Supporting Information for

Original article

Aureane-type sesquiterpene tetraketides as a novel class of immunomodulators with interleukin-17A inhibitory activity

Xin Tang[a,d,†], Chuanxi Wang[b,†], Lei Wang[c,f,†], Feifei Ren[d], Runqiao Kuang[b], Zhenhua Li[a,d], Xue Han[b], Yiming Chen[d], Guodong Chen[b], Xiuqing Wu[d], Jie Liu[c], Hengwen Yang[d], Xingzhong Liu[e], Chen Wang[c,*], Hao Gao[b,*], Zhinan Yin[a,d,*]

[a]*Guangdong Provincial Key Laboratory of Tumor Interventional Diagnosis and Treatment, Zhuhai Institute of Translational Medicine, Zhuhai People's Hospital Affiliated with Jinan University, Jinan University, Zhuhai 519000, China*

[b]*Institute of Traditional Chinese Medicine and Natural Products, College of Pharmacy/Guangdong Province Key Laboratory of Pharmacodynamic Constituents of TCM and New Drugs Research/International Cooperative Laboratory of Traditional Chinese Medicine Modernization and Innovative Drug Development of Ministry of Education (MOE) of China, Jinan University, Guangzhou 510632, China*

[c]*Department of Respirology, Capital Medical University, Beijing 100069, China*

[d]*Biomedical Translational Research Institute, Health Science Center (School of Medicine), Jinan University, Guangzhou 510632, China*

[e]*State Key Laboratory of Mycology, Institute of Microbiology, Chinese Academy of Sciences, Beijing 100190, China*

[f]*Department of Respiratory and Critical Care Medicine, the Second Affiliated Hospital of Xi'an Jiaotong University (Xibei Hospital), Xi'an 710004, China*

Received 1 December 2022; received in revised form 19 February 2023; accepted 13 March 2023

*Corresponding authors.

E-mail addresses: cyh-birm@263.net (Chen Wang), tghao@jnu.edu.cn (Hao Gao), tzhinan@jnu.edu.cn (Zhinan Yin).

[†]These authors made equal contributions to this work.

List of Supporting Information

1. Experimental procedures

1.1. General experimental procedures for the isolation of compounds

A JASCO P1020 digital polarimeter (Jasco International Co. Ltd., Tokyo, Japan) was utilized for the purpose of measuring the optical rotations. A JASCO V-550 UV/vis spectrometer (Jasco International Co. Ltd) was utilized in the recording of the UV spectra and a JASCO J-810 spectrophotometer (Jasco International Co. Ltd) was employed in measuring the ECD spectra, with CH_3OH serving as a solvent. Data in the IR spectrum were obtained by the use of a JASCO FT/IR-480 plus spectrometer (Jasco International Co., Ltd). ^{1}H and ^{13}C NMR spectra were captured using either a Bruker AV 300, Bruker AV 400, or Bruker AV 600 (Bruker BioSpin Group, Faellanden, Switzerland) using solvent signals (DMSO-d_6: δ_H 2.50/δ_C 39.5; CD_3OD: δ_H 3.30/δ_C 49.0) as an internal standard. The Bruker amazon SL mass spectrometer (Bruker Daltonics Inc., MA, USA) was utilized to complete the ESI-MS spectra, and the Waters Synapt G2 mass spectrometer (Waters Corporation, MA, USA) was utilized to acquire the HR-ESI-MS spectra. A UV preparative detector, a twin pump gradient system, and Dr Flash II fraction collector system were installed in the medium-pressure liquid chromatography (MPLC) instrument (Shanghai Lisui E-Tech Co., Ltd., Shanghai, China). The analytical HPLC was carried out on a Dionex HPLC system (Dionex, CA, USA), which was outfitted with an Ultimate 3000 column compartment, Ultimate 3000 diode array detector (DAD), Ultimate 3000 pump, and an Ultimate 3000 autosampler utilizing a reversed-phase C18 column were used for the separation procedure (Gemini 5 μm, 4.6 × 250 mm; Phenomenex, Cheshire, UK). The preparative HPLC was conducted on a shimadzu LC-6-AD liquid chromatography with SPD-20A detector (Shimadzu, Kyoto, Japan) utilizing a reversed-phase C18 column (Gemini 5 μm, 21.2 × 250 mm; Phenomenex). The semi-preparative HPLC was conducted on a shimadzu LC-6AD liquid chromatography with SPD-20A detector (Shimadzu) utilizing a reversed-phase C18 column (5 μm, 10 × 250 mm; YMC Co., Ltd., Kyoto, Japan). Column chromatography (CC) was conducted utilizing a silica gel (200–300 mesh) (Qingdao Haiyang Chemical Co. Ltd., Qingdao, China), Sephadex LH-20 (Amersham Pharmacia Biotech Co., Ltd., GA, USA), and ODS (50 μm, YMC Co., Ltd), respectively.

1.2. Fungal material

The strain ZLW0801-19 was isolated from the mud and obtained from Zhalong Wetland, Heilongjiang Province, China. Premised on its morphological features as well as ribosomal internal transcribed spacer, the strain was identified as *Myrothecium gramineum* (GenBank accession JX077058.1). At a temperature of 25 °C for five days, the fungus was grown in culture on a potato dextrose agar slant. To inoculate the potato dextrose broth that was contained inside the four Erlenmeyer flasks (250 mL), agar plugs were utilized. Each flask contained 100 mL of broth. To prepare the seed culture, a period of five days was spent with each of the four flasks of inoculation medium being agitated on a rotary shaker at a rate of 200 revolutions per minute. Fermentation was carried out in a total of 24 Erlenmeyer flasks, each with a volume of 500 mL and containing 70 g of rice. After adding 105 mL of distilled water to each flask, and the rice was allowed to soak for a whole night before being autoclaved at 120 °C for half an hour. Each flask was then infected with 5 mL of the spore inoculum once the temperature had returned to ambient temperature. The flasks were then kept in an incubator at ambient temperature and in a dark place for 51 days.

1.3. Extraction and isolation

The culture was extracted with EtOAc for three times, and the organic solvent was removed under reduced pressure to obtain the crude product (81.7 g). Then, the crude extract was exposed to open silica-gel CC (5 × 80 cm) using a successive elution of cyclohexane/EtOAc (100:0, 98:2, 95:5, 90:10, 80:20, 70:30, 50:50, and 0:100, v/v, each 6000 mL) and 100% CH_3OH (6000 mL) to afford seven fractions (F1–F7). The fraction F5 (14.4 g) was further separated using the MPLC with an ODS CC (6 × 60 cm), which was eluted with a successive elution of CH_3OH/H_2O (70:30, 80:20, 90:10, and 100:0, v/v, each 2500 mL) with a flow rate of 15 mL/min to afford nine fractions (5.1–5.9). Fraction 5.1 (1.20 g) was subjected to Sephadex LH-20 CC (2 × 150 cm) using an elution of CH_3OH to afford six fractions (5.1.1–5.1.6). Fraction 5.2 (3.44 g) was further exposed to MPLC on ODS CC (4 × 45 cm) using a successive elution of CH_3OH/H_2O (60:40, 70:30, 80:20, 90:10, and 100:0, v/v, each 700 mL) with a flow rate of 15 mL/min to afford five fractions (5.2.1–5.2.5). Purification of fraction 5.2.4 (387 mg) was realized using semi-preparative HPLC with CH_3CN/H_2O (50:50, v/v) at a flow rate of 3 mL/min to obtain compound **9** (t_R: 53.6 min, 26.2 mg). Fraction 5.2.5 (365 mg) was purified using preparative HPLC, and the solvent system CH_3CN/H_2O (55:45, v/v) at a flow rate of 8 mL/min was used to yield compound **11** (t_R: 86.4 min, 7.0 mg). Fraction 5.3 (870 mg) was separated by Sephadex LH-20 CC (2 × 150 cm) using an elution of CH_3OH to afford seven fractions (5.3.1–5.3.7). Fraction 5.3.7 (144 mg) was purified using semi-preparative HPLC with CH_3OH/H_2O (75:25, v/v) at a flow rate of 3 mL/min to yield compounds **1** (t_R: 63.7 min, 17.0 mg) and **4** (t_R: 69.9 min, 17.5 mg). Fraction 5.5 (1.55 g) was purified using preparative HPLC with CH_3OH/H_2O (75:25, v/v) at a flow rate of 8 mL/min to obtain compound **2** (t_R: 73.5 min, 507.0 mg). Fraction 5.7 (1.88 g) was subjected to silica-gel CC (3 × 20 cm) using a successive elution of cyclohexane/EtOAc (90:10, 85:15, 80:20, 75:25, 70:30, 60:40, 50:50, and 0:100, v/v, each 1000 mL) to collected eight fractions (5.7.1–5.7.8). Fraction 5.7.4 (62.1 mg) was purified using semi-preparative HPLC with CH_3OH/H_2O (82:18, v/v) at a flow rate of 3 mL/min to afford compound **5** (t_R: 21.3 min, 12.1 mg). F6 (20.1 g) was further subjected to MPLC on ODS CC (6 × 60 cm) using a successive elution of CH_3OH/H_2O (60:40, 70:30, 80:20, 90:10, and 100:0, v/v, each 2500 mL) with a flow rate of 15 mL/min to afford seven fractions (6.1–6.7). Fraction 6.4 (2.90 g) was subjected to MPLC on ODS CC (4 × 45 cm) using a successive elution of CH_3OH/H_2O (70:30, v/v, each 700 mL) with a flow rate of 15 mL/min to afford five fractions (6.4.1–6.4.5). Fraction 6.4.2 (1.63 g) was purified using preparative HPLC with CH_3OH/H_2O (70:30, v/v) at a flow rate of 8 mL/min to yield compounds **10** (t_R: 25.4 min, 4.0 mg) and **3** (t_R: 35.2 min, 820 mg). Fraction 6.4.3 (212.9 mg) was purified using semi-preparative HPLC with CH_3CN/H_2O (55:45, v/v) at a flow rate of 3 mL/min to yield compounds **6** (t_R: 63.3 min, 10.3 mg) and **7** (t_R: 25.0 min, 10.3 mg). Fraction 6.3 (650 mg) was subjected to silica-gel CC (3 × 20 cm) using a successive elution of cyclohexane/EtOAc (75:25, 70:30, 60:40, 50:50, and 0:100, v/v, each 300 mL) to afford six fractions (6.3.1–6.3.6). Fraction 6.3.6 (349.7 mg) was purified using semi-preparative HPLC with CH_3CN/H_2O (40:60, v/v) at a flow rate of 3 mL/min to yield **8** (t_R: 17.5 min, 7.7 mg).

Myrogramin A (1). Colorless crystal plate; $[\alpha]_D^{29}$ +34.9 (*c* 1.0, CH_3OH); UV (CH_3OH) λ_{max} (log ε) 205 (4.31), 225 (4.28), 221 (4.10), 300 (4.27) nm; ECD (*c* 3.4 × 10^{-4} M CH_3OH) λ_{max} ($\Delta\varepsilon$) 221 (+1.86), 245 (+1.71), 334 (–0.55), 306 (–0.74); IR (KBr) ν_{max} 3399, 3137, 2974, 2929, 2864, 1616, 1430, 1293, 1262, 1117, 1045 cm^{-1}; ^1H NMR (DMSO-d_6, 300 MHz) and ^{13}C NMR (DMSO-d_6, 75 MHz) see Table S1; ESI-MS (positive) *m/z* 373 $[M + H]^+$, 395 $[M + Na]^+$; ESI-MS (negative) *m/z* 371 $[M – H]^–$, 743 $[2M – H]^–$; HR-ESI-MS (positive) *m/z* 373.2379 $[M + H]^+$ (calcd. for $C_{23}H_{33}O_4$,

373.2379).

Myrothecisin C (2). Yellow crystal needle; $[\alpha]_D^{29}$ +57.9 (*c* 1.0, CH_3OH); (CH_3OH) λ_{max} (log ε) 205 (4.27), 223 (4.23), 240 (4.09), 299 (4.27) nm; IR (KBr) ν_{max} 3399, 3160, 2973, 2838, 2868, 1708, 1619, 1435, 1268, 1002 cm^{-1}; ^1H NMR (DMSO-d_6, 400 MHz) and ^{13}C NMR (DMSO-d_6, 100 MHz) see Table S2; ESI-MS (positive) *m/z* 453 $[M + Na]^+$, 883 $[2M + Na]^+$; ESI-MS (negative) *m/z* 429 $[M - H]^-$, 859 $[2M - H]^-$; HR-ESI-MS (positive) *m/z* 453.2261 $[M + Na]^+$ (calcd. for $C_{25}H_{34}O_6Na$, 453.2253).

Myrothecisin D (3). Yellow solid; $[\alpha]_D^{29}$ +36.0 (*c* 1.0, CH_3OH); UV (CH_3OH) λ_{max} (log ε) 206 (4.43), 225 (4.35), 240 (4.18), 299 (4.31) nm; IR (KBr) ν_{max} 3146, 2969, 2929, 2881, 1621, 1625, 1448, 1258 cm^{-1}; ^1H NMR (DMSO-d_6, 300 MHz) and ^{13}C NMR (DMSO-d_6, 75 MHz) see Table S3; ESI-MS (positive) *m/z* 389 $[M + H]^+$, 411 $[M + Na]^+$; ESI-MS (negative) *m/z* 387 $[M - H]^-$, 775 $[2M - H]^-$; HR-ESI-MS (positive) *m/z* 389.2331 $[M + H]^+$ (calcd. for $C_{23}H_{33}O_5$, 389.2328).

Myrogramin B (4). Yellow solid; $[\alpha]_D^{29}$ +32.0 (*c* 1.0, CH_3OH); UV (CH_3OH) λ_{max} (log ε) 205 (4.47), 226 (4.43), 242 (4.31), 300 (4.44) nm; IR (KBr) ν_{max} 3430, 2961, 2931, 2868, 1719, 1622, 1435, 1265, 1039 cm^{-1}; ^1H NMR (DMSO-d_6, 400 MHz) and ^{13}C NMR (DMSO-d_6, 100 MHz) see Table S4; ESI-MS (positive) *m/z* 453 $[M + Na]^+$, 883 $[2M + Na]^+$; ESI-MS (negative) *m/z* 429 $[M - H]^-$, 859 $[2M - H]^-$; HR-ESI-MS (positive) *m/z* 431.2433 $[M + H]^+$ (calcd. for $C_{25}H_{35}O_6$, 431.2434).

Myrogramin C (5). Yellow solid; $[\alpha]_D^{29}$ +41.2 (*c* 1.0, CH_3OH); UV (CH_3OH) λ_{max} (log ε) 205 (4.52), 226 (4.47), 242 (4.31), 298 (4.45) nm; IR (KBr) ν_{max} 3279 ,2934, 2867, 1708, 1618, 1434,1267, 1032 cm^{-1}; ^1H NMR (DMSO-d_6, 400 MHz) and ^{13}C NMR (DMSO-d_6, 100 MHz) see Table S5; ESI-MS (positive) *m/z* 495 $[M + Na]^+$, 967 $[2M + Na]^+$; ESI-MS (negative) *m/z* 471 $[M - H]^-$, 943 $[2M - H]^-$; HR-ESI-MS (positive) *m/z* 495.2368 $[M + Na]^+$ (calcd. for $C_{27}H_{36}O_7Na$, 495.2359).

Myrogramin D (6). Yellow solid; $[\alpha]_D^{29}$ +32.8 (*c* 1.0, CH_3OH); UV (CH_3OH) λ_{max} (log ε) 205 (4.37), 225 (4.35), 239 (4.18), 300 (4.35) nm; ECD (*c* 3.2×10^{-4} M CH_3OH) λ_{max} ($\Delta\varepsilon$) 201 (+1.34), 235 (+2.04), 274 (–0.80), 324 (+0.46); IR (KBr) ν_{max} 3411, 2929, 2858, 1618, 1434, 1386, 1267, 1240, 1125, 1050cm^{-1}; ^1H NMR (DMSO-d_6, 400 MHz) and ^{13}C NMR (DMSO-d_6, 100 MHz) see Table S6; ESI-MS (positive) *m/z* 387 $[M + H]^+$, 409 $[M + Na]^+$; ESI-MS (negative) *m/z* 385 $[M - H]^-$, 771 $[2M - H]^-$; HR-ESI-MS (positive) *m/z* 409.2009 $[M + Na]^+$ (calcd. for $C_{23}H_{30}O_5Na$, 409.2015).

Myrogramin E (7). Yellow solid; $[\alpha]_D^{29}$ +33.4 (*c* 1.0, CH_3OH); UV (CH_3OH) λ_{max} (log ε) 206 (4.36), 226 (4.30), 240 (4.16), 299 (4.33) nm; ECD (*c* 5.8×10^{-4} M CH_3OH) λ_{max} ($\Delta\varepsilon$) 224 (+0.99), 249 (+3.46), 302 (–0.76), 361 (–1.02); IR (KBr) ν_{max} 3399, 2934, 2850, 1617, 1386, 1267, 1245, 1125, 1050, 988 cm^{-1}; ^1H NMR (DMSO-d_6, 400 MHz) and ^{13}C NMR (DMSO-d_6, 100 MHz) see Table S7; ESI-MS (positive) *m/z* 455 $[M + Na]^+$, 895 $[2M + Na]^+$; ESI-MS (negative) *m/z* 431 $[M - H]^-$, 863 $[2M - H]^-$; HR-ESI-MS (positive) *m/z* 455.2415 $[M + Na]^+$ (calcd. for $C_{25}H_{36}O_6Na$, 455.2410).

Myrogramin F (8). Green solid; $[\alpha]_D^{29}$ +37.9 (*c* 1.0, CH_3OH); UV (CH_3OH) λ_{max} (log ε) 215 (4.57), 262 (4.06), 305 (3.27) nm; IR (KBr) ν_{max} 3385, 2929, 2863, 1675, 1452, 1386, 1262 cm^{-1}; ^1H NMR (DMSO-d_6, 300 MHz) and ^{13}C NMR (DMSO-d_6, 75 MHz) see Table S8. ESI-MS (positive) *m/z* 386 $[M + H]^+$, 793 $[2M + Na]^+$; ESI-MS (negative) *m/z* 769 $[2M - H]^-$; HR-ESI-MS (positive) *m/z* 386.2340 $[M + H]^+$ (calcd. for $C_{23}H_{32}NO_4$, 386.2331).

Myrogramin G (9). Green solid; $[\alpha]_D^{29}$ +99.3 (*c* 1.0, CH_3OH); UV (CH_3OH) λ_{max} (log ε) 206

(4.44), 223 (4.46), 240 (4.42), 298 (4.33) nm; ECD (*c* 6.0 × 10^{-4} M CH_3OH) λ_{max} ($\Delta\varepsilon$) 204 (+7.00), 247 (+18.5), 330 (+1.81); IR (KBr) ν_{max} 3283, 2970, 2925, 2867, 1621, 1618, 1430, 1267, 1005 cm^{-1}; ^1H NMR (DMSO-d_6, 300 MHz) and ^{13}C NMR (DMSO-d_6, 75 MHz) see Table S9; ESI-MS (positive) *m/z* 409 $[M + Na]^+$, 795 $[2M + Na]^+$; ESI-MS (negative) *m/z* 385 $[M - H]^-$, 771 $[2M - H]^-$; HR-ESI-MS (positive) *m/z* 387.2176 $[M + H]^+$ (calcd. for $C_{23}H_{31}O_5$, 387.2176).

Myrogramin H (10). White solid; $[\alpha]_D^{29}$ +64.8 (*c* 1.0, CH_3OH); UV (CH_3OH) λ_{max} (log ε) 206 (4.39), 226 (4.06), 289 (3.69) nm; ECD (*c* 6.4 × 10^{-4} M CH_3OH) λ_{max} ($\Delta\varepsilon$) 220 (+3.81), 236 (+3.09), 246 (+3.74), 323 (–0.54); IR (KBr) ν_{max} 3301, 2961, 2872, 1628, 1462, 1284, 1125, 1076 cm^{-1}; ^1H NMR (DMSO-d_6, 300 MHz) and ^{13}C NMR (DMSO-d_6, 75 MHz) see Table S10; ESI-MS (positive) *m/z* 389 $[M + H]^+$, 411 $[M + Na]^+$; ESI-MS (negative) *m/z* 387 $[M - H]^-$, 775 $[2M - H]^-$; HR-ESI-MS (positive) *m/z* 389.2329 $[M + H]^+$ (calcd. for $C_{23}H_{33}O_5$, 389.2328).

Myrogramin I (11). White solid; $[\alpha]_D^{29}$ +79.3 (*c* 1.0, CH_3OH); UV (CH_3OH) λ_{max} (log ε) 206 (4.41), 227 (4.09), 290 (3.76) nm; ECD (*c* 2.9 × 10^{-4} M CH_3OH) λ_{max} ($\Delta\varepsilon$) 220 (+5.47), 235 (+4.19), 246 (+5.58), 320 (–1.30); IR (KBr) ν_{max} 3479, 29743, 2881, 1740, 1623, 1489, 1270, 1045 cm^{-1}; ^1H NMR (DMSO-d_6, 300 MHz) and ^{13}C NMR (DMSO-d_6, 75 MHz) see Table S11; ESI-MS (positive) *m/z* 453 $[M + Na]^+$; ESI-MS (negative) *m/z* 429 $[M - H]^-$, HR-ESI-MS (positive) *m/z* 453.2246 $[M + Na]^+$ (calcd. for $C_{25}H_{34}O_6Na$, 453.2353).

X-ray Crystallographic Analysis of 1. Upon crystallization from MeOH using the vapor diffusion method, colorless plate-like crystals of **1** were obtained. Data were collected using a Sapphire CCD with graphite monochromated Cu Kα radiation, λ = 1.54184 Å at 170.0 K. Crystal data: $C_{24}H_{36}O_5$, M = 404.53, space group monoclinic, *C* 2; unit cell dimensions were determined to be *a* = 25.1808(9) Å, *b* = 7.6024(3) Å, *c* = 12.1145(5) Å, α = 90.00°, β = 90.930(3)°, γ = 90.00 °, *V* = 2318.84(15) $Å^3$, *Z* = 4, *Dx* = 1.159 g/cm^3, F (000) = 880.0, μ (Cu Kα) = 0.638 mm^{-1}. 9310 reflections were collected to θ_{max} = 61.06°, in which 3417 independent unique reflections (R_{int} = 0.0341, R_{sigma} = 0.0333) were used in all calculations. The structure was solved by direct methods using the SHELXS program, and refined by the SHELXL program and full-matrix least-squares calculations[1]. In the structure refinements, hydrogen atoms were placed on the geometrically ideal positions by the "ride on" method. The final refinement gave R_1 = 0.0315 (I > 2σ(I)), wR_2 = 0.0828 (all data), *S* = 1.063, Flack = 0.12(16), and Hooft = 0.16(8). Crystallographic data for myrogramin A (**1**) has been deposited in the Cambridge Crystallographic Data Center as supplementary publication no. CCDC 2223234. Copies of the data can be obtained, free of charge, on application to the Director, CCDC, 12 Union Road, Cambridge CB2 1EZ, UK (fax: +44-(0)1223-336033, or e-mail: deposit@ccdc.cam.ac.uk).

X-ray Crystallographic Analysis of 2. Upon crystallization from MeOH/H_2O using the vapor diffusion method, colorless needle -like crystals of **2** were obtained. Data were collected using a Sapphire CCD with graphite monochromated Cu Kα radiation, λ = 1.54184 Å at 173.00(10) K. Crystal data: $C_{51}H_{74}O_{14}$, M = 911.10, space group monoclinic, *P* 2_1; unit cell dimensions were determined to be *a* = 16.3947(3) Å, *b* = 8.18980(12) Å, *c* = 18.4472(3) Å, α = 90.00°, β = 102.3952 (16)°, γ = 90.00°, *V* = 2419.15(6) $Å^3$, *Z* = 2, *Dx* = 1.251 g/cm^3, F (000) = 984.0, μ (Cu Kα) = 0.735 mm^{-1}. 30758 reflections were collected to θ_{max} = 61.06°, in which 7590 independent unique reflections (R_{int} = 0.0400, R_{sigma} = 0.0330) were used in all calculations. The structure was solved by direct methods using the SHELXS program, and refined by the SHELXL program and full-matrix least-squares calculations[1]. In the structure refinements, hydrogen atoms were placed on the geometrically ideal positions by the "ride on" method. The final refinement gave R_1 = 0.0341 (I >

2σ(I)), wR_2 = 0.0884 (all data), S = 1.037, Flack = -0.04(11), and Hooft = -0.03(6). Crystallographic data for myrothecisin C (**2**) has been deposited in the Cambridge Crystallographic Data Center as supplementary publication no. CCDC 2223235. Copies of the data can be obtained, free of charge, on application to the Director, CCDC, 12 Union Road, Cambridge CB2 1EZ, UK (fax: +44-(0)1223-336033, or e-mail: deposit@ccdc.cam.ac.uk).

1.4. ELISA assays

The cell culture supernatants were collected, and IL-17A concentration was measured using an ELISA kit (Biolegend) as per the guidelines provided by the manufacturer.

1.5. Western blotting

Extraction of whole-cell lysates from cultured splenic cells was done utilizing RIPA lysis buffer (Beyotime Institute of Biotechnology, Shanghai, China) supplemented with complete protease inhibitor (Roche, Basel, Switzerland) on ice for 10 min. The BCA protein assay kit (Beyotime Institute of Biotechnology) was employed in the quantification of the protein supernatants before being boiled with 5 × SDS buffer (Bio Sharp, Hefei, China) at 95 °C for 5 minutes. After being isolated on a 10% polyacrylamide gel, the proteins were deposited onto polyvinylidene fluoride (PVDF) membranes (Millipore). This was followed by the blocking and antibody incubation of the membranes. The ChemiDoc XRS gel imaging system (Bio-RAD, CA, USA) was adopted for the acquisition of western blot images.

1.6. qRT-PCR and bulk RNA-seq analysis

Total RNA from the cells was separated via TRIzol LS reagent (Thermo Fisher Scientific). The RNA was reverse transcribed (RT) into cDNA utilizing the PrimeScript RT reagent kit (TaKaRa, Tokyo, Japan) with gDNA Eraser. Quantitative polymerase qRT-PCR was done as per the recommendations stipulated by the manufacturer of TB green (TaKaRa). Primer sequences for the qPCR assay were as follows: *Il17a* forward (-F), 5′-TTTAACTCCCTTGGCGCAAAA-3′; *Il17a* reverse (-R), 5′-CTTTCCCTCCGCATTGACAC-3′; *Il17f*-F, 5′- TGCTACTGTTGATGTTGGGAC-3′; *Il17f*-R, 5′-AATGCCCTGGTTTTGGTTGAA-3′; *Rorc*-F, 5′-GACCCACACCTCACAAATTGA-3′; *Rorc*-R, 5′-AGTAGGCCACATTACACTGCT-3′; *Rora*-F, 5′-CGAGGTATCTCAGTCACGAAGA-3′; *Rora*-R, 5′-AGTAGGCCACATTACACTGCT-3′; *Irf4*-F, 5′-AGCCCAGCAGGTTCATAACTAC′; *Irf4*-R, 5′-ATGCTTGGCTCAATGGGGAT′; *Batf*-F, 5′-CTGGCAAACAGGACTCATCTG-3′; *Batf*-R, 5′-GGGTGTCGGCTTTCTGTGTC′; *Hprt*-F, 5′-TCAGTCAACGGGGGACATAAA-3′; *Hprt*-R, 5′-GGGGCTGTACTGCTTAACCAG′.

For bulk RNA-seq, 1μg of the extracted RNA was employed in the generation of non-directional RNA-seq libraries by the NEBNext Ultra RNA library prep kit (New England Biolabs, MA, USA). Following the guidelines of the manufacturer, an NovaSeq 6000 sequencing platform (Illumina, CA, USA) was utilized to process the raw data. Subsequently, the alignment of clean reads to the reference genome (mouse genome mm10) was performed. The criteria for genes with significant expression are illustrated below: $|\log_2$ fold change$| > 1$ and P-value < 0.05. KOBAS 3.0 (http://kobas.cbi.pku.edu.cn/help/) was adopted to facilitate the evaluation of the KEGG pathway enrichment analysis predicated on the DEGs.

1.7. Hemodynamic measurements

An ip injection containing 50 mg/kg of pentobarbital, at a concentration of 2%, was used to induce anesthesia in mice. Right ventricular systolic pressure (RVSP) indicated the average pulmonary arterial pressure. When determining the RVSP, our research team typically employed the technique of closed-chest insertion into the right ventricle (RV). Through a xiphocostal angle technique, a needle having a gauge size of 22 that was attached to a pressure transducer and that was integrated with the PowerLab system (AD Instruments, Sydney, Australia) was introduced into the RV of mice that had been administered with anesthesia. The waveform was utilized so that the location of the needle could be confirmed. The pentobarbital sodium solution at a concentration of 2% was used to induce anesthesia in rats (45 mg/kg, ip). To get an accurate reading of the RVSP, a catheter containing heparinized saline was introduced into the RV via the jugular vein. After that, the RVSP was captured by the PowerLab data collecting equipment, and it was afterward converted into a digital form by the LabChart software (AD Instruments). To calculate each patient's specific RVSP, the systolic average of the RV pressure was obtained. Utilizing the LabChart program that was included in the PowerLab system, data were recorded. After that, the animals were slaughtered proceeded by the harvesting of their lungs.

1.8. Lung morphometric analysis

To conduct morphometric analysis, the lung tissue was fixed in paraffin and then sections were cut serially at a thickness of 4 μm. Images of pulmonary arterioles were captured using a digital camera system from Olympus attached to a microscope (Olympus, Tokyo, Japan). Image-Pro Plus 6.0 (Media Cybernetics, MD, USA) was used to do the circumferential measurements on the artery walls. We took measurements of the pulmonary arterioles that had exterior diameters of less than 100 μm and were supplemented either by the alveolar ducts or alveoli. Based on these measurements, we classified the pulmonary arterioles into the following four categories, according to their exterior diameters: 0–25, 26–50, 51–75, and 76–100 μm. The % media thickness (% MT), % MT = (circumference$_{ext}$/π-circumferenceint$_{int}$/π)/(circumference$_{ext}$/π) × 100, where circumference$_{ext}$ and circumference$_{int}$ denoted the circumferences that were respectively bounded by the exterior and interior elastic lamina, was employed as a measuring tool for pulmonary arteriolar remodeling.

1.9. Human Th17 differentiation

Human antibodies and recombinant proteins used for this study were as follows: rhTGF-β1.2, Anti-CD3 (clone OKT3), anti-CD28 (clone CD28.2), and anti-IL-4 (clone MP4-25D2) purchased from Tonbo Biosciences (CA, USA), anti-IFN-γ (clone NIB42, Thermo Fisher Scientific), fluorescence-conjugated anti-CD4 (clone SK3, BD Biosciences), anti-IL-17A (clone BL168, BioLegend), and rhIL-6 (catalog 200-06, PeproTech).

PBMCs were extracted from healthy human peripheral blood by Ficoll-Paque gradient density centrifugation. Negative selection of human naïve $CD4^+$ T cells from the PBMCs was performed with the aid of human naïve $CD4^+$ T cell isolation kit II (StemCell Technologies, BC, Canada). Isolated human naïve $CD4^+$ T cells (5×10^5 cells/mL) were activated in 5 μg/mL anti-CD3-coated plates with soluble 1 μg/mL anti-CD28. Cells culture was undertaken for three days in Th17 culture medium (IMDM complete medium with 0.5 ng/mL rhTGF-β1.2, 10 μg/mL anti-IFN-γ, 10 μg/mL anti-IL-4, and 40 ng/mL rhIL-6). On Day 3, rhIL-6 was supplemented to the medium. On Day 5, the cells were collected and washed twice to remove anti-CD3 Ab and anti-CD28 Ab. The washed

cells were seeded in a new plate with a fresh Th17 medium. On Day 7, the cells were split in a 1:1 ratio and cultured in a fresh Th17 culture medium for an additional two days.

1.10. Isolation of CNS-infiltrating lymphocytes

After mice were euthanized, their brain and spinal cord tissues were dissected and placed in 100 mm dishes containing pre-cooled PBS at 4°C. The CNS tissues were then homogenized with a plunger from a 5-mL syringe on a 70-μm cell mesh. After centrifugation, lymphocytes from the CNS were enriched by centrifugation at room temperature for 20 minutes at 1260 g using discontinuous Percoll density gradients of 40% and 70%. Set the acceleration to 6 and the deceleration to 2. Transfer 40% to 70% of the mist layer (lymphocytes) into a 15 mL centrifuge tube, add PBS and centrifuge at 2200 rpm for 10 min. The cell pellets were washed and then resuspended in culture media or PBS for subsequent cell counting and flow cytometry analysis.

2. Supplementary figures for pharmacological activities

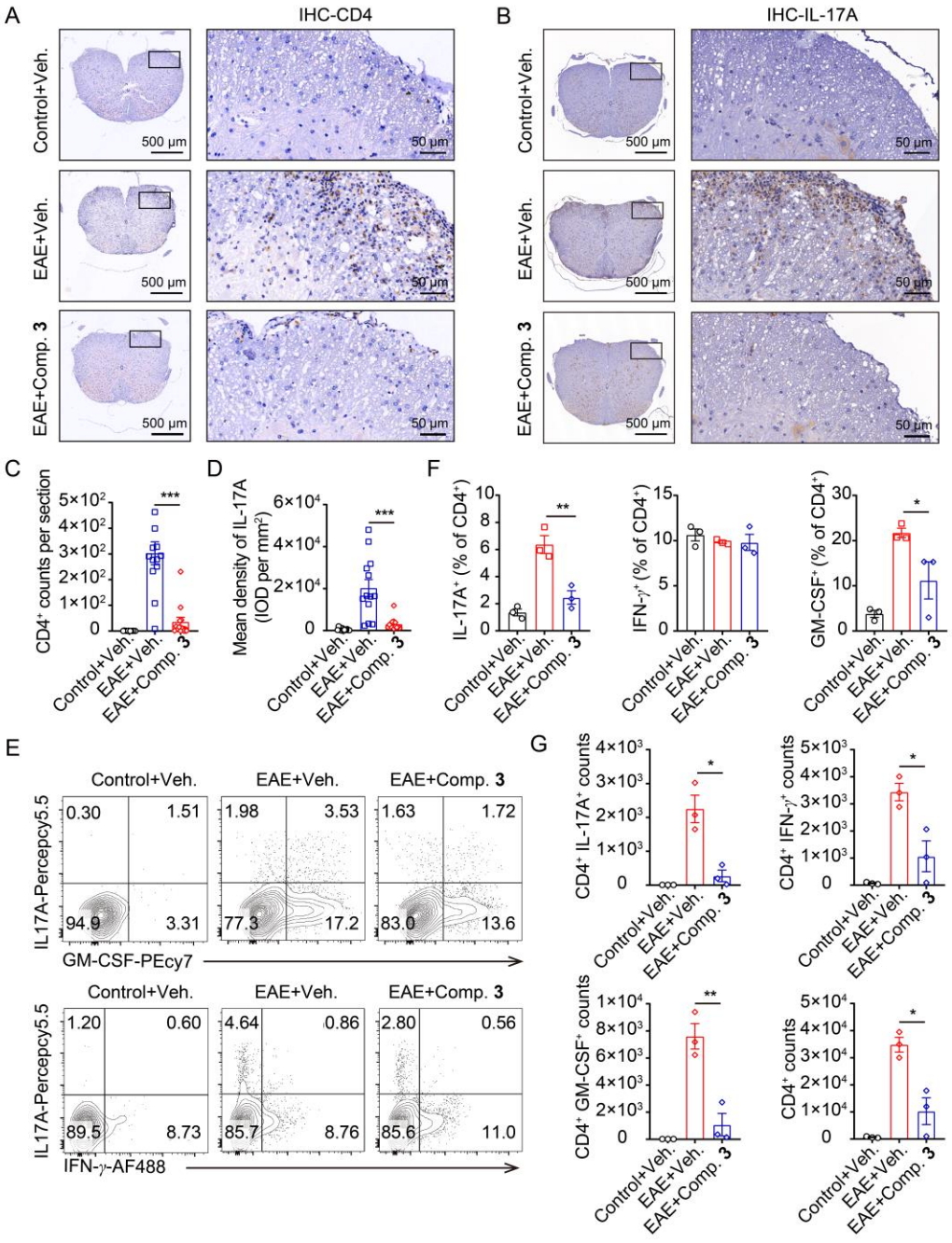

Figure S1 Compound **3** suppresses the infiltration of IL-17A-producing $CD4^+$ T cells in MOG35-55-elicited EAE diseases. (A–D) Mice were administered with compound **3** starting on the same day of MOG immunization (Day 0) and euthanized on Day 15 for flow cytometry analysis. (A and C) Representative IHC images for CD4 staining of the spinal cord and statistical histograms for the absolute number of infiltrating $CD4^+$ T cells. (B and D) Representative IHC images for IL-17A staining of the spinal cord and statistical histograms of the mean density of IL-17A expression. (E–G) Mice were treated with compound **3** beginning on Day 0 and euthanized on Day 19 for IHC analysis. (E and F) Illustrative flow cytometry staining and statistical analysis for the frequency of CNS-infiltrating IFN-γ, GM-CSF, and IL-17A gated on $CD4^+$ T cells. (G) Statistical histograms for the absolute number of $CD4^+$ $IL\text{-}17A^+$, $CD4^+$ $GM\text{-}CSF^+$, $CD4^+$ $IFN\text{-}\gamma^+$, and $CD4^+$ T cells in CNS-

infiltrating lymphocytes. Veh. represents vehicle; Comp. **3** represents compound **3**. Data were represented as mean ± SEM. $^{*}P < 0.05$, $^{**}P < 0.01$, $^{***}P < 0.001$ *vs*. EAE + veh. group.

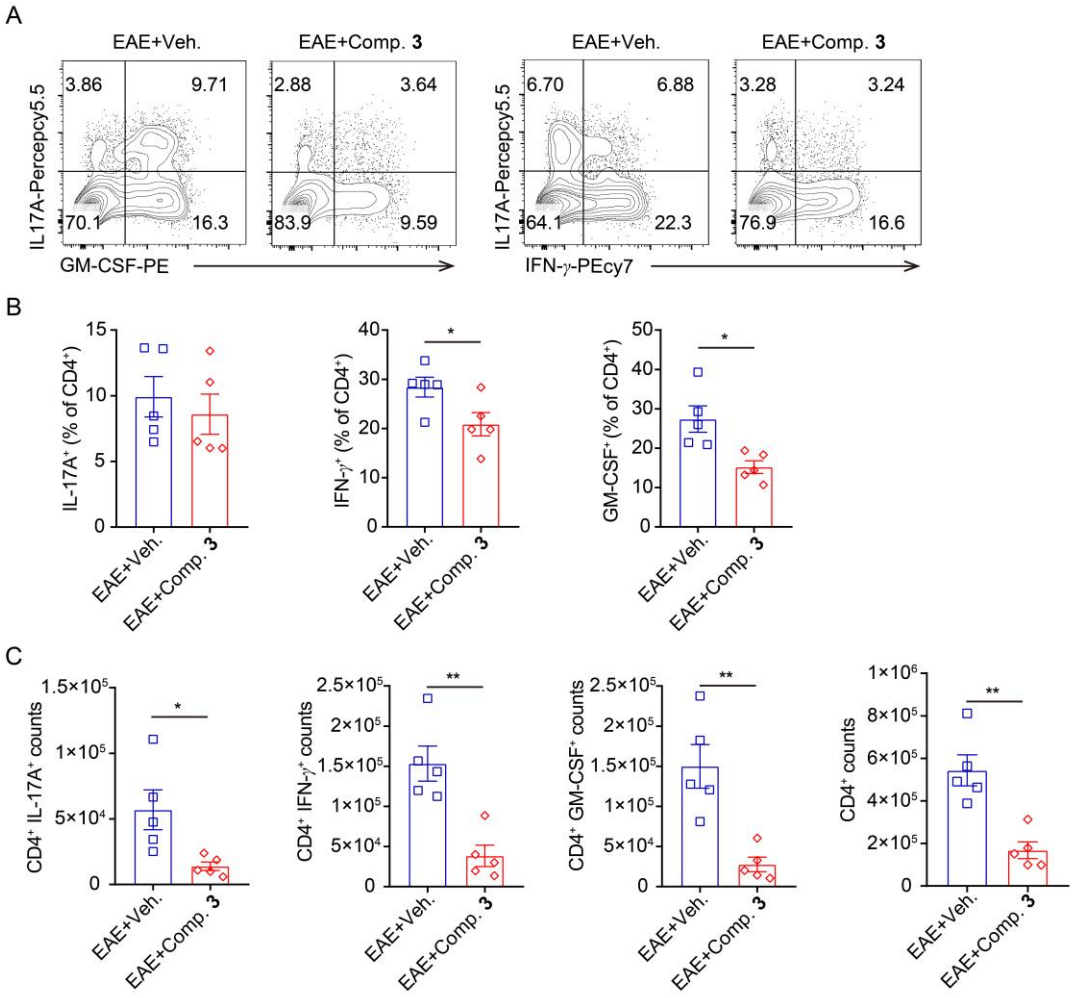

Figure S2 Compound **3** reduces the infiltration of pro-inflammatory immune cells into the CNS after induction of EAE. (A) EAE mice were treated with vehicle or compound **3** beginning at Day 10 (clinical score reached 0.5–1) and euthanized on Day 15. Representative flow cytometry plots of CNS-infiltrating IL-17A, GM-CSF, and IFN-γ gated $CD4^+$ T cells. (B) Statistical histograms for the percentages of CNS-infiltrating IFN-γ, GM-CSF, and IL-17A in $CD4^+$ T cells. (C) Statistical histograms for the absolute number of $CD4^+$ $IL\text{-}17A^+$, $CD4^+$ $GM\text{-}CSF^+$, $CD4^+$ $IFN\text{-}\gamma^+$, and $CD4^+$ T cells in CNS-infiltrating lymphocytes. Veh. represents vehicle; Comp. **3** represents compound **3**. Data were mean ± SEM. $^{*}P < 0.05$, $^{**}P < 0.01$, $^{***}P < 0.001$ *vs*. EAE + veh. group.

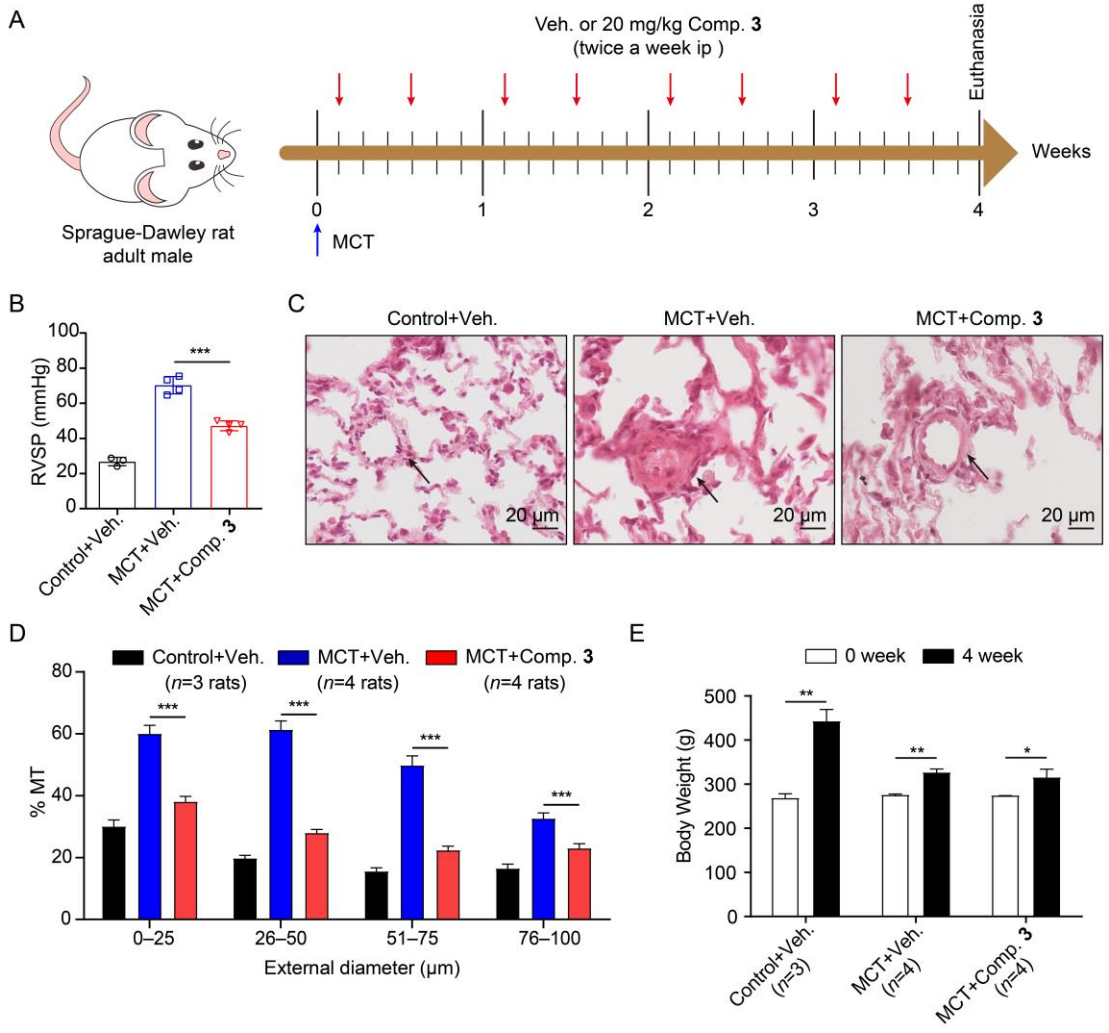

Figure S3 Compound **3** improves MCT-induced PH. (A) Experimental schematic of the MCT-induced rat model. (B) RVSP of rats treated with or without MCT (Control + Vehicle, MCT + Vehicle, or MCT + Compound **3**). (C) Images showing H&E staining of pulmonary arterioles. The arrows represented pulmonary arterioles. (D) The proportion of the medial thickness of the pulmonary arterioles in mice relative to its exterior diameter. (E) Weight gain in the three groups. Veh. represents vehicle; Comp. **3** represents compound **3**; MCT represents monocrotaline. $^{*}P < 0.05$, $^{**}P < 0.01$, $^{***}P < 0.001$ between indicated groups.

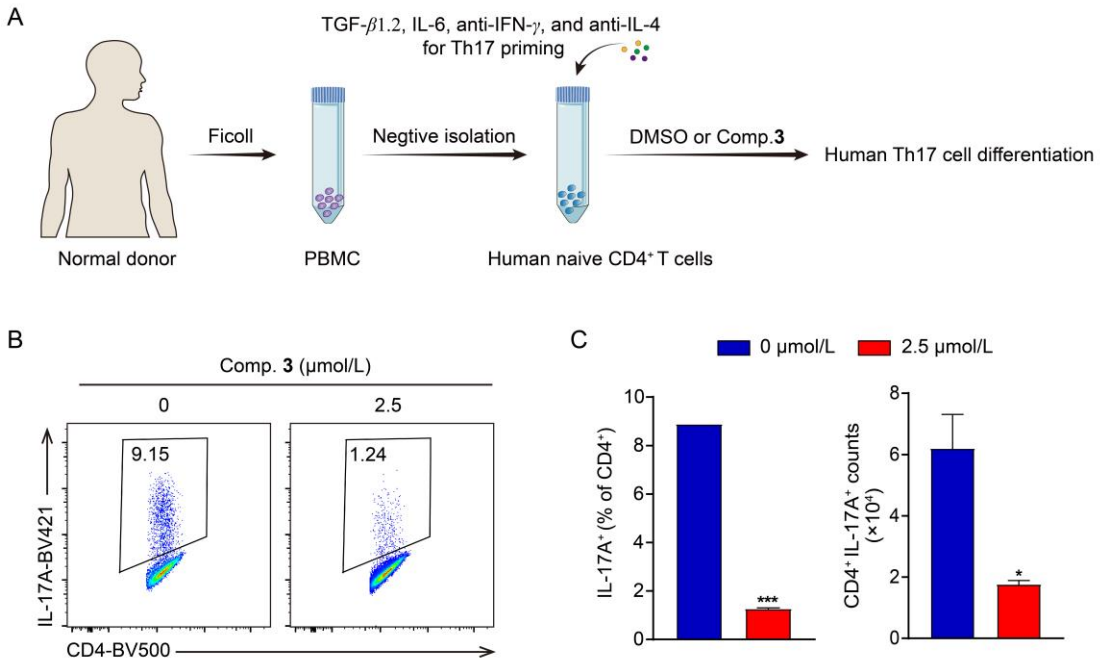

Figure S4 Compound **3** suppresses human Th17 differentiation. (A) The schematic diagram of human Th17 cell differentiation. (B) Illustrative flow cytometry plots of IL-17A production gated on $CD4^+$ T cells with DMSO or 2.5 μmol/L compound **3**. (C) Statistical histograms for the proportion and the absolute number of $CD4^+$ $IL\text{-}17A^+$ T cells. Data were mean ± SD for $n = 3$. $^*P < 0.05$, $^{***}P < 0.001$ *vs*. compound **3** (0 μmol/L) group.

3. NMR assignments of compounds 1–11

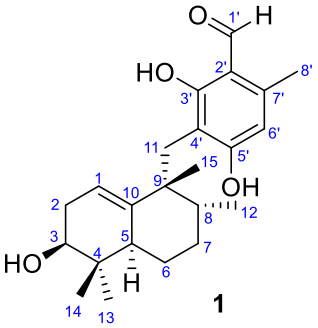

1

Table S1 NMR assignments for **1**.

position	δ_C[a], type	δ_H[a,c] (*J* in Hz)	^{1}H–^{1}H COSY[b]	HMBC[b]	ROESY[b]
1	116.3, CH	4.89	2a, 2b, 5	3, 5, 9	15
2	31.6, CH_2	1.74, Ha	1, 2b, 3	1, 3, 10	14
		1.71, Hb	1, 2a, 3	1, 3, 4, 10	
3	71.5, CH	3.30, dd (7.8, 7.5)	2a, 2b, OH-3	4, 13, 14	5, 13
4	36.9, C				
5	43.6, CH	2.45	1, 6a, 6b	4, 6, 10	3, 7b, 11a, 13
6	26.6, CH_2	1.79, Ha	5, 6b	5, 10	
		1.11, Hb	5, 6a, 7a, 7b	5, 10	8, 14
7	30.3, CH_2	1.53, Ha	6b, 7b, 8	6, 8	
		1.50, Hb	6b, 7a, 8	6, 8	5, 11a, 11b, 12
8	42.8, CH	1.28	7a, 7b, 12	7, 9, 12, 15	6b, 15
9	43.7, C				
10	143.0, C				
11	23.2, CH_2	2.62, d (12.7), Ha	11b	9, 10, 15, 4', 5', 6'	5, 7b
		2.48, d (12.7), Hb	11a	9, 10, 15, 4', 5', 6'	7b, 12
12	17.2, CH_3	1.03, d (6.6)	8	7, 8, 9, 15	7b, 11b
13	25.2, CH_3	0.95, s		3, 4, 5, 14	3, 5
14	14.8, CH_3	0.59, s		3, 4, 5, 13	2a, 6b
15	22.9, CH_3	0.91, s		8, 9, 10, 11, 12	1, 8
1'	193.5, CH	9.94, s		2', 3'	8'
2'	111.6, C				
3'	164.9, C				
4'	110.6, C				
5'	164.9, C				
6'	109.8, CH	6.23, s	8'	2', 4', 5', 8'	
7'	141.7, C				
8'	17.7, CH_3	2.42, s	6'	2', 6', 7'	1'
OH-3		4.15, br.s	3		
OH-3'		12.87, s			
OH-5'		10.55, br.s			

[a] The data recorded in DMSO-d_6 (^{1}H NMR for 300 MHz, ^{13}C NMR for 75 MHz)

[b] The data recorded in DMSO-d_6 (^{1}H NMR for 400 MHz, ^{13}C NMR for 100 MHz)

[c] Indiscernible signals owing to overlapping or having complex multiplicity are reported without designating multiplicity.

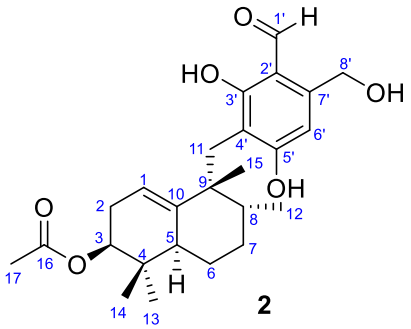

2

Table S2 NMR assignments for **2** in DMSO-d_6 (400 MHz for ^{1}H; 100 MHz for ^{13}C).

position	δ_C, type	δ_H[a] (J in Hz)	^{1}H–^{1}H COSY	HMBC	ROESY
1	114.7, CH	4.94	2a, 2b, 5	3, 5, 9	15
2	27.9, CH_2	1.86, Ha	1, 2b, 3	1, 3, 10	14
		1.84, Hb	1, 2a, 3	1, 3, 10	
3	75.6, CH	4.62, dd (6.9, 6.4)	2a, 2b	4, 16	5, 13
4	35.6, C				
5	43.3, CH	2.56	1, 6b	4, 6, 10	3, 7b, 11a, 13
6	26.7, CH_2	1.78, Ha	6b, 7a, 7b	5	
		1.15, Hb	5, 6a, 7a, 7b		8, 14
7	30.2, CH_2	1.54, Ha	6a, 6b, 7b, 8	6, 8, 12	
		1.52, Hb	6a, 6b, 7a, 8	8	5, 11a, 11b, 12
8	43.1, CH	1.30	7a, 7b, 12	7, 12	6b, 15
9	43.7, C				
10	143.9, C				
11	23.4, CH_2	2.68, d (12.9), Ha	11b	9, 10, 15, 4', 5', 6'	5, 7b, 12
		2.52, d (12.9), Hb	11a	9, 10, 15, 4', 5', 6'	7b, 12
12	17.1, CH_3	1.03, d (6.7)	8	7, 8, 9, 15	7b, 11a, 11b
13	24.9, CH_3	0.88, s		3, 4, 5, 14	3, 5
14	16.7, CH_3	0.73, s		3, 4, 5, 13	2a, 6b
15	22.9, CH_3	0.95, s		8, 9, 10, 11, 12	1, 8
16	169.9, C				
17	21.0, CH_3	1.98, s		16	
1'	193.4, CH	9.96, s		2', 3'	8'
2'	110.3, C				
3'	164.4, C				
4'	111.3, C				
5'	164.7, C				
6'	107.3, CH	6.51, s		2', 4', 5', 8'	OH-5', OH-8'
7'	145.4, C				
8'	59.9, CH_2	4.71, d (5.4)	OH-8'	2', 6', 7'	1'
OH-3'		12.84, s		3', 4'	
OH-5'		10.58, s		4', 5'	6'
OH-8'		5.37, t (5.4)	8'	8'	6'

[a] Indiscernible signals owing to overlapping or having complex multiplicity are reported without designating multiplicity.

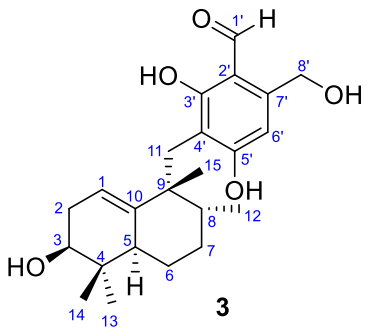

3

Table S3 NMR assignments for **3**.

position	δ_C[a], type	δ_H[a,c] (*J* in Hz)	^{1}H–^{1}H COSY[b]	HMBC[b]	ROESY[b]
1	116.3, CH	4.87	2a, 2b, 5	3, 5, 9	15
2	31.6, CH_2	1.73, Ha	1, 2b, 3	1, 3, 10	14
		1.70, Hb	1, 2a, 3	1, 3, 4, 10	
3	71.5, CH	3.31	2a, 2b, OH-3		5, 13
4	36.9, C				
5	43.7, CH	2.45	1, 6b	4, 6, 10	3, 7b, 11a, 13
6	26.7, CH_2	1.79, Ha	6b	5, 10	
		1.11, Hb	5, 6a, 7a, 7b	5	8, 14
7	30.3, CH_2	1.52, Ha	6b, 7b, 8	6, 8, 12	
		1.50, Hb	6b, 7a, 8	8	5, 11a, 11b, 12
8	42.8, CH	1.28	7a, 7b, 12	7, 9, 12, 15	6b, 15
9	43.7, C				
10	143.0, C				
11	23.3, CH_2	2.63, d (12.8), Ha	11b	9, 10, 15, 3', 4', 5'	5, 7b
		2.49, d (12.8), Hb	11a	9, 10, 15, 3', 4', 5'	7b, 12
12	17.2, CH_3	1.02, d (6.7)	8	7, 8, 9, 15	7b, 11b
13	25.2, CH_3	0.95, s		3, 4, 5, 14	3, 5
14	14.8, CH_3	0.59, s		3, 4, 5, 13	2a, 6b
15	22.8, CH_3	0.90, s		8, 9, 10, 11, 12	1, 8
1'	193.5, CH	9.96, s		2', 3'	8'
2'	110.2, C				
3'	164.8, C				
4'	111.3, C				
5'	164.6, C				
6'	107.2, CH	6.50, s	8'	2', 4', 5', 8',	
7'	145.4, C				
8'	59.8, CH_2	4.71, d (3.4)	6'	2', 6', 7'	1'
OH-3		4.15, d (4.4)	3		
OH-3'		12.79, s			
OH-5'		10.56, br.s		4', 5'	
OH-8'		5.38, t (3.4)			

[a] The data recorded in DMSO-d_6 (^{1}H NMR for 300 MHz, ^{13}C NMR for 75 MHz)

[b] The data recorded in DMSO-d_6 (^{1}H NMR for 400 MHz, ^{13}C NMR for 100 MHz)

[c] Indiscernible signals owing to overlapping or having complex multiplicity are reported without designating multiplicity.

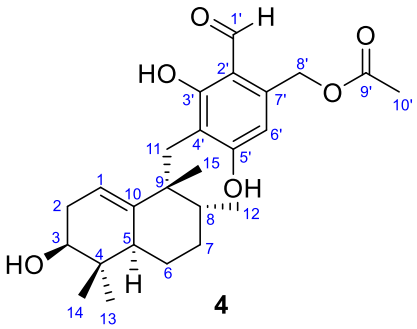

4

Table S4 NMR assignments for **4** in DMSO-d_6 (400 MHz for ^{1}H; 100 MHz for ^{13}C).

position	δ_C, type	δ_H[a] (J in Hz)	^{1}H–^{1}H COSY	HMBC	ROESY
1	116.3, CH	4.88	2a, 2b, 5	3, 5, 9	15
2	31.6, CH_2	1.72, Ha	1, 2b, 3	1, 3, 10	14
		1.70, Hb	1, 2a, 3	1, 3, 10	
3	71.5, CH	3.29, dd (7.6, 7.2)	2a, 2b, OH-3	13	5, 13
4	36.9, C				
5	43.7, CH	2.45, br.d (11.7)	1, 6b	10	3, 7b, 11a, 13
6	26.6, CH_2	1.78, Ha	6b, 7a	5, 10	
		1.10, Hb	5, 6a, 7a, 7b	5, 10	8, 14
7	30.3, CH_2	1.52, Ha	6b, 7b, 8	6, 8	
		1.50, Hb	6a, 6b, 7a, 8	6	5, 11a, 11b, 12
8	42.9, CH	1.28	7a, 7b, 12	12	6b, 15
9	43.7, C				
10	143.0, C				
11	23.4, CH_2	2.65, d (12.9), Ha	11b	9, 10, 15, 3', 4', 5'	5, 7b, 12
		2.52, d (12.9), Hb	11a	9, 10, 15, 3', 4', 5'	7b, 12
12	17.2, CH_3	1.03, d (6.7)	8	7, 8, 9, 15	7b, 11a, 11b
13	25.2, CH_3	0.94, s		3, 4, 5, 14	3, 5
14	14.8, CH_3	0.59, s		3, 4, 5, 13	2a, 6b
15	22.9, CH_3	0.91, s		8, 9, 10, 11, 12	1, 8
1'	193.2, CH	9.90, s		2', 7'	8'
2'	110.3, C				
3'	164.8, C				
4'	112.9, C				
5'	164.9, C				
6'	109.2, CH	6.46, s	8'	2', 4', 5', 8'	
7'	138.5, C				
8'	62.3, CH_2	5.29, s	6'	2', 6', 7', 9'	1'
9'	169.9, C				
10'	20.7, CH_3	2.07, s		9'	
OH-3		4.15, br.s	3		
OH-3'		12.79, s			
OH-5'		10.80, br.s			

[a] Indiscernible signals owing to overlapping or having complex multiplicity are reported without designating multiplicity.

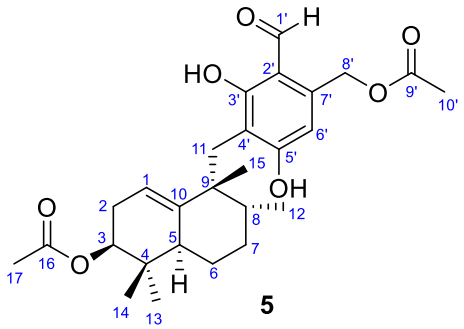

5

Table S5 NMR assignments for **5** in DMSO-d_6 (400 MHz for ^{1}H; 100 MHz for ^{13}C).

position	δ_C, type	$\delta_H{}^a$ (J in Hz)	^{1}H–^{1}H COSY	HMBC	ROESY
1	114.8, CH	4.94	2a, 2b, 5	3, 5, 9	15
2	27.9, CH_2	1.87, Ha	1, 2b, 3	1, 3, 10	14
		1.85, Hb	1, 2a, 3	1, 3, 10	
3	75.5, CH	4.59, dd (6.7, 6.3)	2a, 2b	4, 13, 16	5, 13
4	35.6, C				
5	43.4, CH	2.50	1, 6b	4, 6, 10	3, 7b, 13
6	26.7, CH_2	1.78, Ha	6b	5, 10	
		1.13, Hb	5, 6a, 7a, 7b	5, 10	
7	30.2, CH_2	1.54, Ha	6b, 7b, 8	8	
		1.52, Hb	6b, 7a, 8	8	5, 11a, 11b, 12
8	43.1, CH	1.31	7a, 7b, 12	12	15
9	43.7, C				
10	143.8, C				
11	23.6, CH_2	2.70, d (12.9), Ha	11b	9, 10, 15, 3', 4', 5'	7b, 12
		2.52, d (12.9), Hb	11a	9, 10, 15, 3', 4', 5'	7b, 12
12	17.0, CH_3	1.03, d (6.7)	8	7, 8, 9, 15	7b, 11a, 11b
13	24.9, CH_3	0.87, s		3, 4, 5, 13	3, 5
14	16.6, CH_3	0.72, s		3, 4, 5, 14	2a
15	23.0, CH_3	0.96, s		8, 9, 10, 11, 12	1, 8
16	169.8, C				
17	21.0, CH_3	1.98, s		16	
1'	193.2, CH	9.92, s		2', 3'	
2'	110.5, C				
3'	164.7, C				
4'	113.0, C				
5'	164.3, C				
6'	109.1, CH	6.47, s	8'	2', 4', 5', 8'	
7'	138.6, C				
8'	62.2, CH_2	5.29, s	6'	2', 6', 7', 9'	
9'	169.9, C				
10'	20.7, CH_3	2.07, s		9'	
OH-3'		12.82, s		2', 3', 4'	
OH-5'		10.74, br.s			

[a] Indiscernible signals owing to overlapping or having complex multiplicity are reported without designating multiplicity.

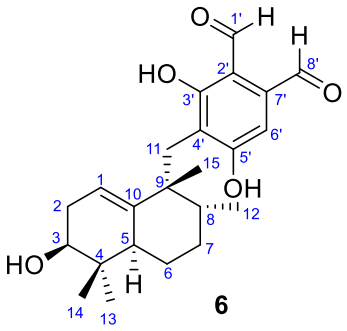

6

Table S6 NMR assignments for **6** in DMSO-d_6 (400 MHz for ^{1}H; 100 MHz for ^{13}C).

position	δ_C, type	$\delta_H{}^a$ (J in Hz)	^{1}H–^{1}H COSY	HMBC	ROESY
1	116.6, CH	4.88	2a, 2b, 5	3, 5, 9	15
2	31.5, CH_2	1.72, Ha	1, 2b, 3	1, 3, 10	14
		1.70, Hb	1, 2a, 3	1, 3, 10	
3	71.4, CH	3.28, dd (7.6, 7.5)	2a, 2b, OH-3		5, 13
4	36.9, C				
5	43.7, CH	2.44, br.d (12.9)	1, 6b	10	3, 7b, 11a, 13
6	26.5, CH_2	1.78, Ha	6b		
		1.09, Hb	5, 6a, 7a, 7b	5, 7	8, 14
7	30.3, CH_2	1.54, Ha	6b, 7b, 8	6, 8	
		1.52, Hb	6b, 7a, 8	6, 8	5, 11a, 11b, 12
8	42.9, CH	1.31	7a, 7b, 12	7, 9, 12, 15	6b, 15
9	44.0, C				
10	142.8, C				
11	24.0, CH_2	2.75, d (12.9), Ha	11b	9, 10, 15, 3', 4', 5'	5, 7b, 12
		2.60, d (12.9), Hb	11a	9 ,10, 15, 3', 4', 5'	7b, 12
12	17.1, CH_3	1.04, d (6.7)	8	7, 8, 9, 15	7b, 11a, 11b
13	25.1, CH_3	0.95, s		3, 4, 5, 14	3, 5
14	14.7, CH_3	0.59, s		3, 4, 5, 13	2a, 6b
15	22.9, CH_3	0.94, s		8, 9, 10, 11, 12	1, 8
1'	194.4, CH	10.54, s		2', 3', 7'	8'
2'	110.4, C				
3'	164.7, C				
4'	119.0, C				
5'	164.0, C				
6'	113.7, CH	6.99, s		2', 4', 5', 8'	8'
7'	136.0, C				
8'	192.9, CH	10.15, s		2', 6', 7'	1', 6'
OH-3		4.14, br.s	3		
OH-3'		12.93, br.s		2', 3', 4'	

[a] Indiscernible signals owing to overlapping or having complex multiplicity are reported without designating multiplicity.

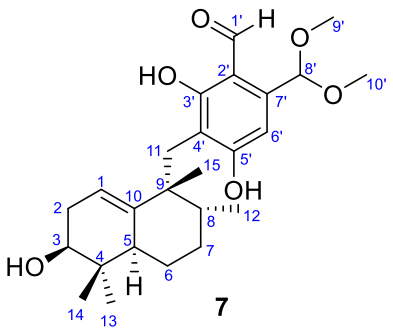

7

Table S7 NMR assignments for **7** in DMSO-d_6 (400 MHz for ^{1}H; 100 MHz for ^{13}C).

position	δ_C, type	δ_H[a] (J in Hz)	^{1}H–^{1}H COSY	HMBC[b]	ROESY
1	116.5, CH	4.86	2a, 2b, 5	3, 5, 9	15
2	31.7, CH_2	1.70, Ha	1, 2b, 3	1, 3, 4, 10	14
		1.68, Hb	1, 2a, 3	1, 3, 4, 10	
3	71.5, CH	3.33	2a, 2b, OH-3	4	5, 13
4	36.9, C				
5	43.8, CH	2.44, br.d (12.1)	1, 6a, 6b	4, 6, 10	3, 7b, 11a, 13
6	26.5, CH_2	1.78, Ha	6b, 7a, 7b	5, 10	
		1.09, Hb	6a, 7a, 7b	5	14
7	30.4, CH_2	1.53, Ha	6a, 6b, 7b, 8	8	
		1.51, Hb	6a, 6b, 7a, 8	6, 8	5, 11a, 11b, 12
8	42.8, CH	1.30	7a, 7b, 12	7, 9, 12	15
9	43.8, C				
10	142.8, C				
11	23.5, CH_2	2.67, d (12.8), Ha	11b	9, 10, 15, 3', 4', 5'	5, 7b, 12
		2.50, d (12.8), Hb	11a	9, 10, 15, 3', 4', 5'	7b, 12
12	17.2, CH_3	1.03, d (6.7)	8	7, 8, 9, 15	7b, 11a, 11b
13	25.1, CH_3	0.93, s		3, 4, 5, 14	3, 5
14	14.7, CH_3	0.58, s		3, 4, 5, 13	2a, 6b
15	23.2, CH_3	0.92, s		8, 9, 10, 11, 12	1, 8
1'	194.1, CH	10.05, s		2', 3', 7'	
2'	109.6, C				
3'	165.0, C				
4'	112.9, C				
5'	163.9, C				
6'	107.3, CH	6.62, s		2', 4', 5', 8'	8'
7'	140.2, C				
8'	101.3, CH	5.68, s		2', 6', 7', 9', 10'	3, 9', 10'
9'	53.2, CH_3	3.28, s		8'	8'
10'	53.3, CH_3	3.27, s		8'	8'
OH-3		4.13, br.s	3		
OH-3'		12.88, s		2', 3', 4'	
OH-5'		10.68, br.s			

[a] Indiscernible signals owing to overlapping or having complex multiplicity are reported without designating multiplicity.

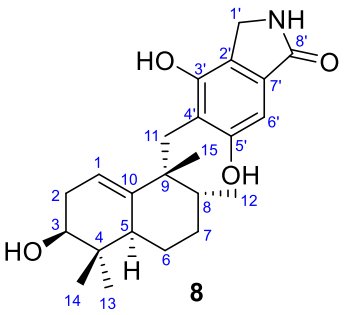

8

Table S8 NMR assignments for **8**.

position	δ_C[a], type	δ_H[a,c] (*J* in Hz)	^{1}H–^{1}H COSY[b]	HMBC[b]	ROESY[b]
1	116.2,	4.82	2a, 2b, 5	3, 5, 9	15
2	31.7, CH_2	1.73, Ha	1, 2b, 3	1, 10	14
		1.69, Hb	1, 2a, 3	1, 10	
3	71.3, CH	3.39	2a, 2b, OH-3	4	5, 13
4	36.9, C				
5	43.7, CH	2.50	1, 6a, 6b	4, 6, 10	3, 7b, 11a, 13
6	26.7, CH_2	1.79, Ha	5, 6b	10	
		1.10, Hb	5, 6a, 7a, 7b	10	8, 14
7	30.4, CH_2	1.54, Ha	6b, 7b, 8	8	
		1.52, Hb	6b, 7a, 8	8	5, 11a, 11b, 12
8	43.1, CH	1.29	7a, 7b, 12	15	6b, 15
9	43.9, C				
10	143.1, C				
11	24.8, CH_2	2.73, d (12.5), Ha	11b	9, 10, 15, 3', 4', 5'	5a, 7b, 12
		2.60, d (12.5), Hb	11a	9, 10, 15, 3', 4', 5'	7b, 12
12	17.3, CH_3	1.05, d (6.7)	8	7, 8, 9	7b, 11a, 11b
13	25.1, CH_3	0.95, s		3, 4, 5, 14	3, 5
14	14.8, CH_3	0.59, s		3, 4, 5, 13	2a, 6b
15	23.1, CH_3	0.95, s		8, 9, 10, 11, 12	1, 8
1'	43.0, CH_2	4.15, br.d (16.9), Ha	1'b, NH	2', 3', 7', 8'	
		4.05, br.d (16.9), Hb	1'a, NH	2', 3', 7', 8'	
2'	120.3, C				
3'	151.7, C				
4'	117.4, C				
5'	157.7, C				
6'	99.6, CH	6.56, s		2', 4', 5', 8'	OH-5'
7'	131.0, C				
8'	170.6, C				
OH-3		4.06, d (5.2)	3		
OH-3'		8.88, s			
OH-5'		9.23, s		4', 5'	6'
NH		8.24, br.s	1'a, 1'b	1', 2', 7', 8'	

[a] The data recorded in DMSO-d_6 (^{1}H NMR for 300 MHz, ^{13}C NMR for 75 MHz)

[b] The data recorded in DMSO-d_6 (^{1}H NMR for 400 MHz, ^{13}C NMR for 100 MHz)

[c] Indiscernible signals owing to overlapping or having complex multiplicity are reported without designating multiplicity.

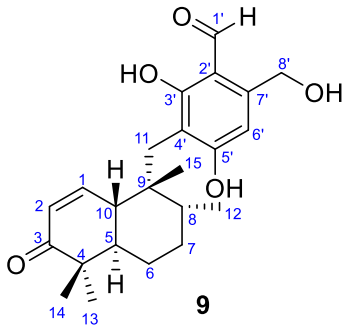

9

Table S9 NMR assignments for **9**.

position	δ_C[a], type	δ_H[a,c] (*J* in Hz)	^{1}H–^{1}H COSY[b]	HMBC[b]	ROESY[b]
1	148.9, CH	6.79, br.d (10.5)	2, 5, 10	2, 3, 5, 9, 10	15
2	127.8, CH	5.78, dd (10.5, 3.2)	1, 10	4, 10	13
3	204.1, C				
4	45.2, C				
5	42.7, CH	2.63	1, 6a, 6b, 10	1, 4, 6, 10	7b, 13
6	22.9, CH_2	1.62, Ha	5, 6b	5, 7, 8	10
		1.06, Hb	5, 6a, 7a, 7b	5, 7	
7	29.5, CH_2	1.43, Ha	6b, 7b, 8	6, 8	
		1.35, Hb	6b, 7a, 8	5, 6, 8, 12	5, 11a, 11b
8	39.6, CH	1.30	7a, 7b, 12	7, 12	10, 15
9	40.6, C				
10	43.1, CH	2.84	1, 2, 5	1, 2, 5, 9, 15	6a, 8, 14, 15
11	21.8, CH_2	2.71, d (13.5), Ha	11b	8, 9, 10, 15, 3', 4', 5'	7b
		2.63, d (13.5), Hb	11a	8, 9, 10, 15, 3', 4', 5'	7b, 12
12	15.8, CH_3	0.93, d (6.3)	8	7, 8, 9	11b
13	24.3, CH_3	1.08, s		3, 4, 5, 14	2, 5
14	22.1, CH_3	0.99, s		3, 4, 5, 13	10
15	23.1, CH_3	0.97, s		8, 9, 10, 11, 12	1, 8, 10
1'	193.8, CH	9.99, s		2', 3'	
2'	110.5, C				
3'	164.6, C				
4'	111.3, C				
5'	164.5, C				
6'	107.6, CH	6.59, s	8'	2', 4', 5', 8'	
7'	146.0, C				
8'	59.8, CH_2	4.73, s	6'	2', 6', 7'	
OH-3'		13.03, s		2', 3', 4'	
OH-8'		5.39, br.s			

[a] The data recorded in DMSO-d_6 (^{1}H NMR for 300 MHz, ^{13}C NMR for 75 MHz)

[b] The data recorded in DMSO-d_6 (^{1}H NMR for 400 MHz, ^{13}C NMR for 100 MHz)

[c] Indiscernible signals owing to overlapping or having complex multiplicity are reported without designating multiplicity.

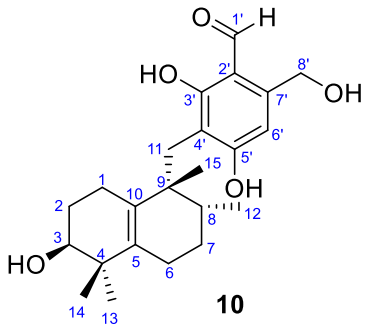

10

Table S10 NMR assignments for **10**.

position	δ_C[a], type	δ_H[a,c] (*J* in Hz)	$^1H–^1H$ COSY[b]	HMBC[b]	NOESY[b]
1	23.0, CH_2	1.89, Ha	1b	2, 10	
		1.34, Hb	1a, 2b	10	
2	26.4, CH_2	1.37, Ha	2b, 3	1, 3, 4, 10	13
		1.24, Hb	1b, 2a, 3	1, 3, 4, 10	
3	73.0, CH	3.17, dd (4.7, 1.8)	2a, 2b, OH-3	1, 2, 4, 5	13, 14
4	38.7, C				
5	131.4, C				
6	24.6, CH_2	1.99, Ha	6b, 7a, 7b	4, 5, 7, 10	8, 14
		1.93, Hb	6a, 7a, 7b	4, 5, 7, 10	13
7	26.7, CH_2	1.75, Ha	6a, 6b, 7b, 8	8, 12	11a, 11b, 12
		1.50, Hb	6a, 6b, 7a	12	12, 13
8	39.9, CH	1.40	7a, 12	7, 9, 12, 15	6a, 15
9	41.4, C				
10	132.7, C				
11	26.9, CH_2	2.64, d (12.8), Ha	11b	9, 10, 15, 3', 4', 5'	7a, 12
		2.42, d (12.8), Hb	11a	9, 10, 15, 3', 4', 5'	7a, 12
12	16.8, CH_3	0.99, d (6.8)	8	7, 8, 9, 15	7b, 11a, 11b
13	26.9, CH_3	0.90, s		3, 4, 5, 14	2a, 3, 6b, 7b
14	22.7, CH_3	0.87, s		3, 4, 5, 13	3, 6a
15	23.7, CH_3	1.03, s		8, 9, 10, 11, 12	8
1'	193.2,	9.96, s		2', 3', 7'	8'
2'	110.2, C				
3'	164.4, C				
4'	112.6, C				
5'	164.4, C				
6'	107.5,	6.51, s	8'	2', 4', 5', 8'	
7'	145.4, C				
8'	59.8, CH_2	4.71, s	6'	2', 6', 7'	1'
OH-3		4.04, br.s	3		
OH-3'		12.76, s		2', 3', 4'	
OH-8'		5.35, br.s		8'	

[a] The data recorded in DMSO-d_6 (^1H NMR for 300 MHz, ^{13}C NMR for 75 MHz)

[b] The data recorded in DMSO-d_6 (^1H NMR for 600 MHz, ^{13}C NMR for 150 MHz)

[c] Indiscernible signals owing to overlapping or having complex multiplicity are reported without designating multiplicity.

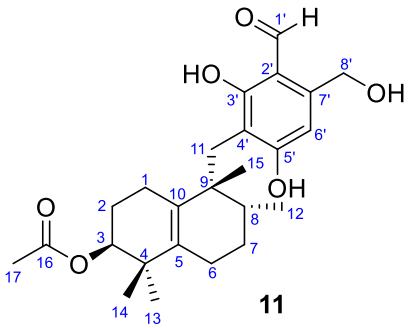

11

Table S11 NMR assignments for **11**.

position	δ_C[a], type	δ_H[a,d] (*J* in Hz)	^{1}H–^{1}H COSY[b]	HMBC[c]	NOESY[c]
1	22.5,	1.75, Ha	1b	2, 9, 5, 10	
		1.40, Hb	1a, 2b	2, 9, 5, 10	
2	23.1,	1.38, Ha	2b	1, 3, 4, 10	13
		1.23, Hb	1b, 2a, 3	1, 3, 10	
3	76.4, CH	4.53	2b	1, 2, 4, 5, 16	13, 14
4	37.3, C				
5	130.5, C				
6	24.8,	1.98, Ha	6b, 7a, 7b	4, 5, 10	8, 14
		1.78, Hb	6a, 7a, 7b	5, 10	13
7	26.7,	1.55, Ha	6a, 6b, 7b	8, 12	11a, 11b, 12
		1.48, Hb	6a, 6b, 7a, 8	12	12, 13
8	40.1, CH	1.43	7b, 12	7, 12, 15	6a, 15
9	41.5, C				
10	133.2, C				
11	27.1,	2.63, d (12.8), Ha	11b	9, 10, 15, 3', 4', 5'	7a, 12
		2.44, d (12.8), Hb	11a	9, 10, 15, 3', 4', 5'	7a, 12
12	16.8,	1.01, d (6.7)	8	7, 8, 9	7b, 11a, 11b
13	26.9,	0.97, s		3, 4, 5, 14	2a, 3
14	22.7,	0.86, s		3, 4, 5, 13	3, 6a
15	23.6,	1.05, s		8, 9, 10, 11, 12	8
16	170.1, C				
17	21.0,	1.93, s		16	
1'	193.2,	9.94, s		2', 3'	
2'	110.1, C				
3'	165.2, C				
4'	112.4, C				
5'	164.4, C				
6'	107.7,	6.52, s	8'	2', 4', 5', 8'	
7'	145.5, C				
8'	59.9,	4.70, s	6'	2', 6', 7'	
OH-3'		12.82, br.s			

[a] The data recorded in DMSO-d_6 (^{1}H NMR for 300 MHz, ^{13}C NMR for 75 MHz)

[b] The data recorded in DMSO-d_6 (^{1}H NMR for 400 MHz, ^{13}C NMR for 100 MHz)

[c] The data recorded in DMSO-d_6 (^{1}H NMR for 600 MHz, ^{13}C NMR for 150 MHz)

[d] Indiscernible signals owing to overlapping or having complex multiplicity are reported without designating multiplicity.

4. Alkaline hydrolysis of compounds 2, 4, and 5

4.1. Alkaline hydrolysis of 2

Compound **2** (1 mg) was dissolved in 2% CH_3ONa/CH_3OH (3 mL), and the mixture was stirred at 50 °C for 12 h. HCOOH (10%) was used for neutralizing, and the resulting solution was extracted with EtOAc. Following extraction, the EtOAc layer was collected and evaporated completely. CH_3OH was used to dissolve the resulting residue. The obtained mixture was purified by means of semi-preparative RP-HPLC with CH_3OH/H_2O (75:25, v/v) at a flow rate of 3 mL/min, and compound **2a** (0.8 mg) was obtained as the final product. Compounds **2a** and **3** were identical on the basis of the same ^{1}H NMR data and HPLC profiles (Fig. S5 and S6).

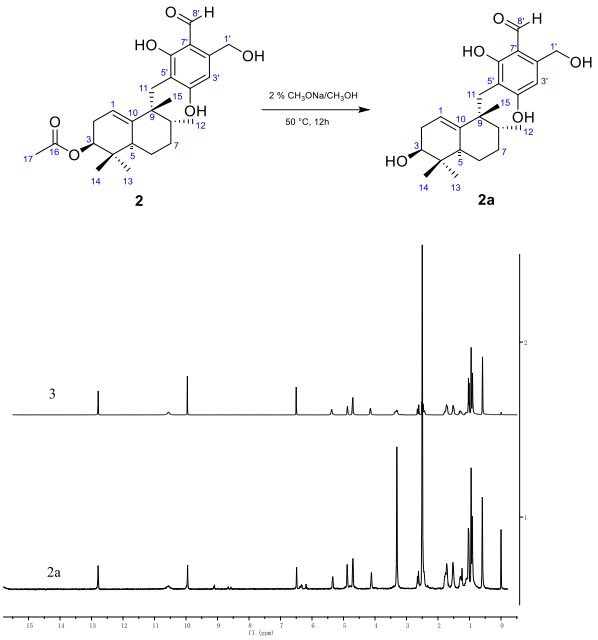

Figure S5 Compounds **2a** and **3** were compared by analyzing the ^{1}H NMR profiles (400 MHz, in DMSO-d_6).

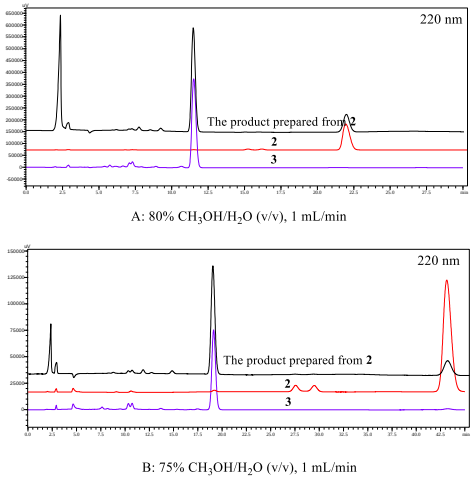

Figure S6 Compounds **2** and **3**, and the product prepared from **2** were compared by analyzing the HPLC profiles (Phenomenex 5μ-C18, 4.6 × 250 mm).

4.2. Alkaline hydrolysis of 4

Compound **4** (1 mg) was dissolved in 2% CH_3ONa/CH_3OH (3 mL), and the resulting mixture was stirred at 50 °C for 12 h. HCOOH (10%) was used for neutralization. The resulting mixture was extracted with EtOAc, and the EtOAc layer was collected and evaporated. The obtained residue was dissolved in CH_3OH, and the mixture was purified by semi-preparative RP-HPLC with CH_3OH/H_2O (75:25, v/v) at a flow rate of 3 mL/min. Compound **4a** (0.8 mg) was finally obtained. Compounds **4a** and **3** were identical based on the same ^{1}H NMR data and HPLC profiles (Fig. S7 and S8).

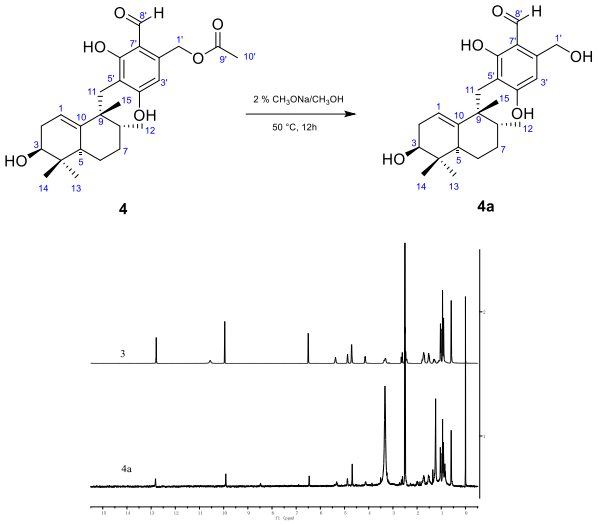

Figure S7 Compounds **4a** and **3** were compared by analyzing the ^{1}H NMR profiles (400 MHz, in DMSO-d_6).

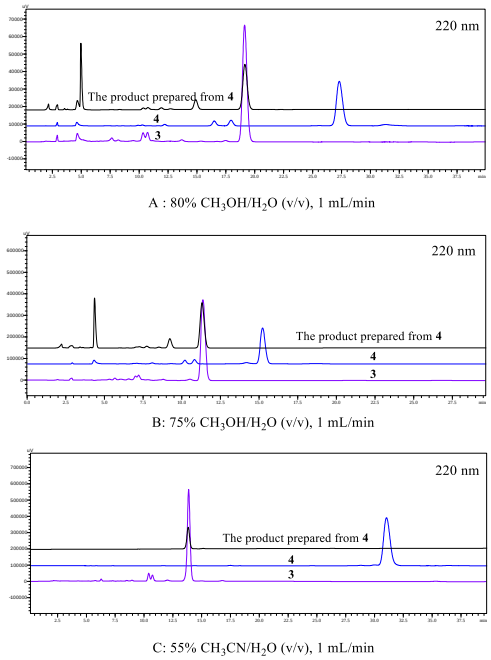

Figure S8 Compounds **3** and **4**, and the product prepared from **4** were compared by analyzing the HPLC profiles (Phenomenex 5μ-C18, 4.6 × 250 mm).

4.3. Alkaline hydrolysis of 5

Compound **5** (1 mg) dissolved in 2% CH_3ONa/CH_3OH (3 mL). The resulting mixture was subjected to stirring at 50 °C for 12 h. HCOOH was used for sample neutralization. The obtained solution was extracted with EtOAc, and the EtOAc layer collected. Subsequently, the collected organic layer was evaporated, and the obtained residue was dissolved in CH_3 OH. The mixture was purified by semi-preparative RP-HPLC with CH_3OH/H_2O (75:25, v/v) at flow rate of 3 mL/min. Finally, compound **5a** (0.7 mg) was obtained. Compounds **5a** and **3** were identical as per the same ^{1}H NMR data and HPLC profiles (Fig. S9 and S10).

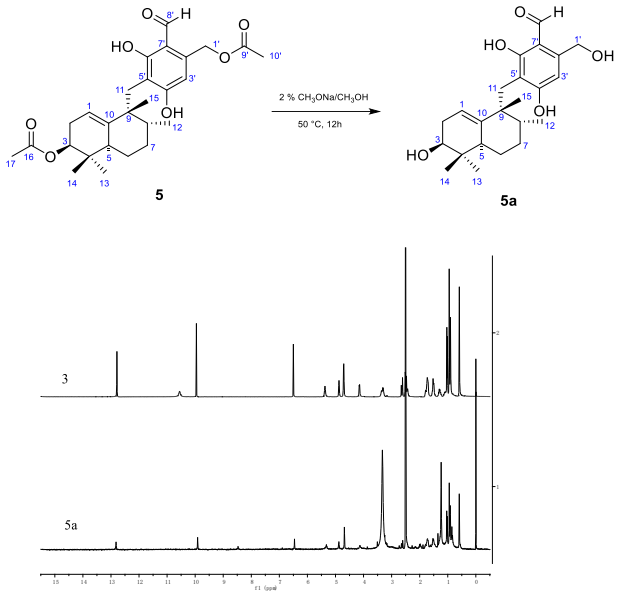

Figure S9 Compounds **5a** and **3** were compared by analyzing the ^{1}H NMR profiles (400 MHz, in DMSO-d_6).

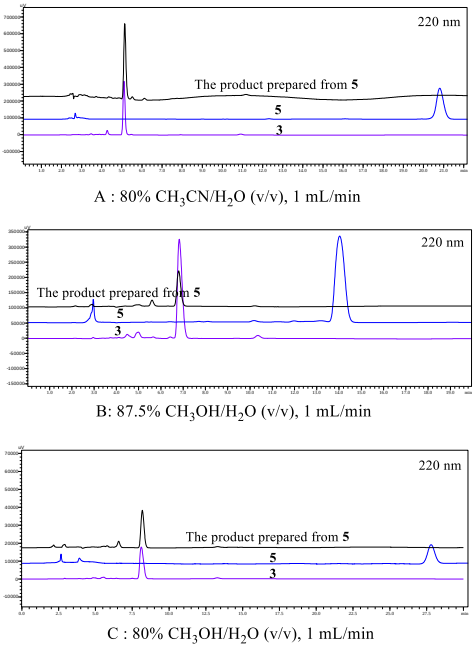

Figure S10 The samples of **3** and **5**, and the product prepared from **5** were compared by analyzing the HPLC profiles (Phenomenex 5μ-C18, 4.6 × 250 mm).

5. Quantum chemical ECD calculations of compounds 9 and 10

5.1. Quantum chemical ECD calculation of 9

SMILES codes were generated by converting the molecules of (5*S*,8*S*,9*S*,10*R*)-**9** and (5*R*,8*R*,9*R*,10*S*)-**9**. Following this, CORINA version 3.4 was used to generate the initial 3D structures. Conformer databases were generated in CONFLEX version 7.0 using the MMFF94s force-field, with an energy window for acceptable conformers (ewindow) of 5 kcal mol^{-1} higher than that of the ground state, a maximum number of conformations per molecule (maxconfs) of 100, and an RMSD cutoff (rmsd) of 0.5Å. Each conformer of the acceptable conformers was subsequently optimized in Gaussian09 using the HF/6-31G(d) technique. The dihedral angles were obtained when the structures were further optimized at the APFD/6-31G(d) level. After that, the eleven lowest energy conformers were identified. ECD calculations of the optimized conformers were conducted using Gaussian09 [APFD/6-311++G(2d,p)]. The polarizable-conductor calculation model (IEFPCM, methanol as the solvent) was used to account for the solvent effect. The experimental and calculated spectra were compared using the SpecDis software. This software was also utilized to apply a UV shift to the ECD spectra, Boltzmann weighting of the spectra, and Gaussian broadening of the excitations. Calculated ECD spectra for (5*S*,8*S*,9*S*,10*R*)-**9** and (5*R*,8*R*,9*R*,10*S*)-**9** (UV correction = 10 nm, band width σ = 0.3 eV) and experimental ECD spectrum of **9** are shown in Fig. 1D.

Table S12 Conformers distribution of (5*S*,8*S*,9*S*,10*R*)-**9** and (5*R*,8*R*,9*R*,10*S*)-**9** in solvated model calculations at the APFD/6-31G(d) level.

Conformers	Contribution %
1	37.03
2	36.71
3	6.29
4	4.47
5	4.09
6	3.66
7	1.88
8	1.67
9	1.54
10	1.48
11	1.18

5.2. Quantum chemical ECD calculations of 10

SMILES codes were generated by converting the molecules of (3*R*,8*S*,9*S*)-**10** and (3*S*,8*R*,9*R*)-**10**. Following this, CORINA version 3.4 was used to generate the initial 3D structures. Conformer databases were generated in CONFLEX version 7.0 using the MMFF94s force-field, with an energy window for acceptable conformers (ewindow) of 5 kcal mol^{-1} higher than that of the ground state, a maximum number of conformations per molecule (maxconfs) of 100, and an RMSD cutoff (rmsd) of 0.5Å. Each conformer of the acceptable conformers was subsequently optimized in Gaussian09 using the HF/6-31G(d) technique. The dihedral angles were obtained when the structures were further optimized at the APFD/6-31G(d) level. After that, the five conformers with the lowest energy were identified. ECD calculations of the optimized conformers were conducted using Gaussian09 [APFD/6-311++G(2d,p)]. The polarizable-conductor calculation model (IEFPCM, methanol as the solvent) was used to account for the solvent effect. The experimental and calculated spectra were

compared using SpecDis software. This software was also utilized to apply a UV shift to the ECD spectra, Boltzmann weighting of the spectra, and Gaussian broadening of the excitations.

Table S13 Conformers distribution of (3*R*,8*S*,9*S*)-**10** and (3*S*,8*R*,9*R*)-**10** in solvated model calculations at the APFD/6-31G(d) level.

Conformers	Contribution %
1	64.11
2	20.89
3	6.10
4	5.31
5	3.59

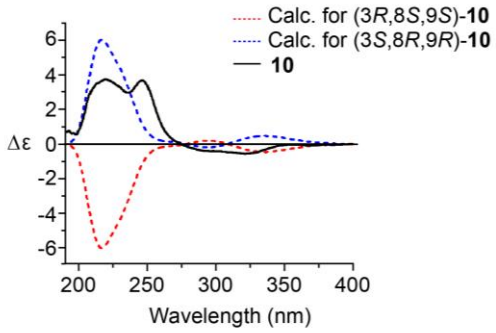

Figure S11 Calculated ECD spectra for (3*R*,8*S*,9*S*)-**10** and (3*S*,8*R*,9*R*)-**10** (UV correction = 0 nm, band width σ = 0.3 eV) and experimental ECD spectrum of **10**.

6. The 1D and 2D NMR spectra of compounds 1–11

The 1D and 2D NMR spectra of myrogramin A (**1**)

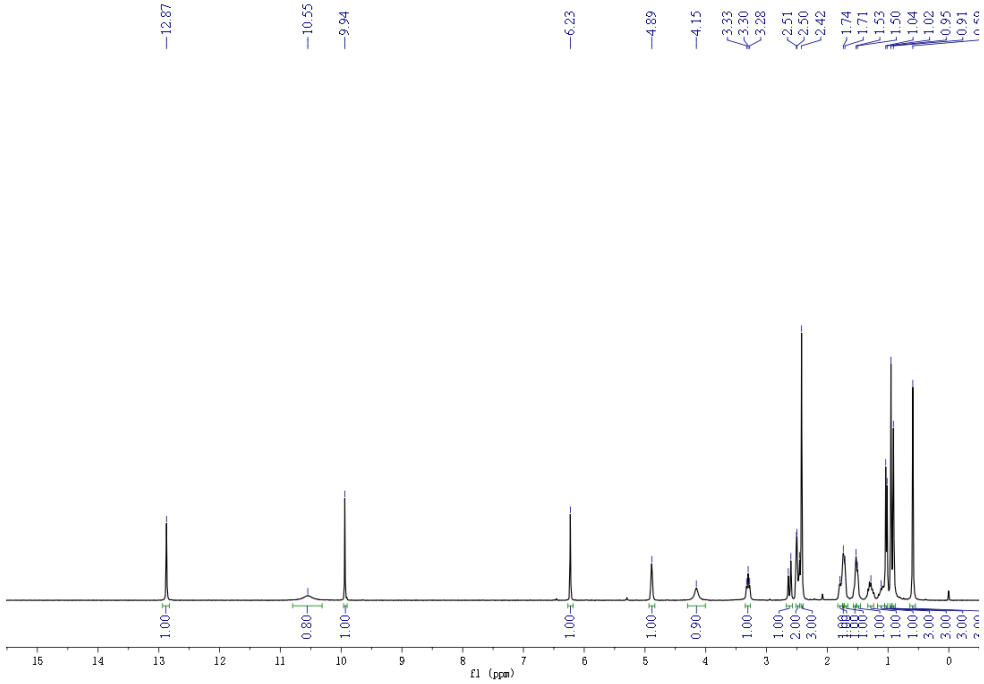

Figure S12 ^{1}H NMR (300 MHz, DMSO-d_6) spectrum for myrogramin A (**1**).

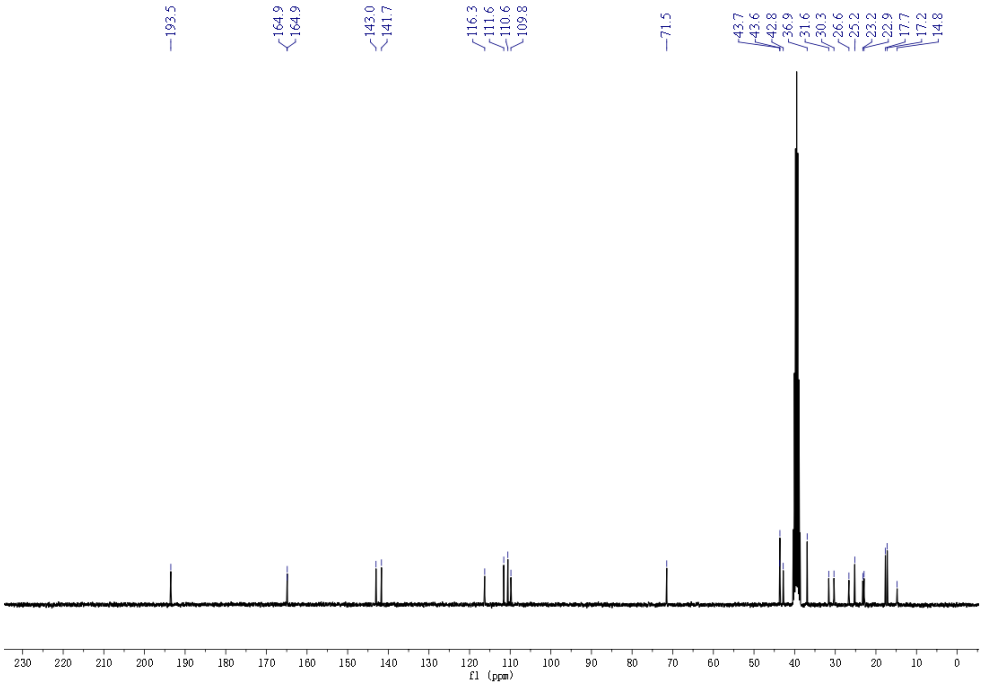

Figure S13 ^{13}C NMR (75 MHz, DMSO-d_6) spectrum for myrogramin A (**1**).

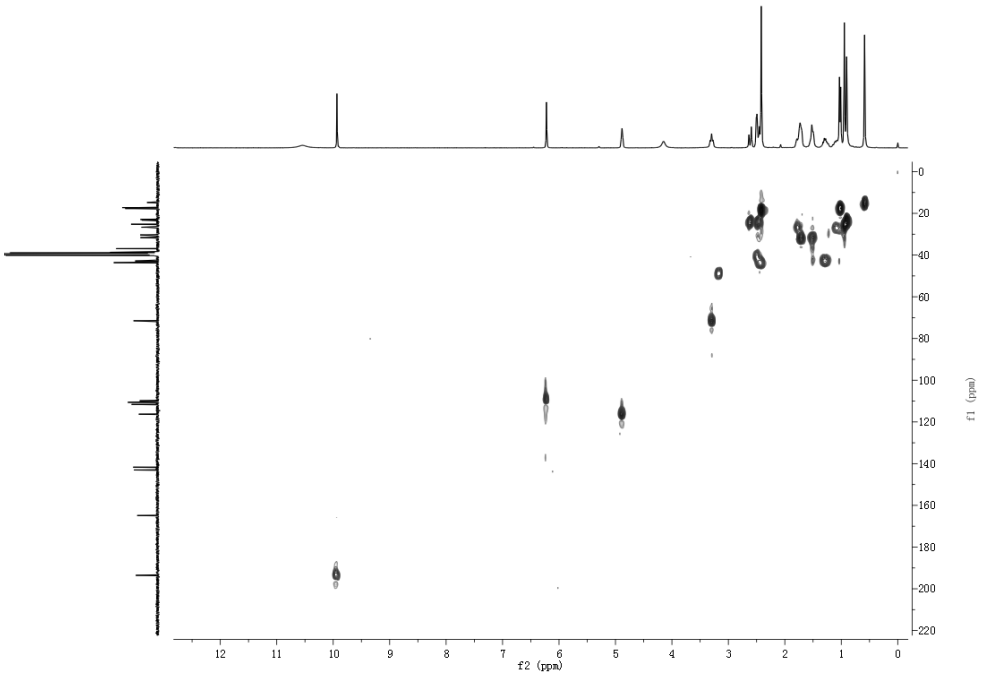

Figure S14 HSQC (400 MHz, DMSO-d_6) spectrum for myrogramin A (**1**).

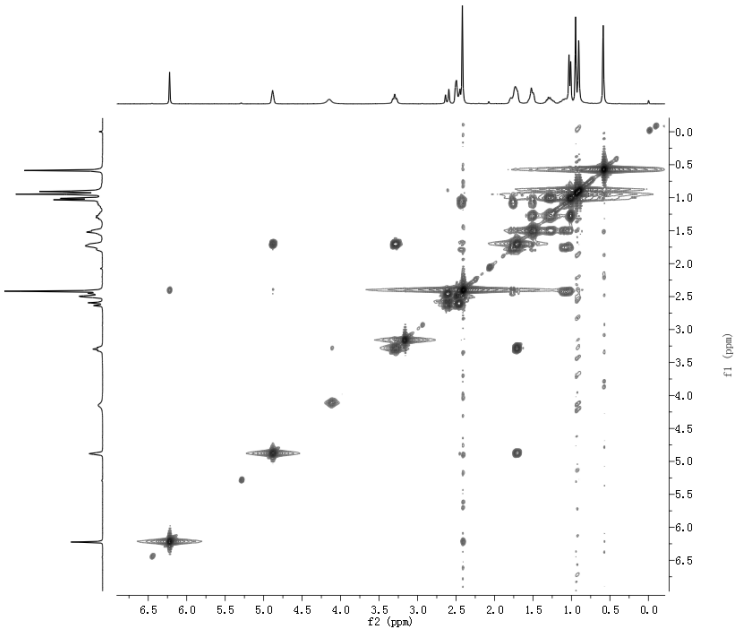

Figure S15 ^{1}H-^{1}H COSY (400 MHz, DMSO-d_6) spectrum for myrogramin A (**1**).

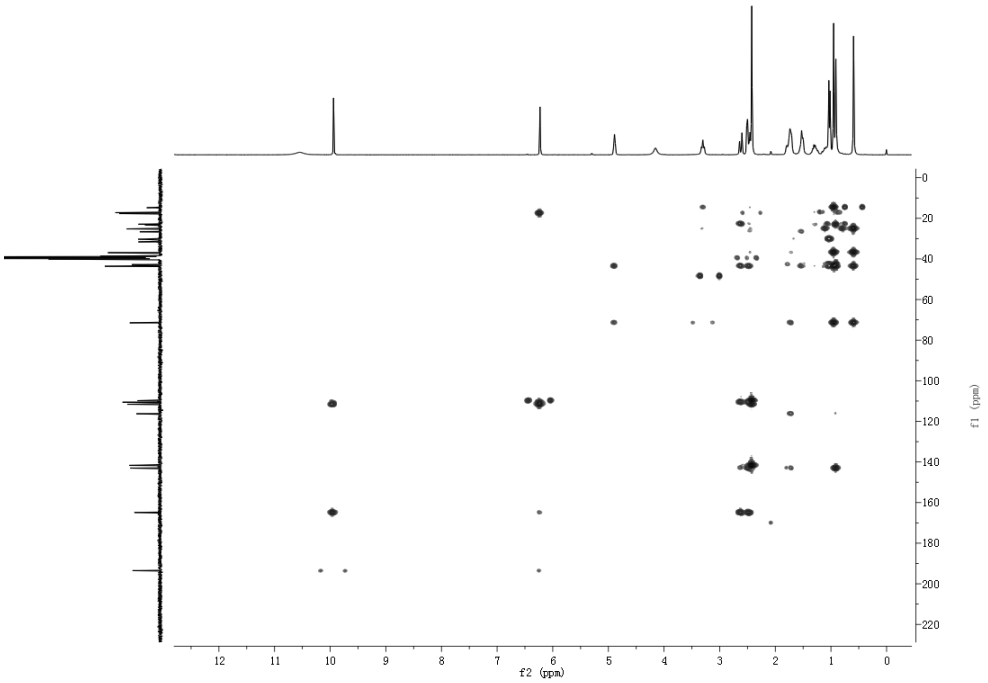

Figure S16 HMBC (400 MHz, DMSO-d_6) spectrum for myrogramin A (**1**).

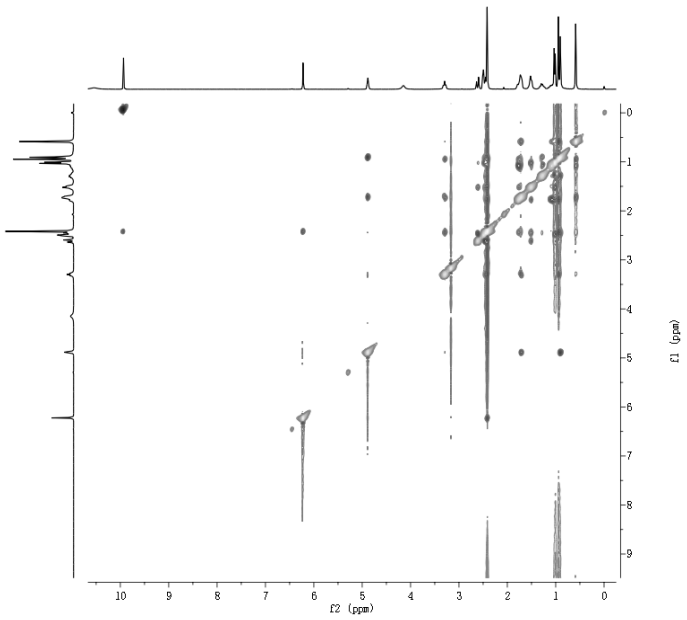

Figure S17 ROESY (400 MHz, DMSO-d_6) spectrum for myrogramin A (**1**).

The 1D and 2D NMR spectra of myrothecisin C (**2**)

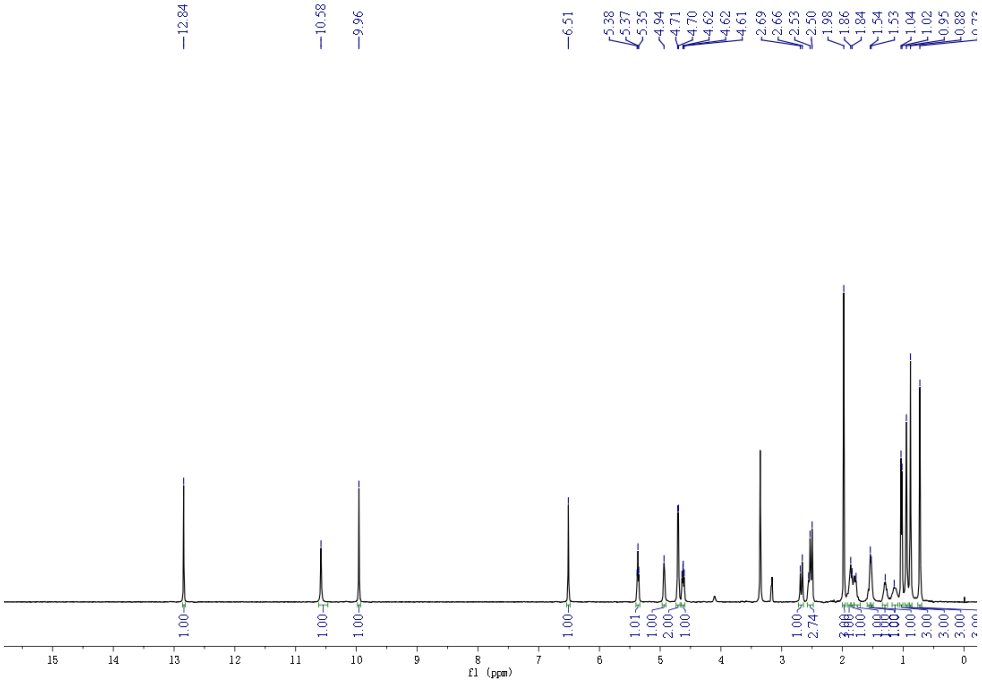

Figure S18 ^{1}H NMR (400 MHz, DMSO-d_6) spectrum for myrothecisin C (**2**).

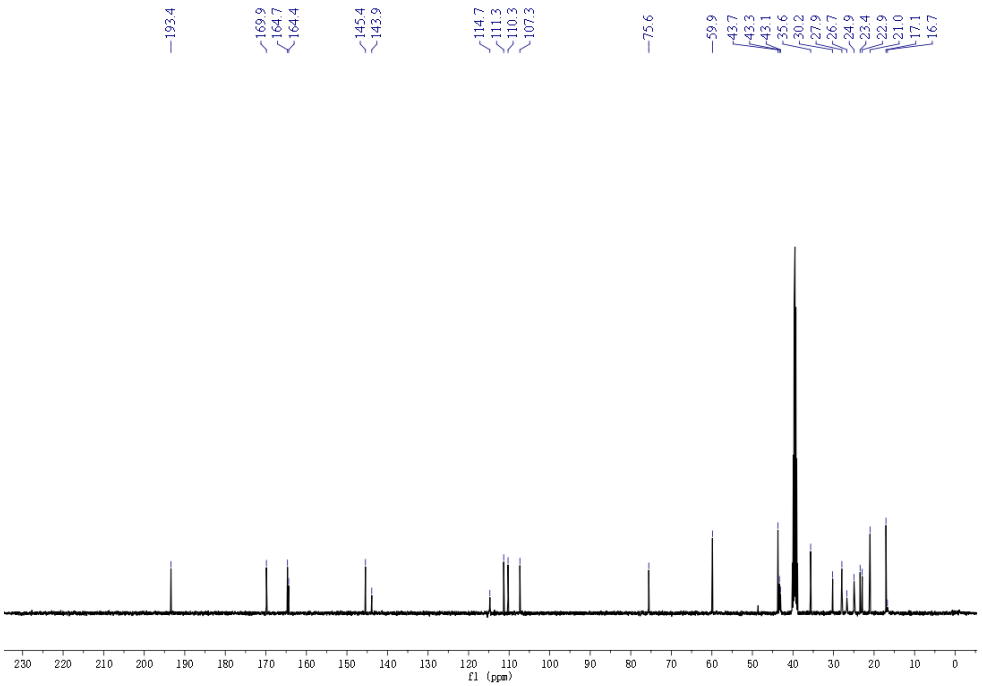

Figure S19 ^{13}C NMR (100 MHz, DMSO-d_6) spectrum for myrothecisin C (**2**).

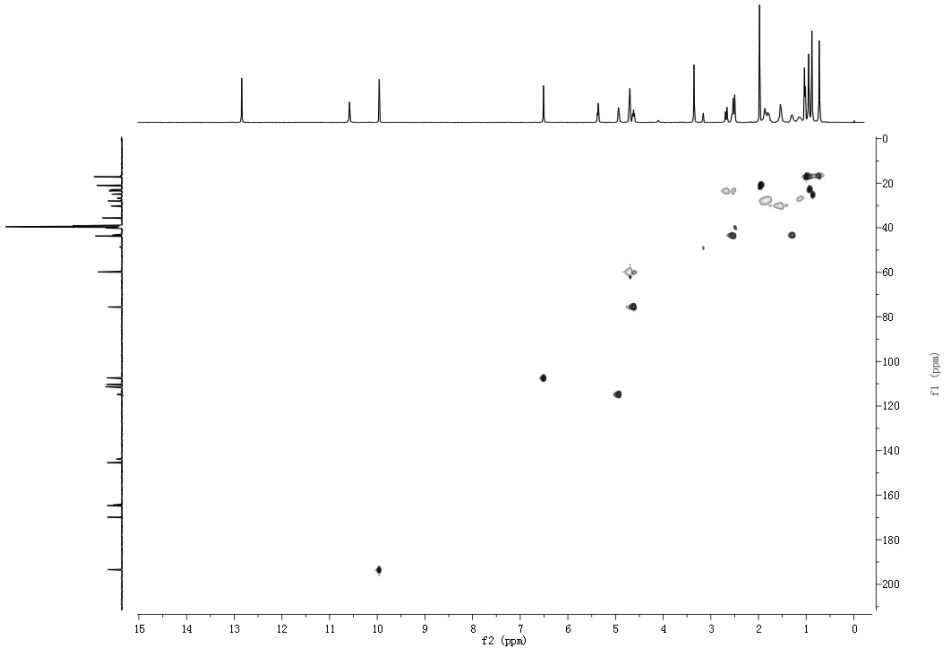

Figure S20 HSQC (300 MHz, DMSO-d_6) spectrum for myrothecisin C (**2**).

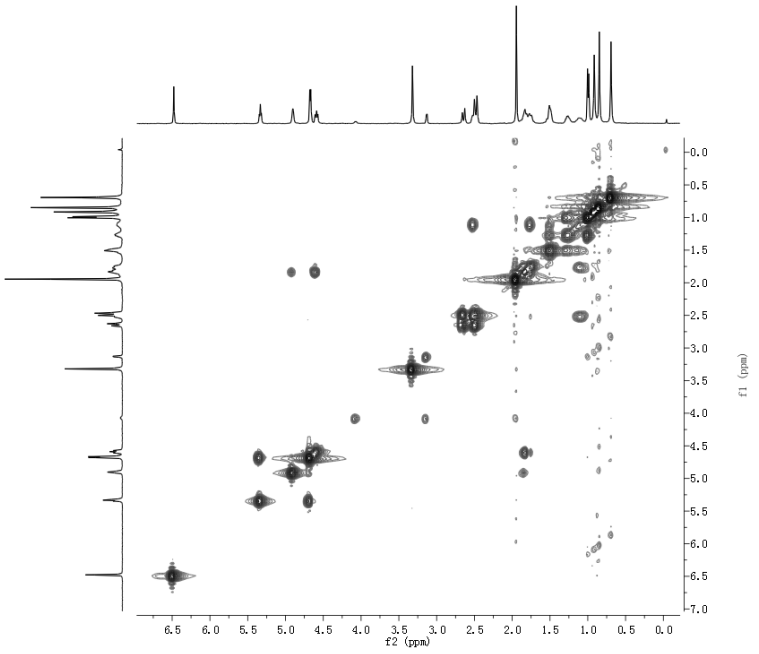

Figure S21 ^{1}H-^{1}H COSY (400 MHz, DMSO-d_6) spectrum for myrothecisin C (**2**).

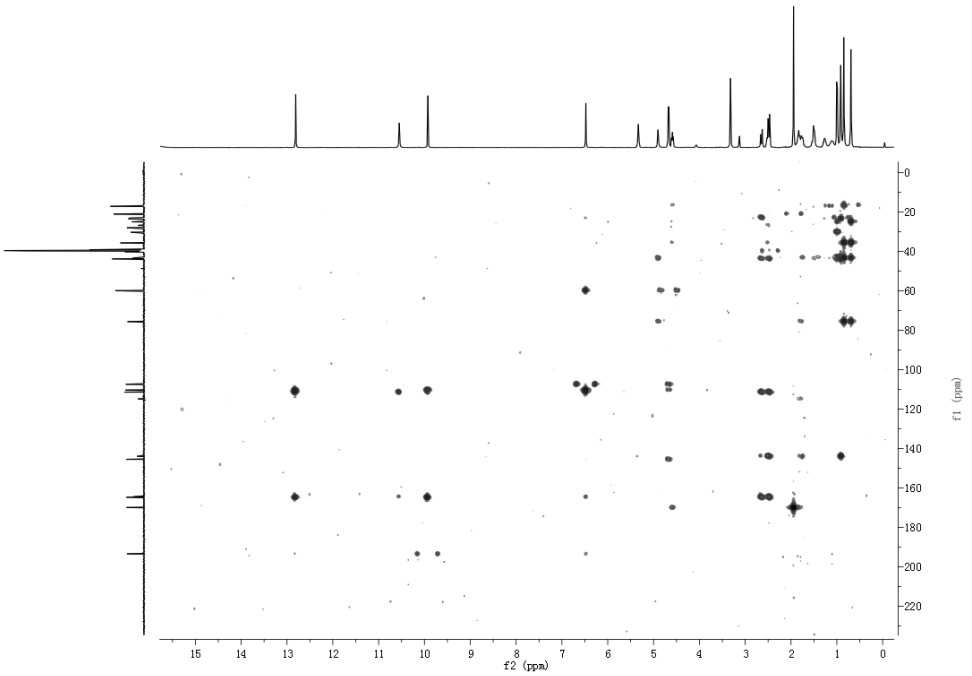

Figure S22 HMBC (400 MHz, DMSO-d_6) spectrum for myrothecisin C (**2**).

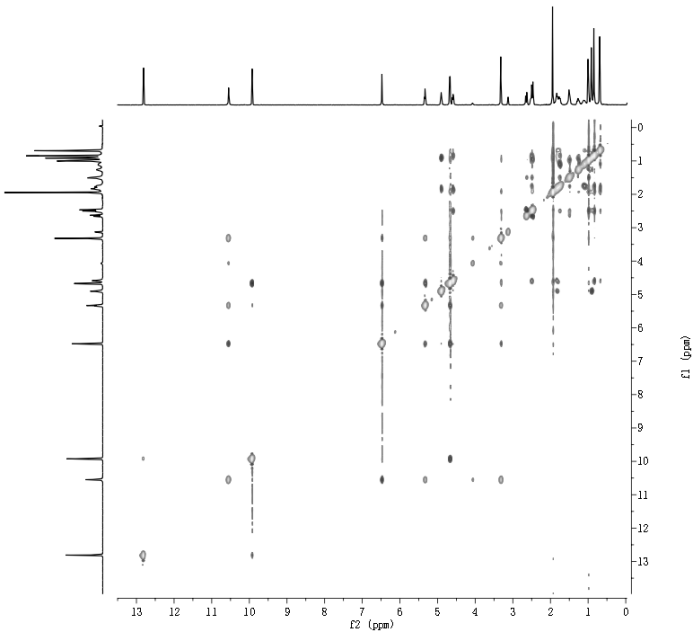

Figure S23 ROESY (400 MHz, DMSO-d_6) spectrum for myrothecisin C (**2**).

The 1D and 2D NMR spectra of myrothecisin D (**3**)

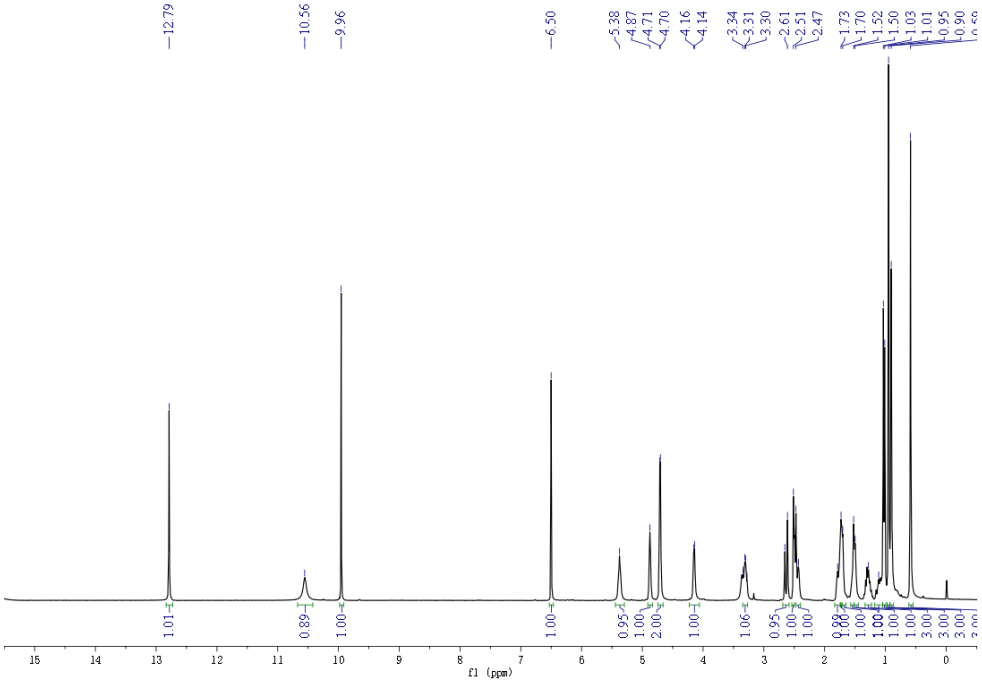

Figure S24 ^{1}H NMR (300 MHz, DMSO-d_6) spectrum for myrothecisin D (**3**).

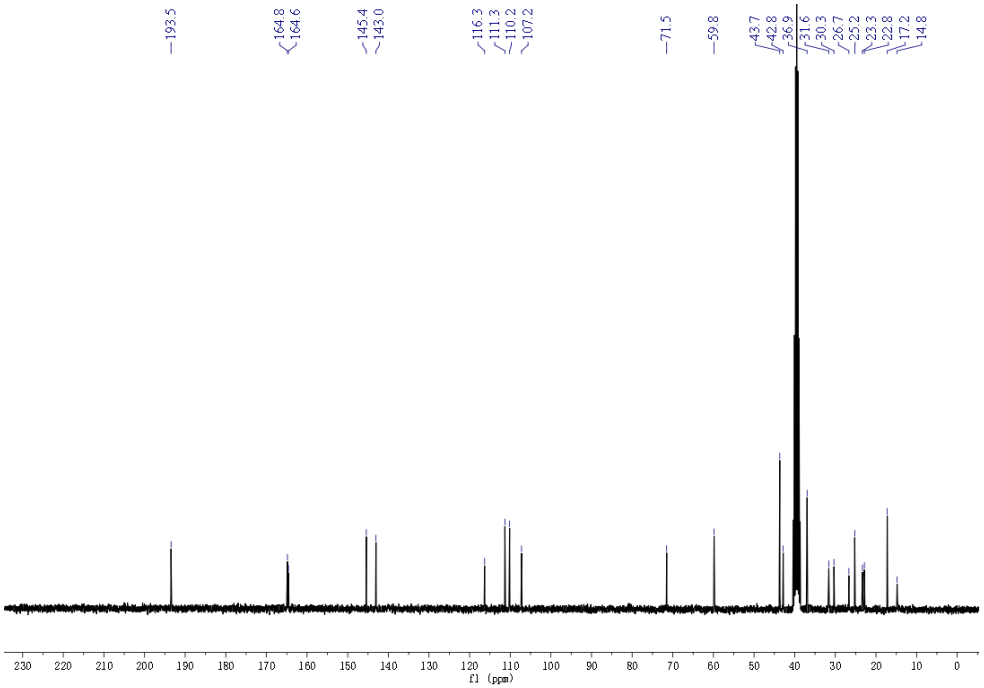

Figure S25 ^{13}C NMR (75 MHz, DMSO-d_6) spectrum for myrothecisin D (**3**).

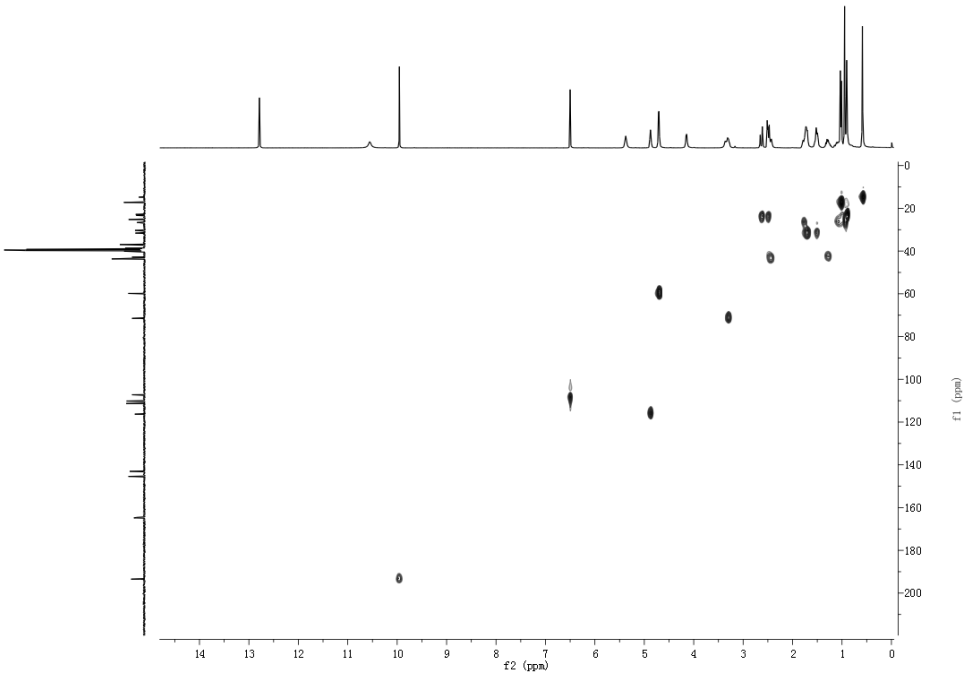

Figure S26 HSQC (400 MHz, DMSO-d_6) spectrum for myrothecisin D (**3**).

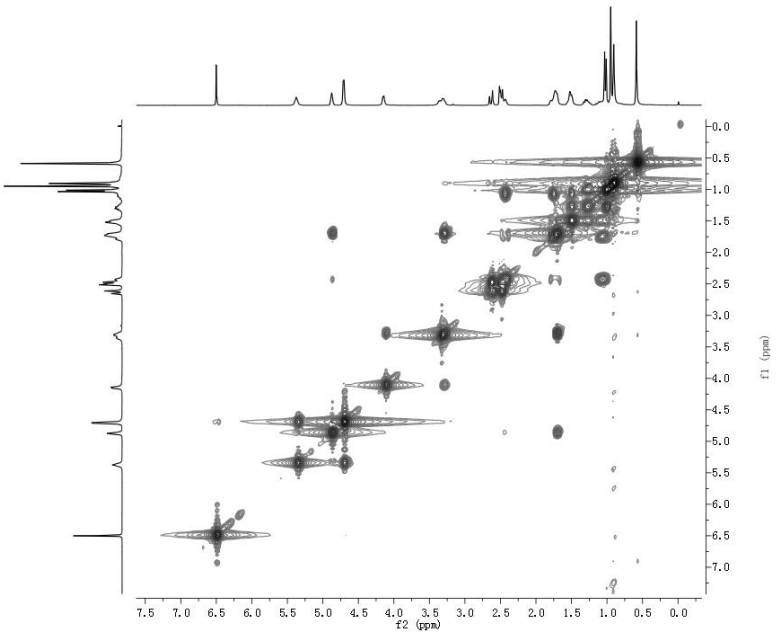

Figure S27 ^{1}H-^{1}H COSY (400 MHz, DMSO-d_6) spectrum for myrothecisin D (**3**).

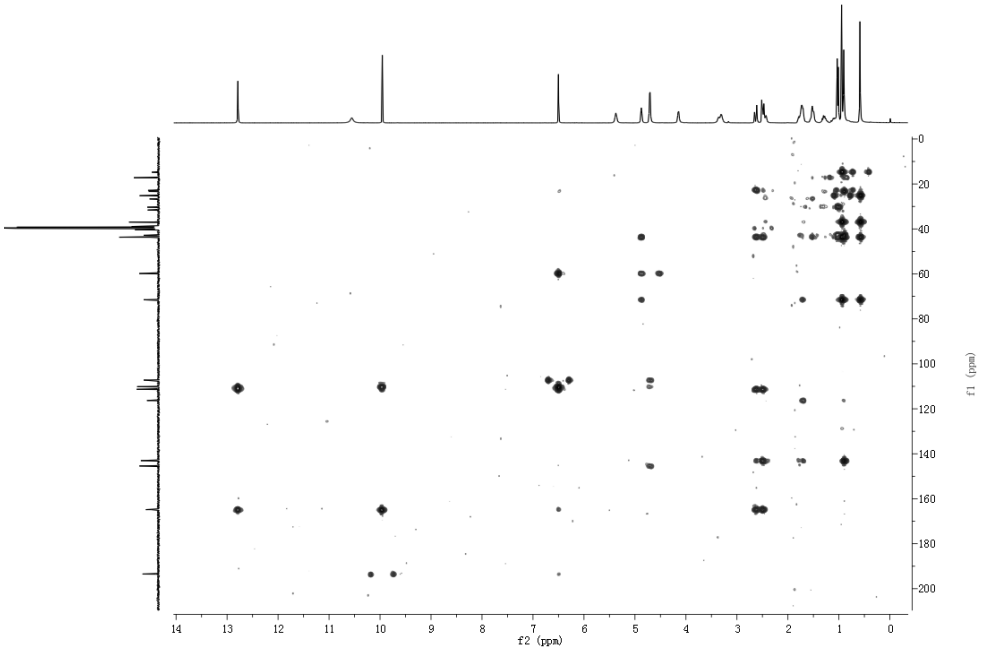

Figure S28 HMBC (400 MHz, DMSO-d_6) spectrum for myrothecisin D (**3**).

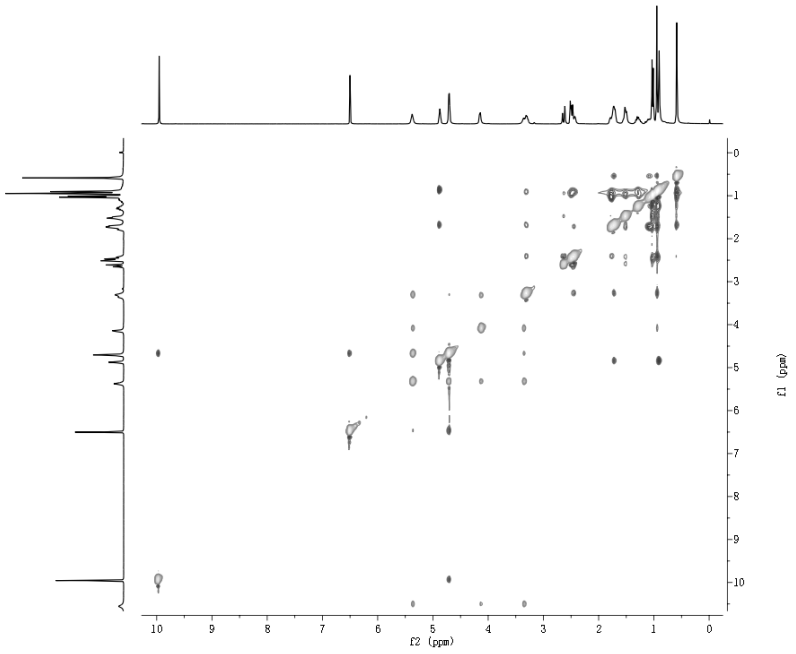

Figure S29 ROESY (400 MHz, DMSO-d_6) spectrum for myrothecisin D (**3**).

The 1D and 2D NMR spectra of myrogramin B (**4**)

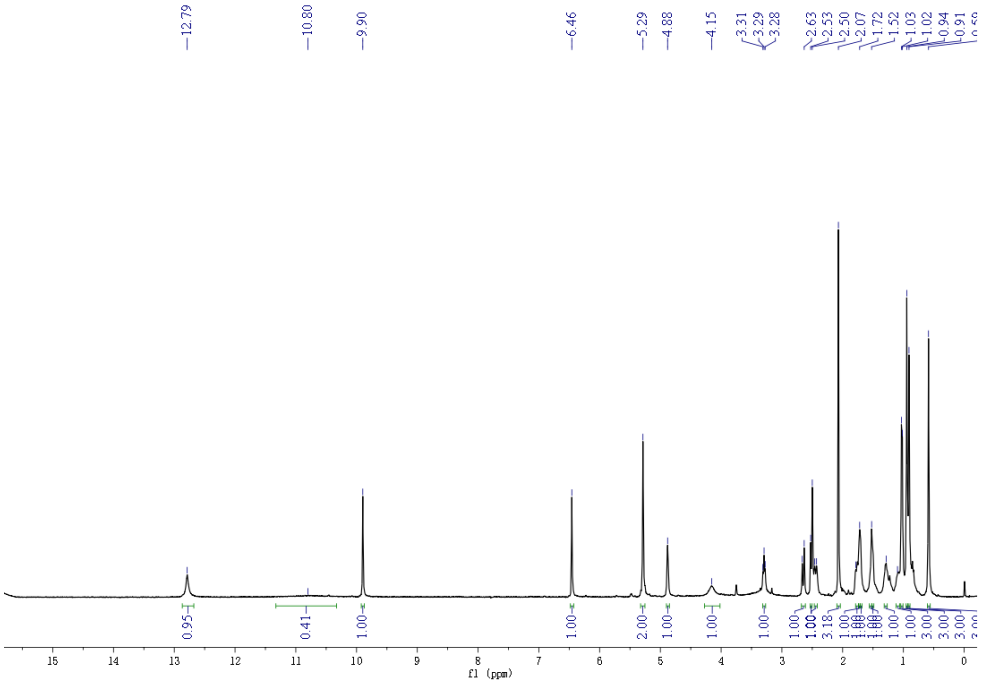

Figure S30 ^{1}H NMR (400 MHz, DMSO-d_6) spectrum for myrogramin B (**4**).

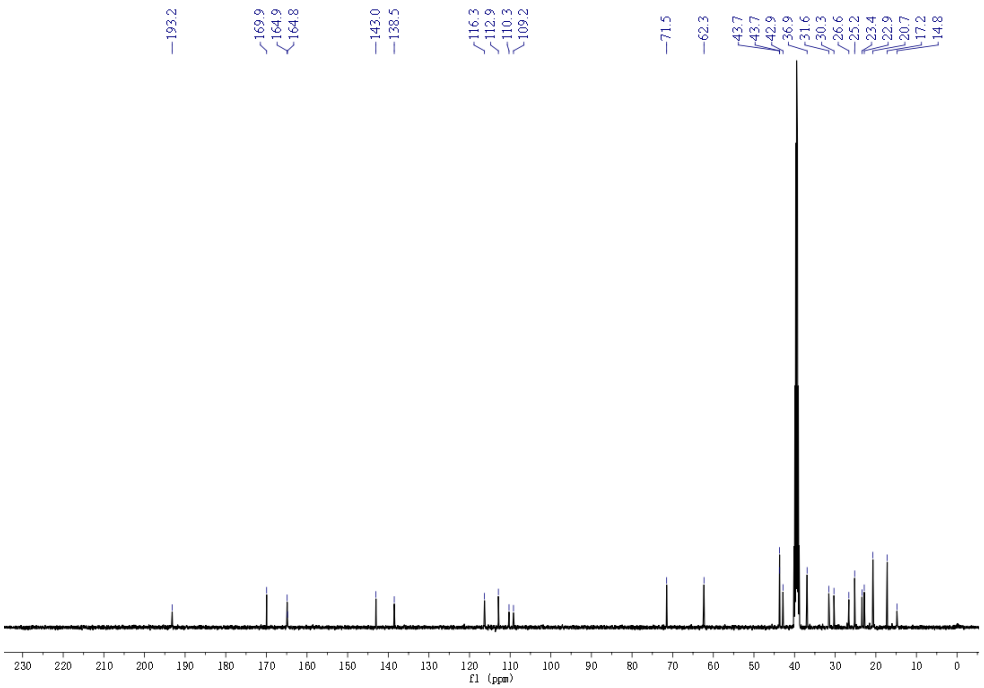

Figure S31 ^{13}C NMR (100 MHz, DMSO-d_6) spectrum for myrogramin B (**4**).

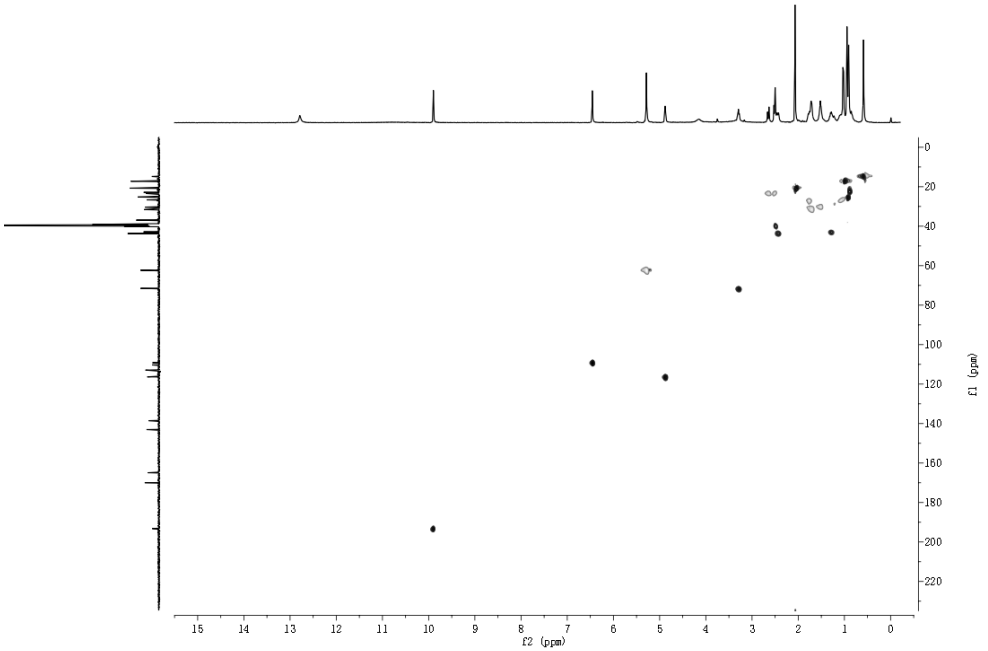

Figure S32 HSQC (300 MHz, DMSO-d_6) spectrum for myrogramin B (**4**).

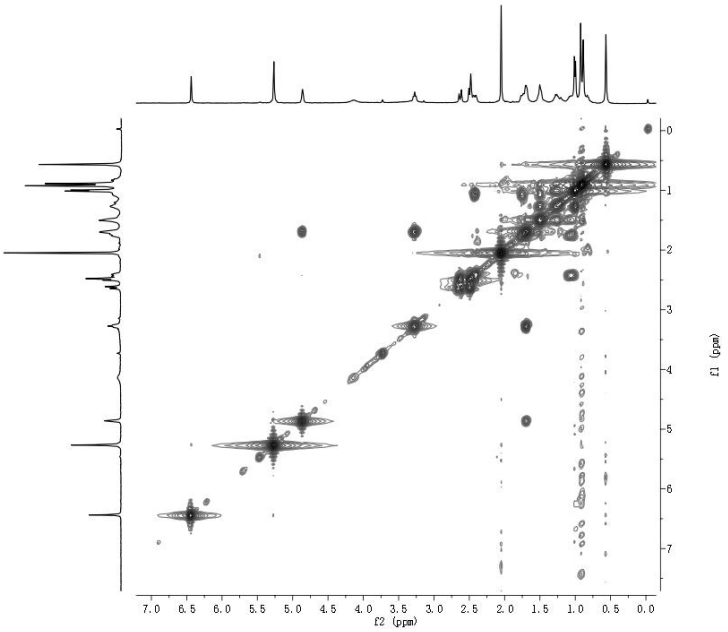

Figure S33 ^{1}H-^{1}H COSY (400 MHz, DMSO-d_6) spectrum for myrogramin B (**4**).

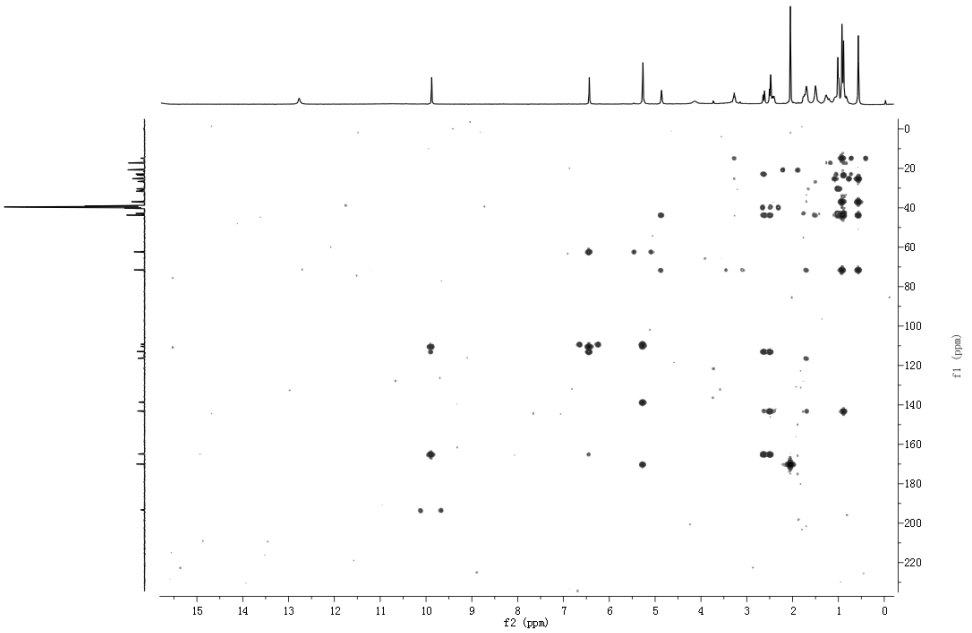

Figure S34 HMBC (400 MHz, DMSO-d_6) spectrum for myrogramin B (**4**).

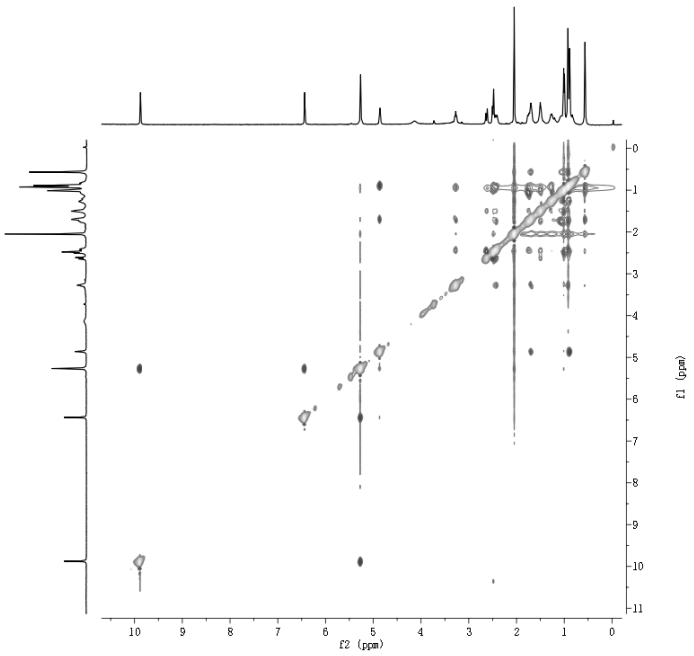

Figure S35 ROESY (400 MHz, DMSO-d_6) spectrum for myrogramin B (**4**).

The 1D and 2D NMR spectra of myrogramin C (**5**)

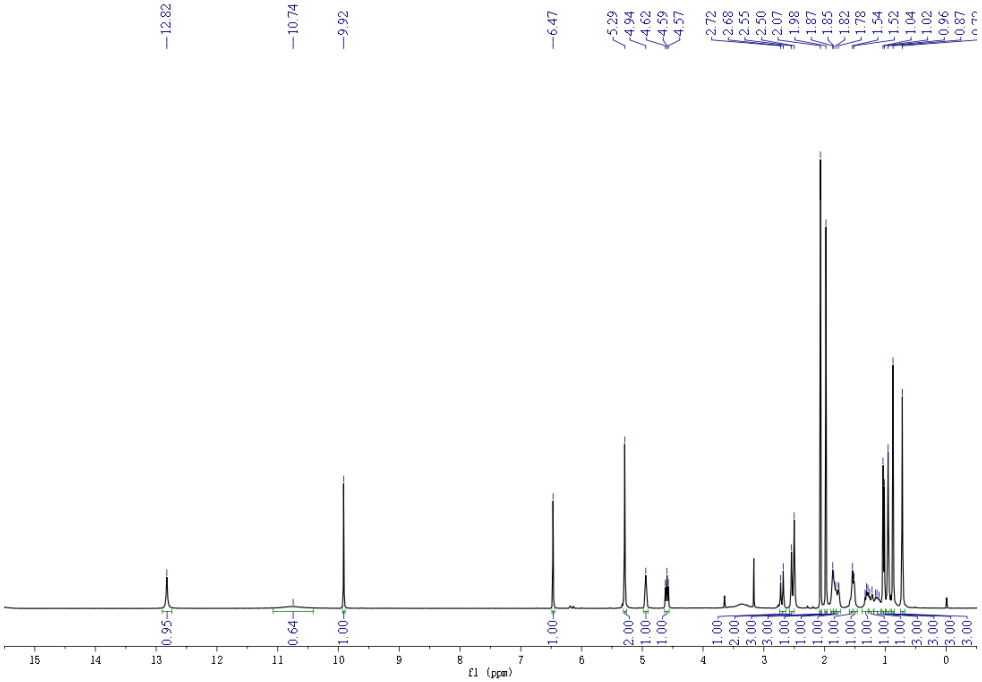

Figure S36 ^{1}H NMR (400 MHz, DMSO-d_6) spectrum for myrogramin C (**5**).

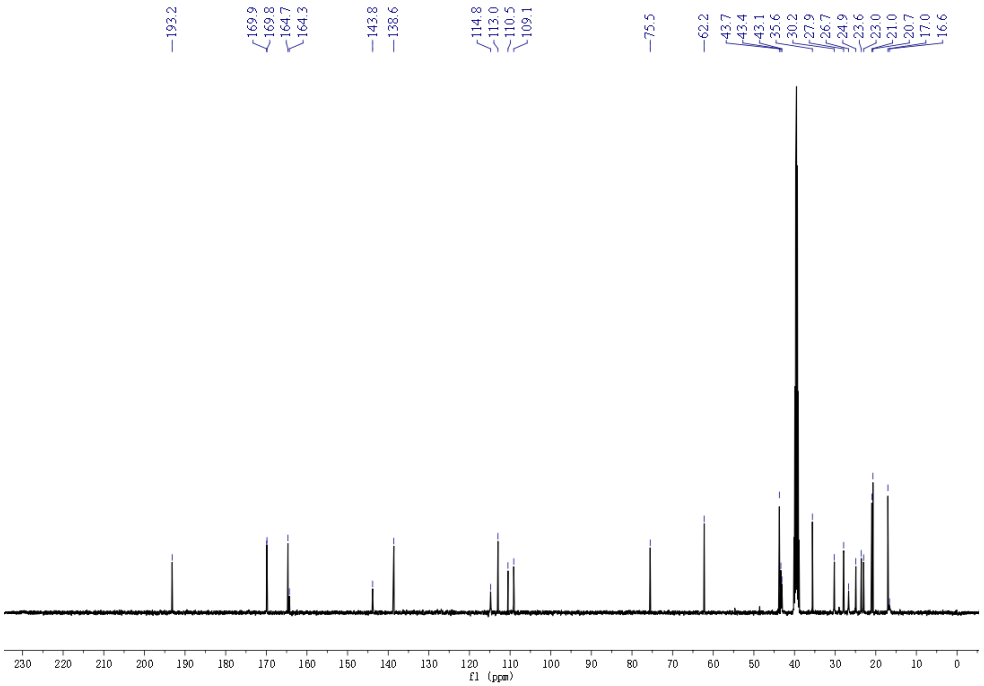

Figure S37 ^{13}C NMR (100 MHz, DMSO-d_6) spectrum for myrogramin C (**5**).

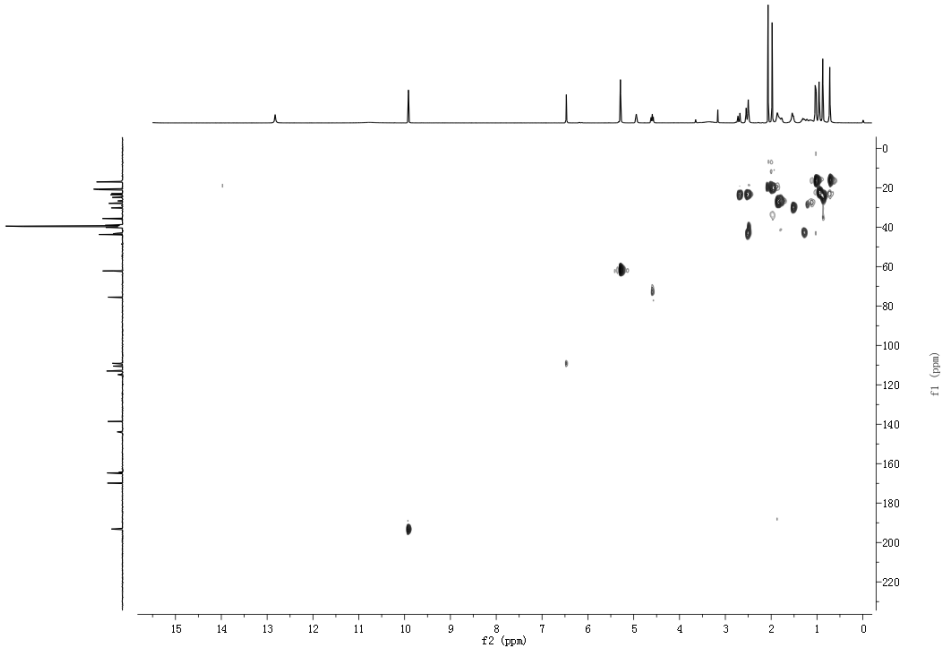

Figure S38 HSQC (400 MHz, DMSO-d_6) spectrum for myrogramin C (**5**).

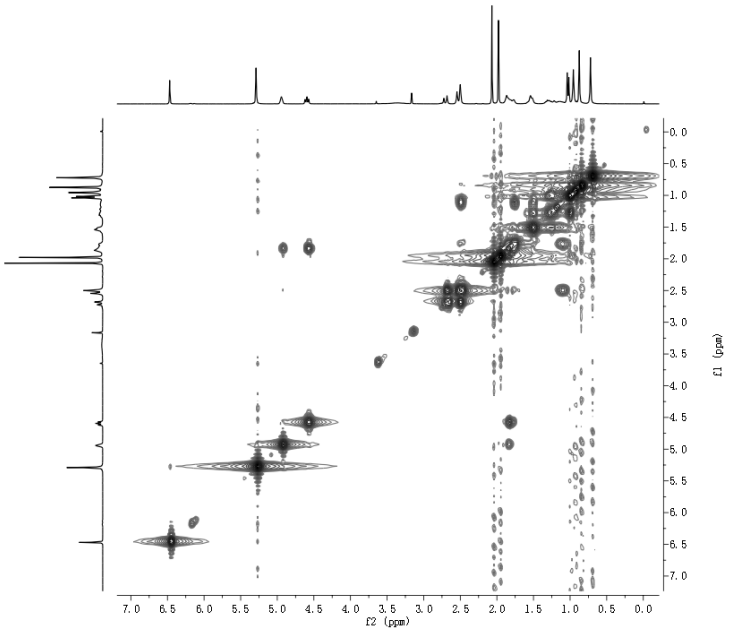

Figure S39 ^{1}H-^{1}H COSY (400 MHz, DMSO-d_6) spectrum for myrogramin C (**5**).

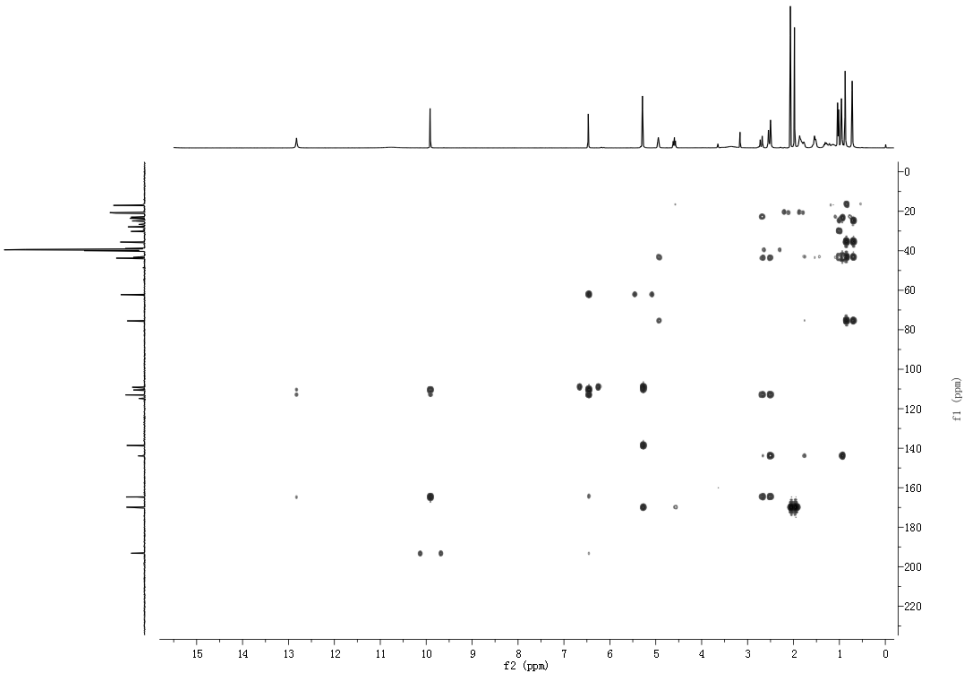

Figure S40 HMBC (400 MHz, DMSO-d_6) spectrum for myrogramin C (**5**).

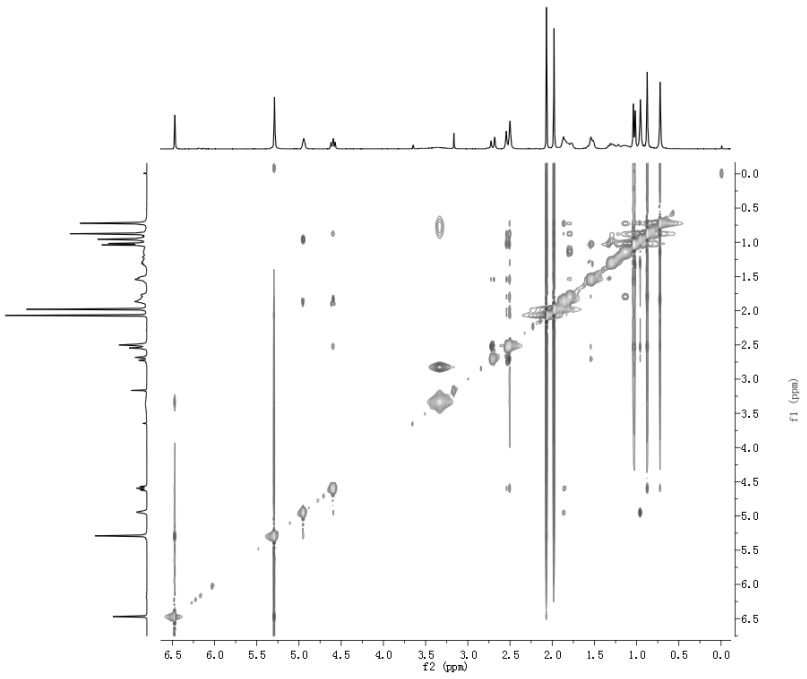

Figure S41 ROESY (400 MHz, DMSO-d_6) spectrum for myrogramin C (**5**).

The 1D and 2D NMR spectra of myrogramin D (**6**)

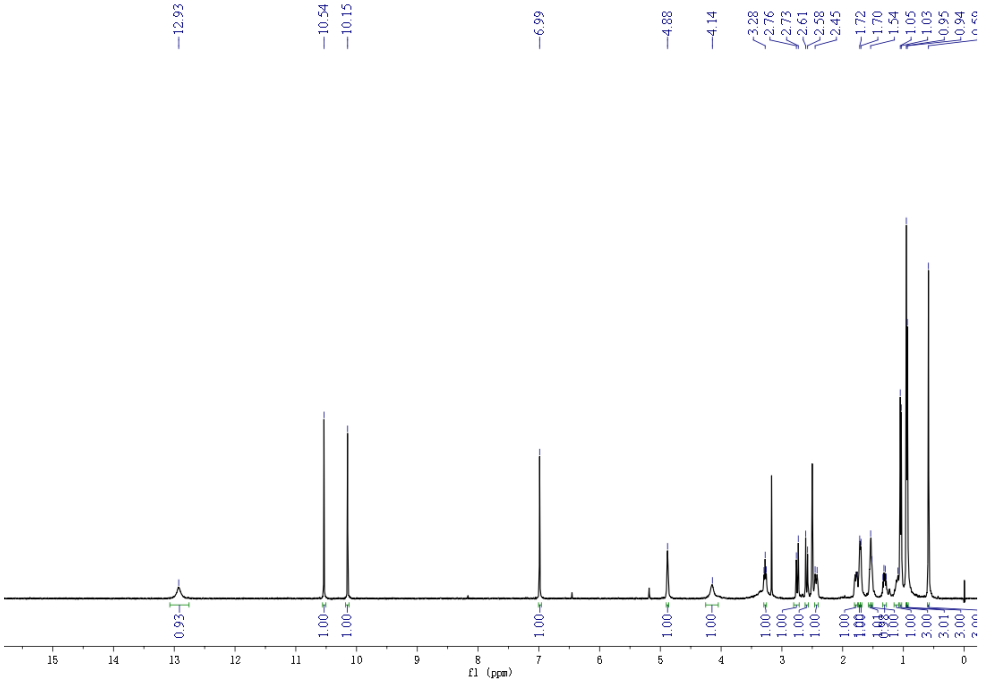

Figure S42 ^{1}H NMR (400 MHz, DMSO-d_6) spectrum for myrogramin D (**6**).

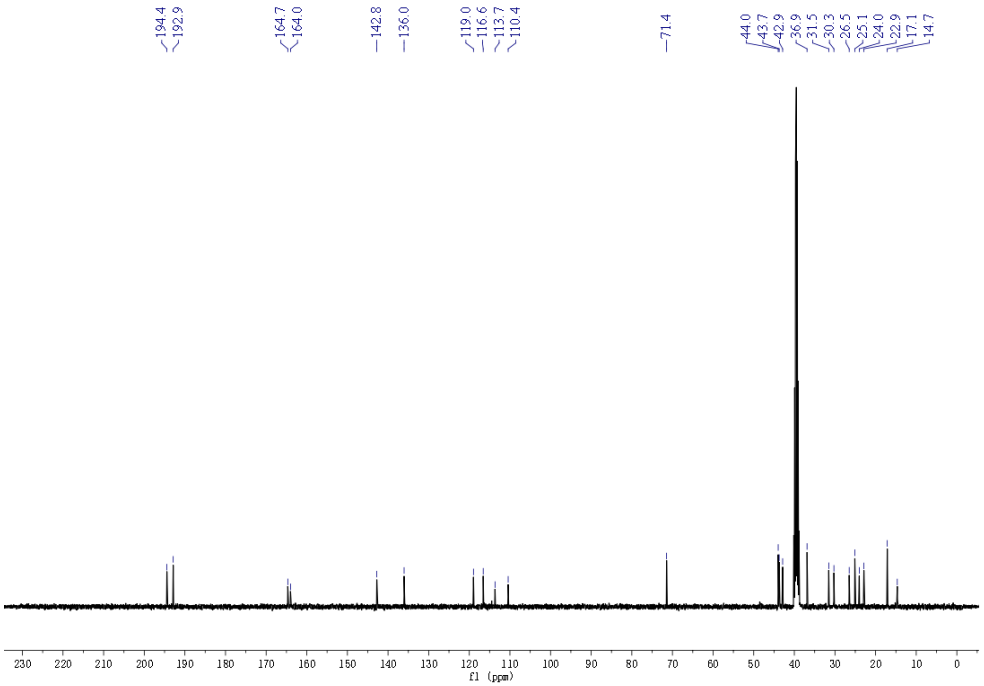

Figure S43 ^{13}C NMR (100 MHz, DMSO-d_6) spectrum for myrogramin D (**6**).

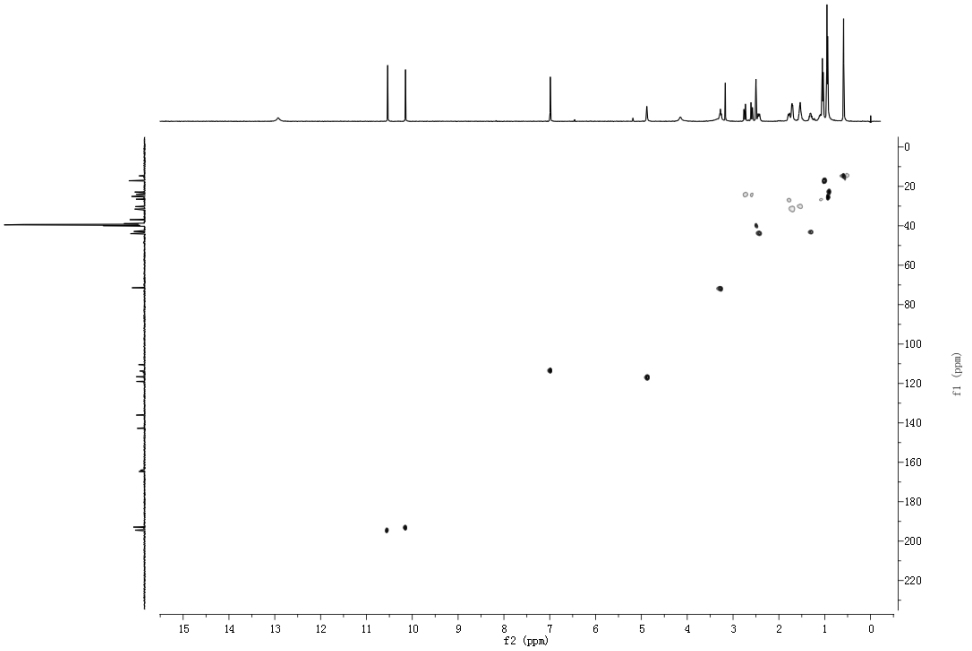

Figure S44 HSQC (300 MHz, DMSO-d_6) spectrum for myrogramin D (**6**).

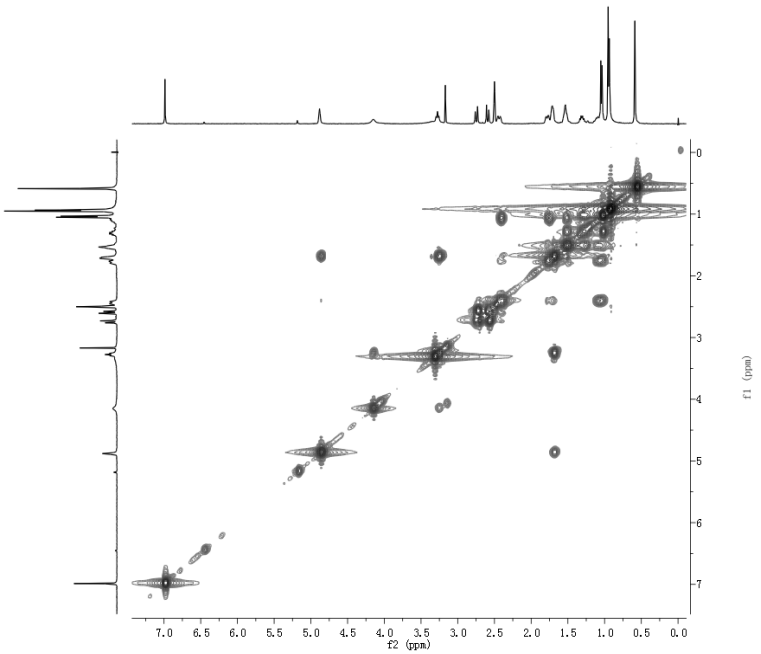

Figure S45 ^{1}H-^{1}H COSY (400 MHz, DMSO-d_6) spectrum for myrogramin D (**6**).

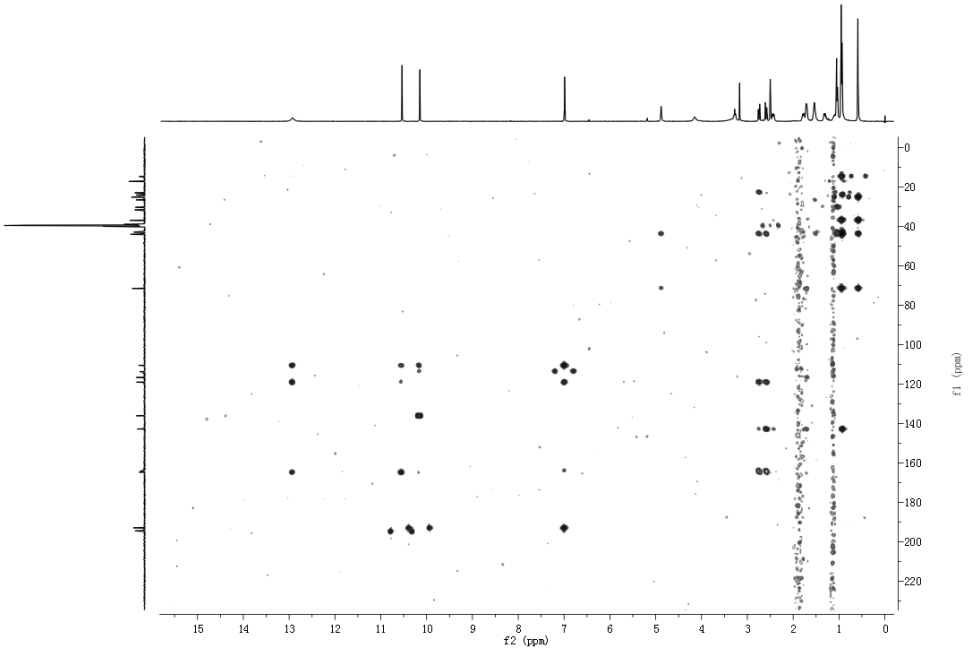

Figure S46 HMBC (400 MHz, DMSO-d_6) spectrum for myrogramin D (**6**).

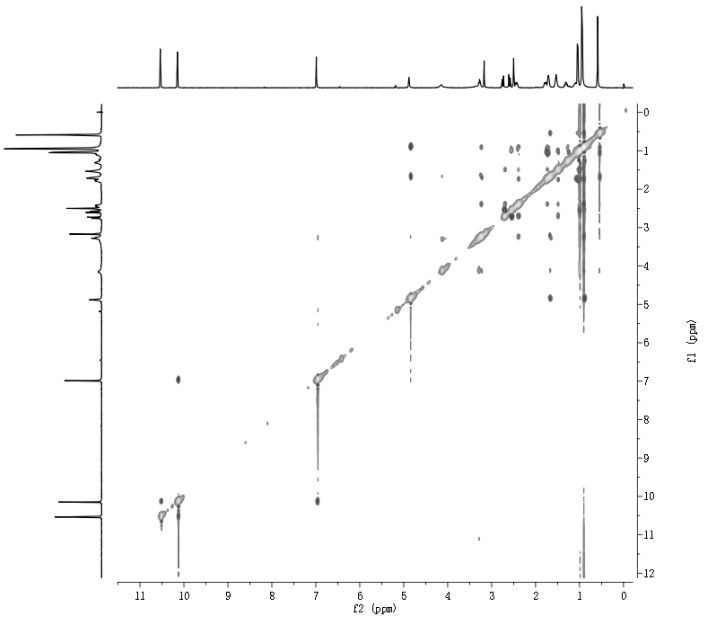

Figure S47 ROESY (400 MHz, DMSO-d_6) spectrum for myrogramin D (**6**).

The 1D and 2D NMR spectra of myrogramin E (**7**)

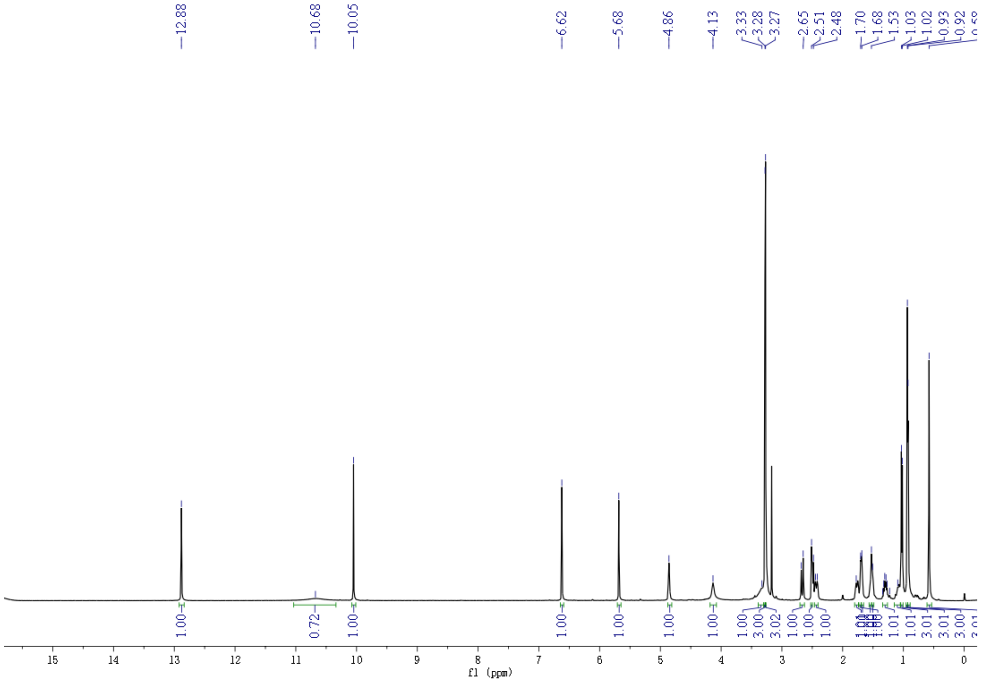

Figure S48 ^{1}H NMR (400 MHz, DMSO-d_6) spectrum for myrogramin E (**7**).

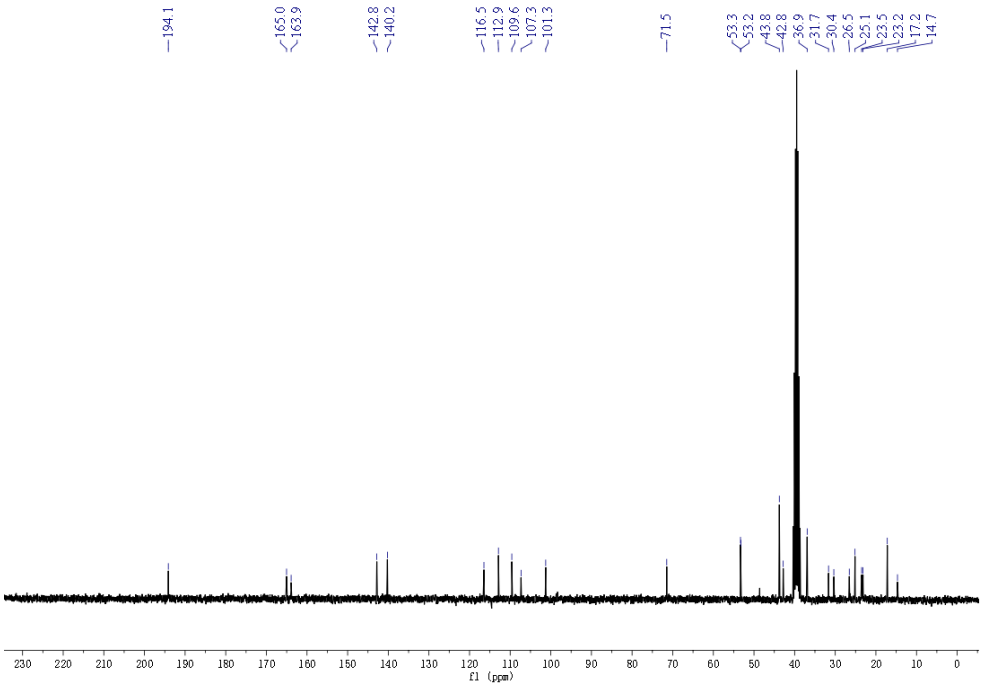

Figure S49 ^{13}C NMR (100 MHz, DMSO-d_6) spectrum for myrogramin E (**7**).

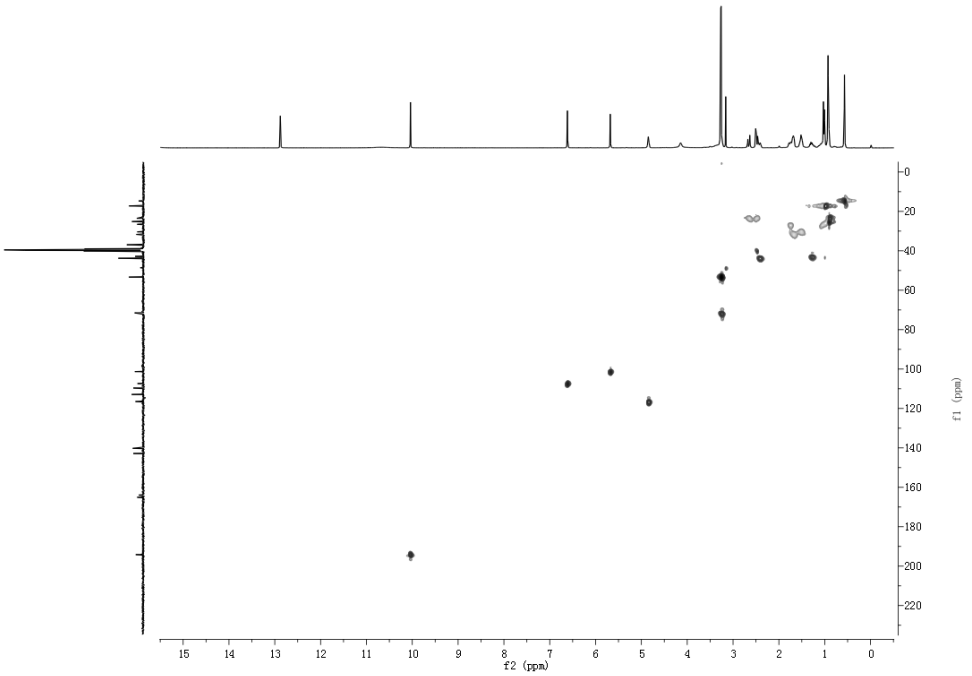

Figure S50 HSQC (300 MHz, DMSO-d_6) spectrum for myrogramin E (**7**).

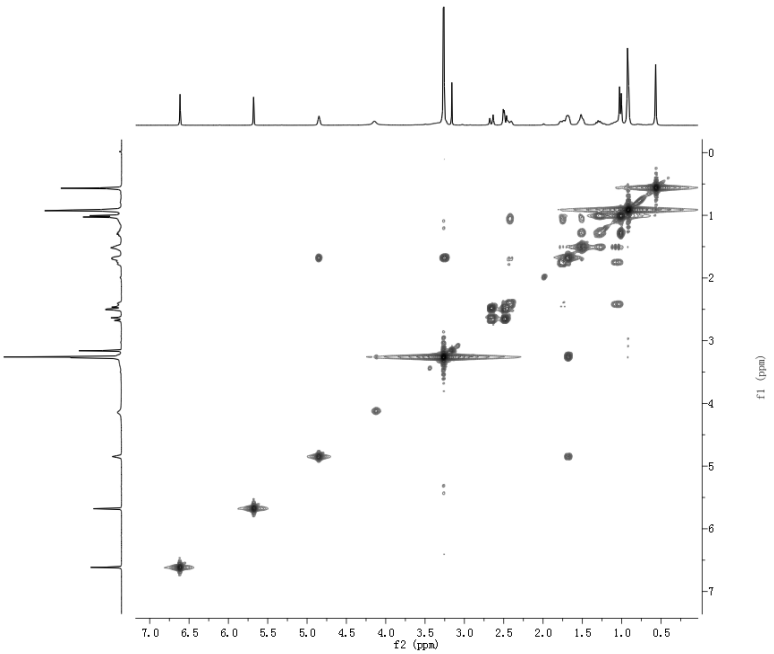

Figure S51 ^{1}H-^{1}H COSY (400 MHz, DMSO-d_6) spectrum for myrogramin E (**7**).

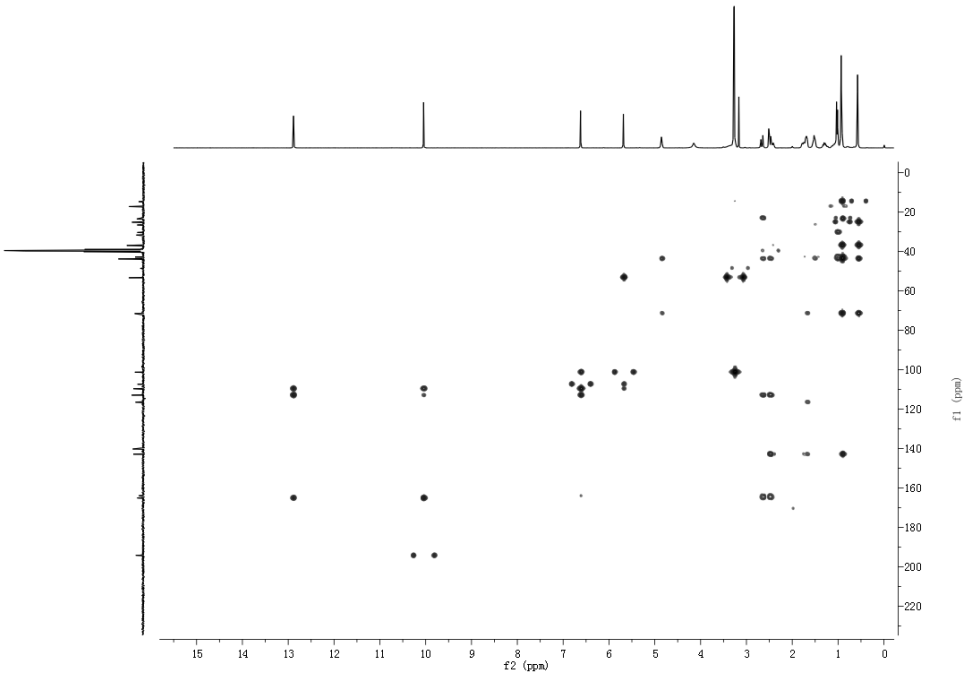

Figure S52 HMBC (400 MHz, DMSO-d_6) spectrum for myrogramin E (**7**).

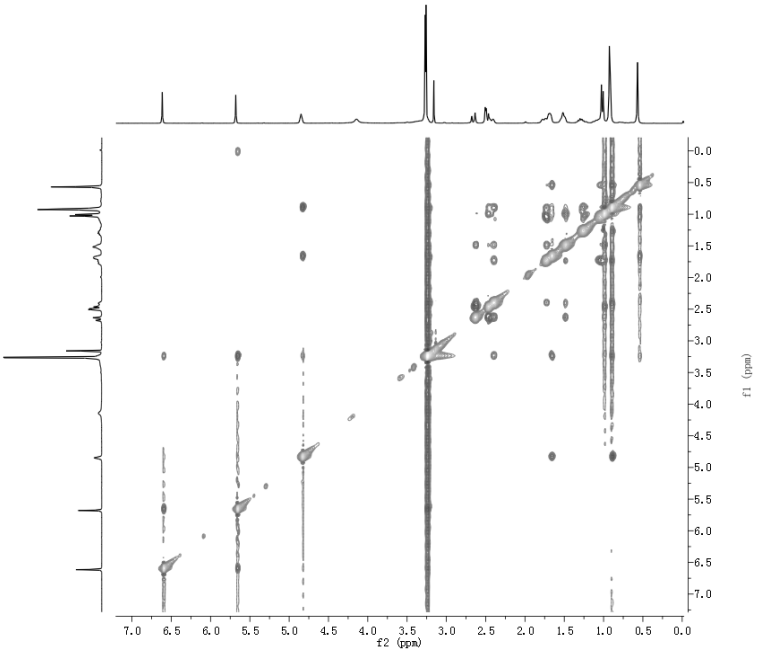

Figure S53 ROESY (400 MHz, DMSO-d_6) spectrum for myrogramin E (**7**).

The 1D and 2D NMR spectra of myrogramin F (**8**)

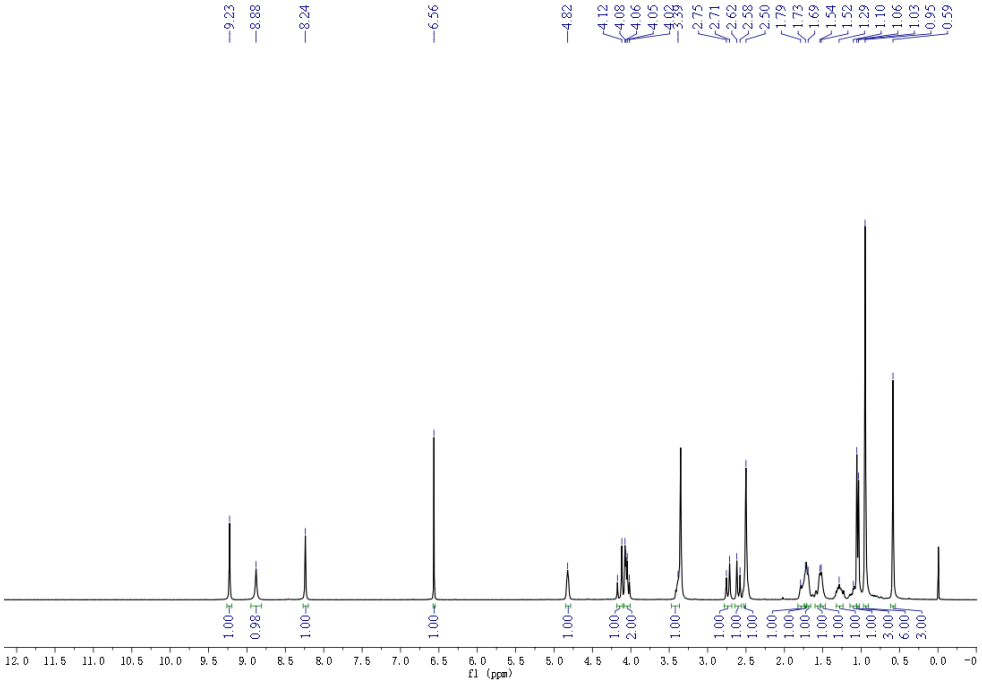

Figure S54 ^{1}H NMR (300 MHz, DMSO-d_6) spectrum for myrogramin F (**8**).

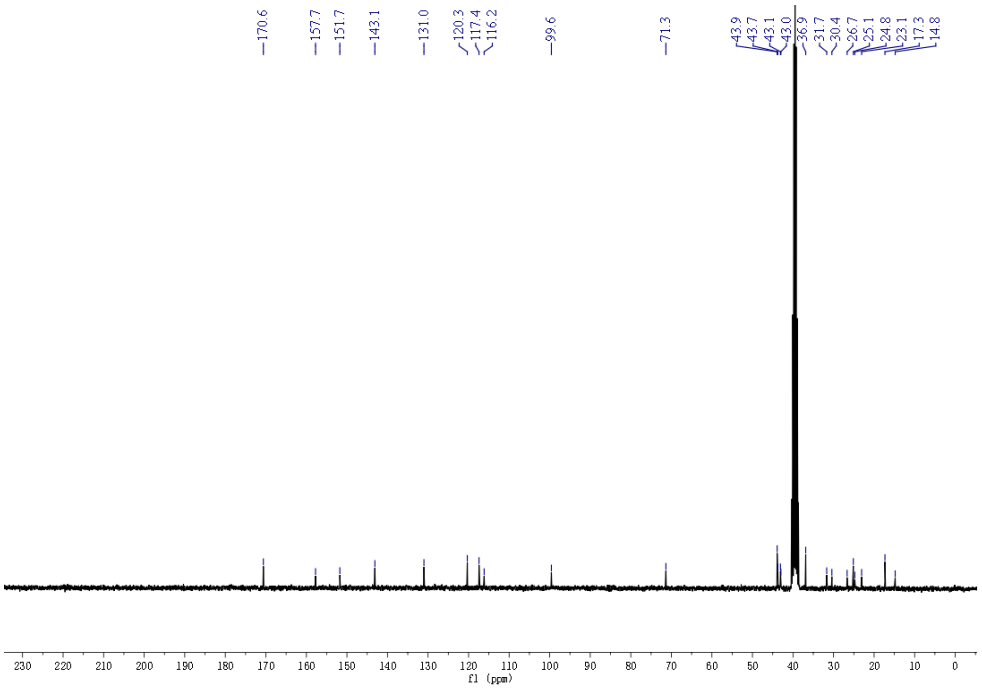

Figure S55 ^{13}C NMR (75 MHz, DMSO-d_6) spectrum for myrogramin F (**8**).

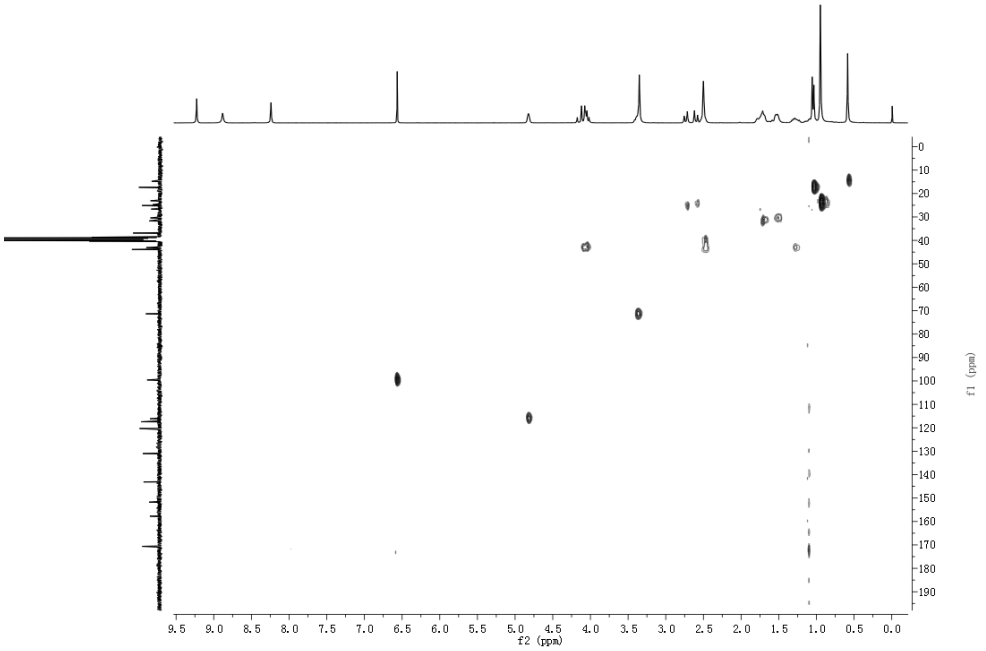

Figure S56 HSQC (400 MHz, DMSO-d_6) spectrum for myrogramin F (**8**).

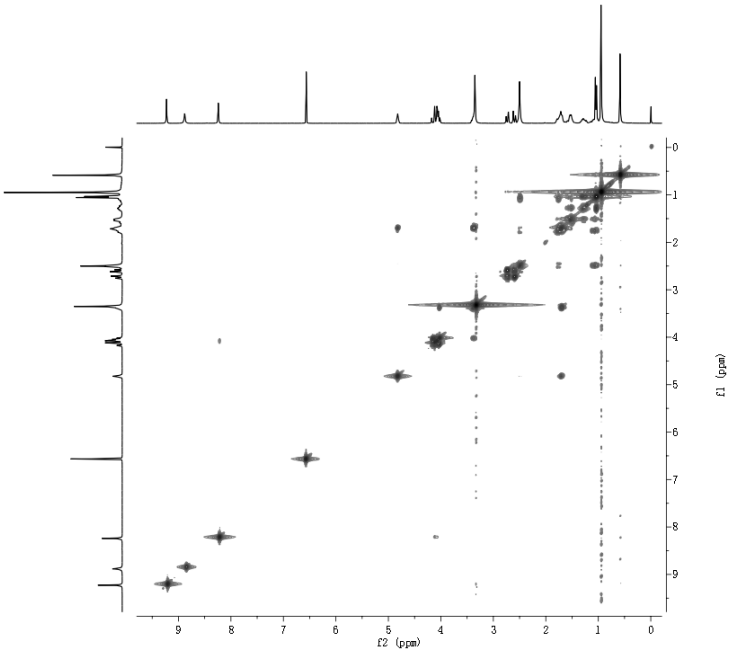

Figure S57 ^{1}H-^{1}H COSY (400 MHz, DMSO-d_6) spectrum for myrogramin F (**8**).

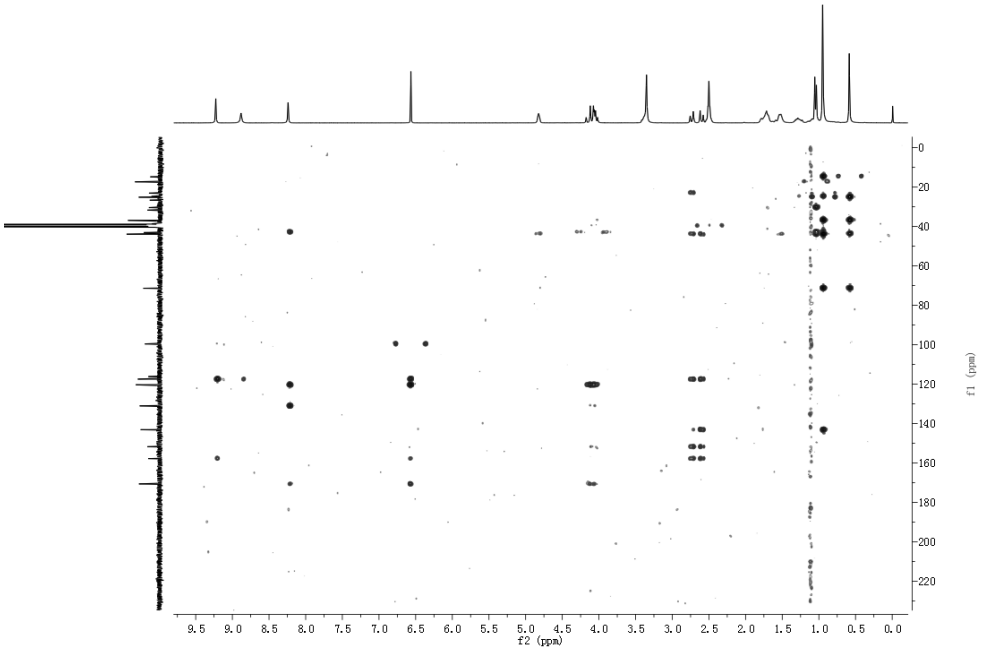

Figure S58 HMBC (400 MHz, DMSO-d_6) spectrum for myrogramin F (**8**).

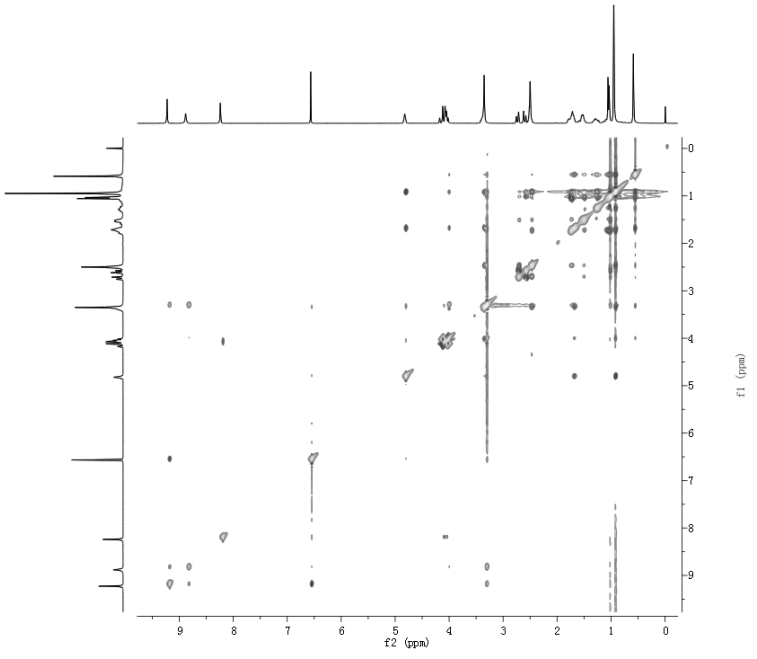

Figure S59 ROESY (400 MHz, DMSO-d_6) spectrum for myrogramin F (**8**).

The 1D and 2D NMR spectra of myrogramin G (**9**)

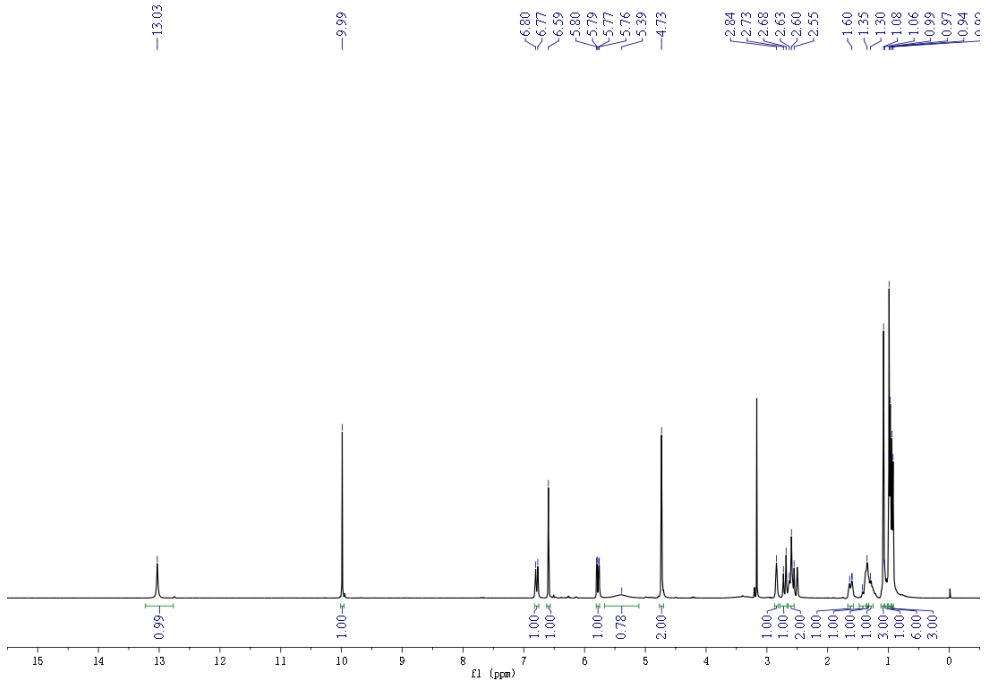

Figure S60 ^{1}H NMR (300 MHz, DMSO-d_6) spectrum for myrogramin G (**9**).

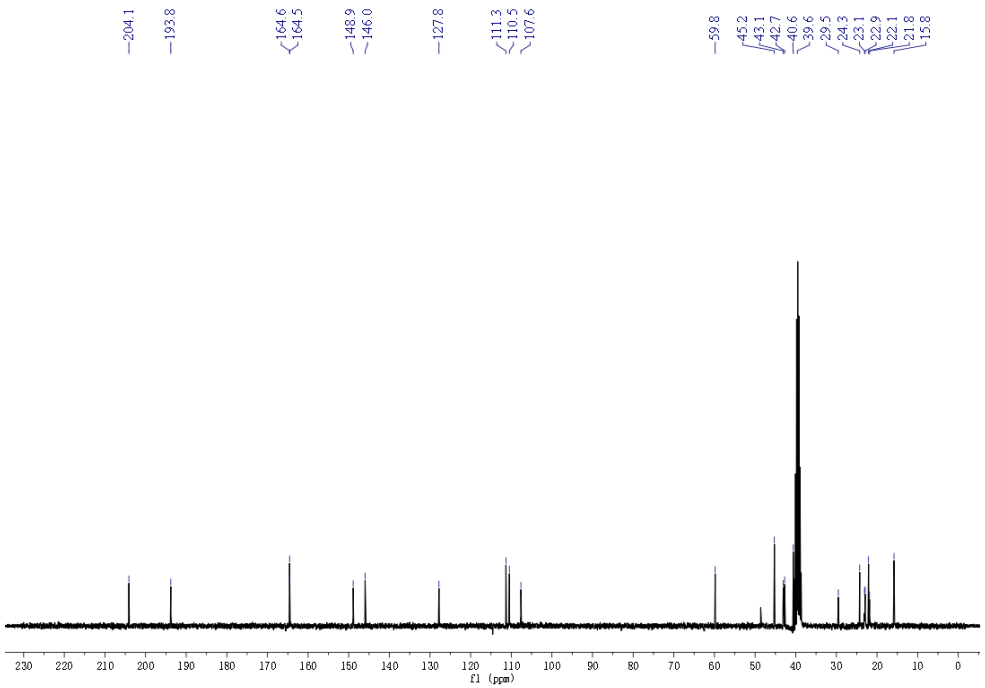

Figure S61 ^{13}C NMR (75 MHz, DMSO-d_6) spectrum for myrogramin G (**9**).

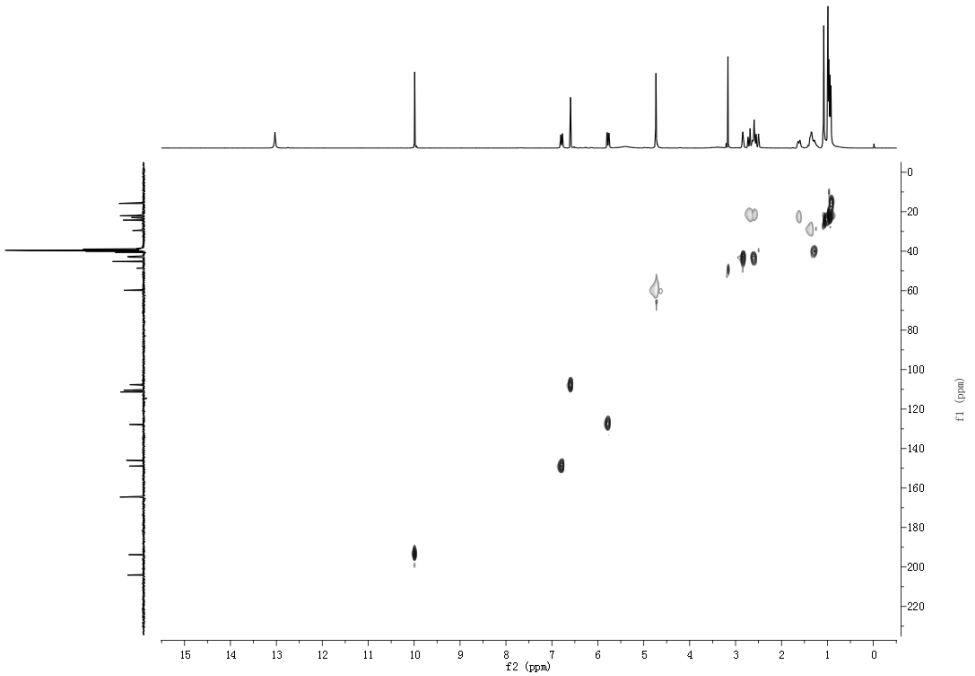

Figure S62 HSQC (300 MHz, DMSO-d_6) spectrum for myrogramin G (**9**).

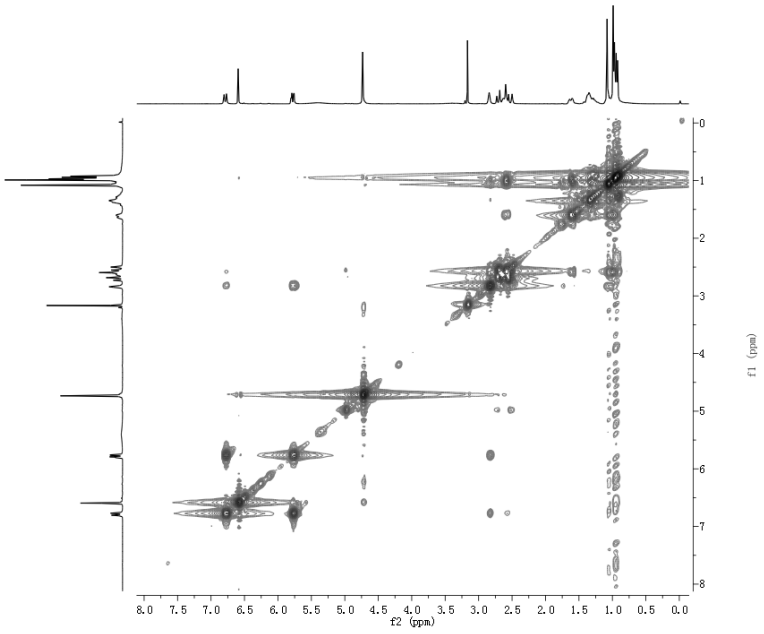

Figure S63 ^{1}H-^{1}H COSY (400 MHz, DMSO-d_6) spectrum for myrogramin G (**9**).

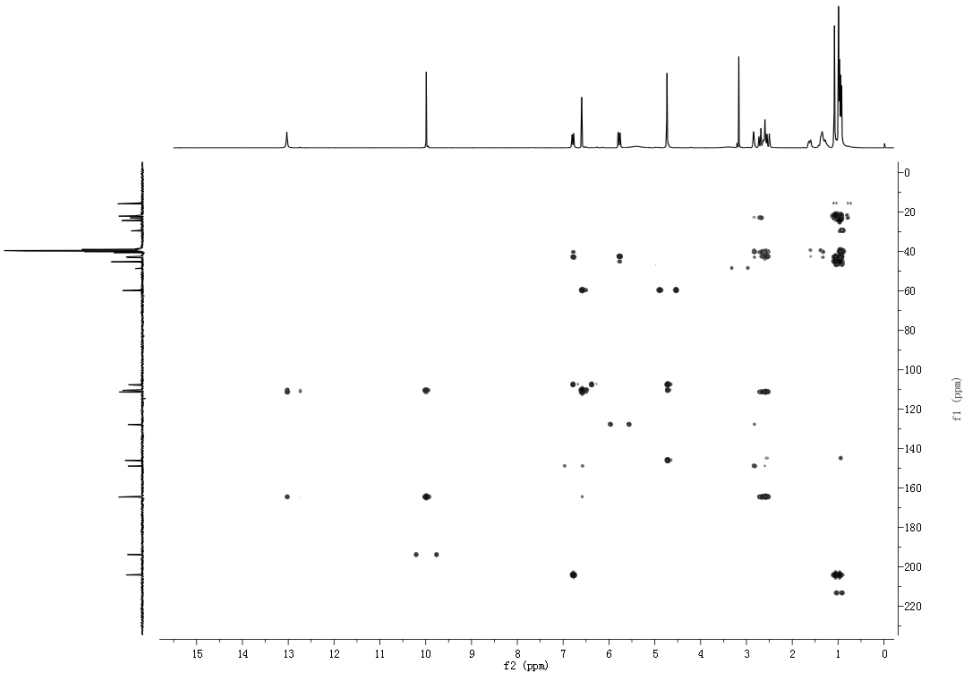

Figure S64 HMBC (400 MHz, DMSO-d_6) spectrum for myrogramin G (**9**).

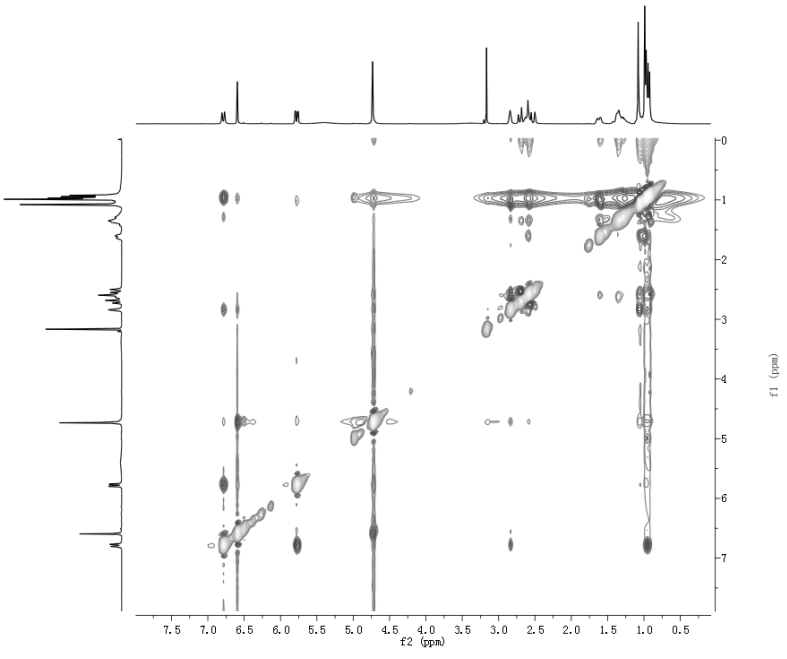

Figure S65 ROESY (400 MHz, DMSO-d_6) spectrum for myrogramin G (**9**).

The 1D and 2D NMR spectra of myrogramin H (**10**)

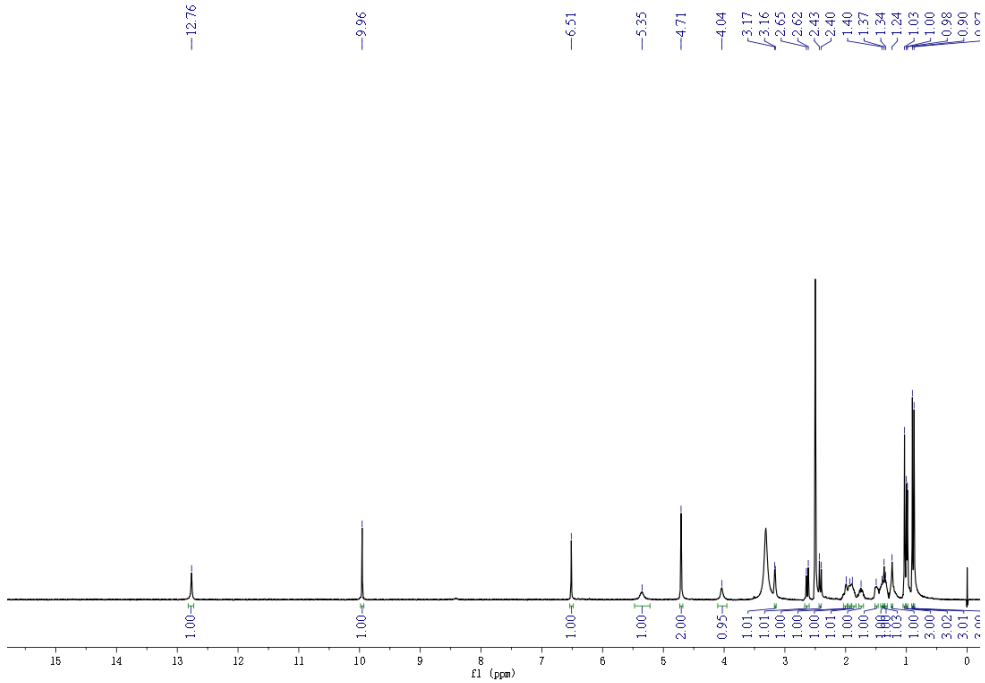

Figure S66 ^{1}H NMR (300 MHz, DMSO-d_6) spectrum for myrogramin H (**10**).

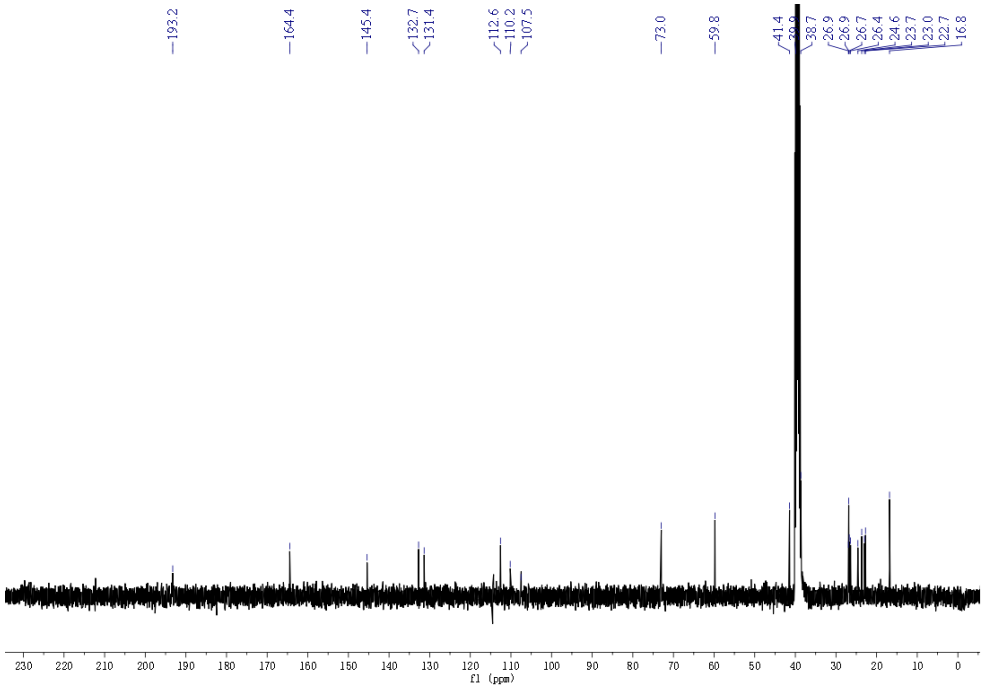

Figure S67 ^{13}C NMR (75 MHz, DMSO-d_6) spectrum for myrogramin H (**10**).

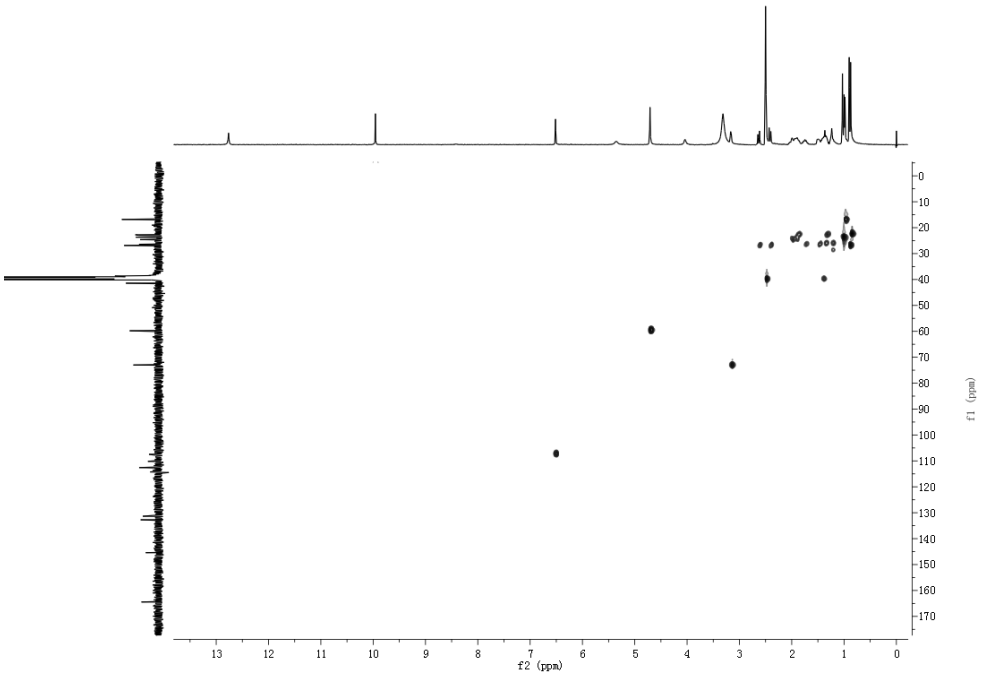

Figure S68 HSQC (600 MHz, DMSO-d_6) spectrum for myrogramin H (**10**).

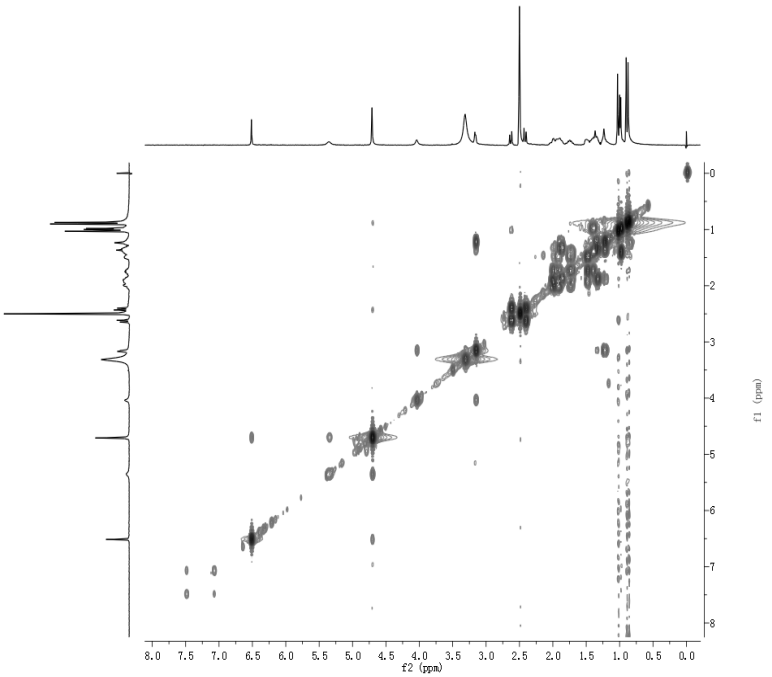

Figure S69 ^{1}H-^{1}H COSY (600 MHz, DMSO-d_6) spectrum for myrogramin H (**10**).

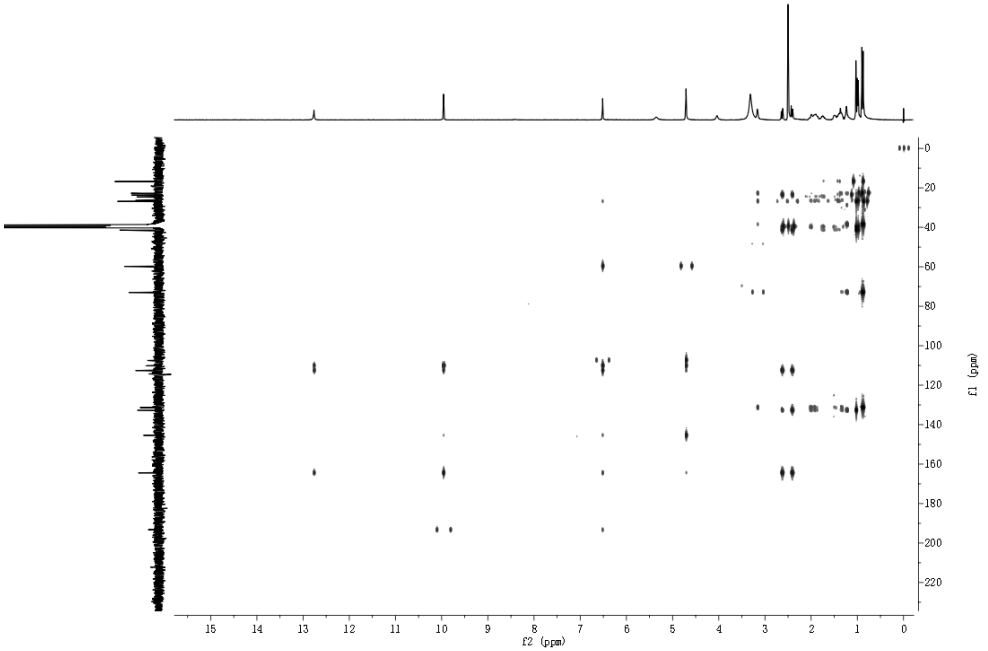

Figure S70 HMBC (600 MHz, DMSO-d_6) spectrum for myrogramin H (**10**).

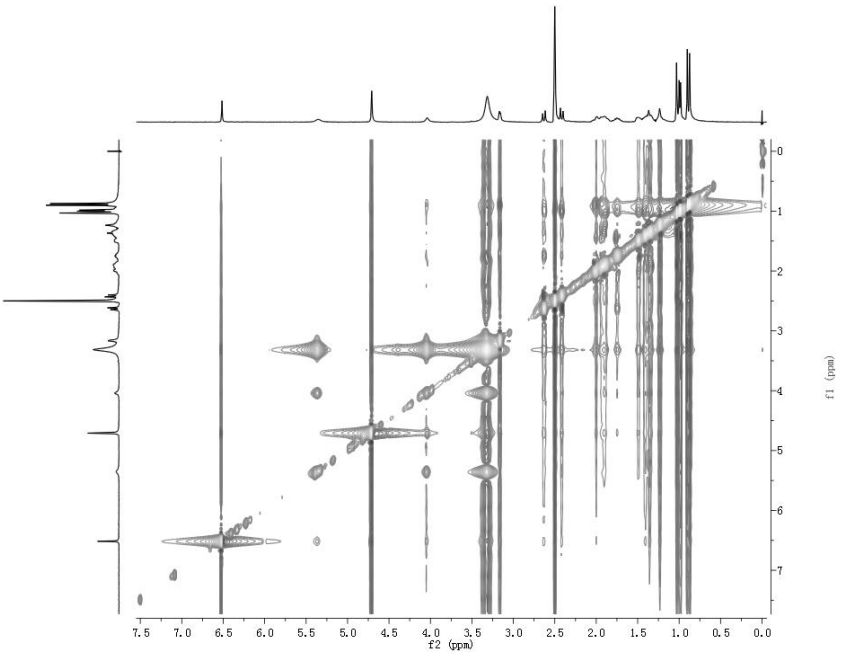

Figure S71 NOESY (600 MHz, DMSO-d_6) spectrum for myrogramin H (**10**).

The 1D and 2D NMR spectra of myrogramin I (**11**)

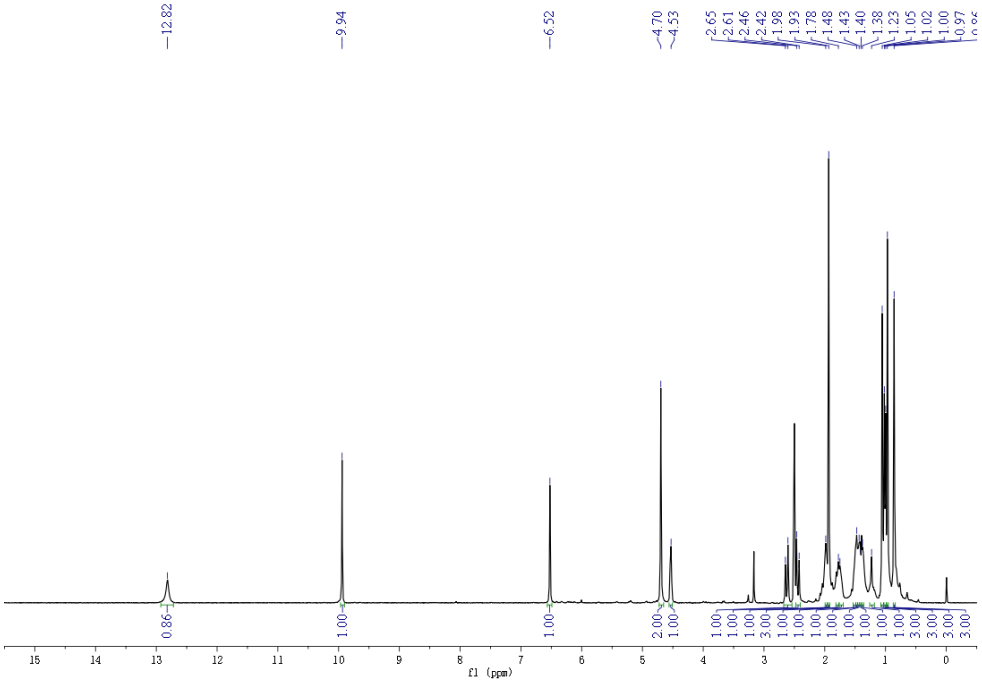

Figure S72 ^{1}H NMR (300 MHz, DMSO-d_6) spectrum for myrogramin I (**11**).

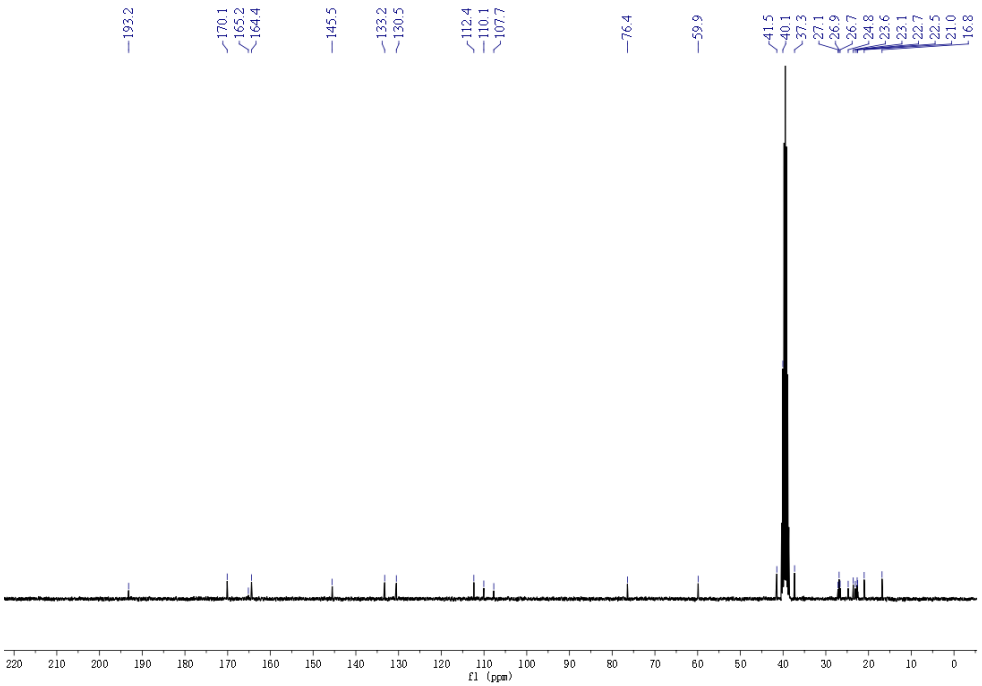

Figure S73 ^{13}C NMR (75 MHz, DMSO-d_6) spectrum for myrogramin I (**11**).

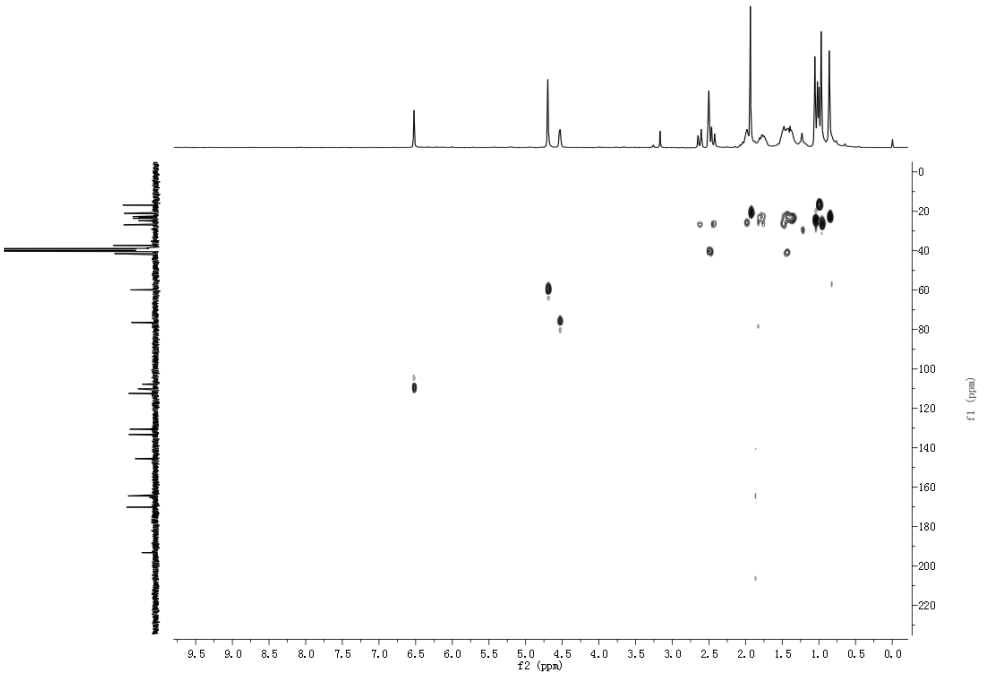

Figure S74 HSQC (400 MHz, DMSO-d_6) spectrum for myrogramin I (**11**).

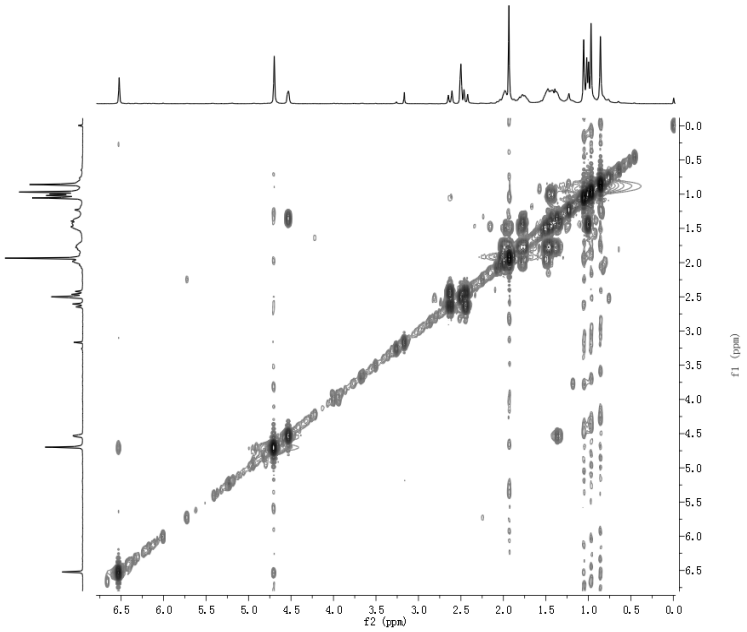

Figure S75 ^{1}H-^{1}H COSY (400 MHz, DMSO-d_6) spectrum for myrogramin I (**11**).

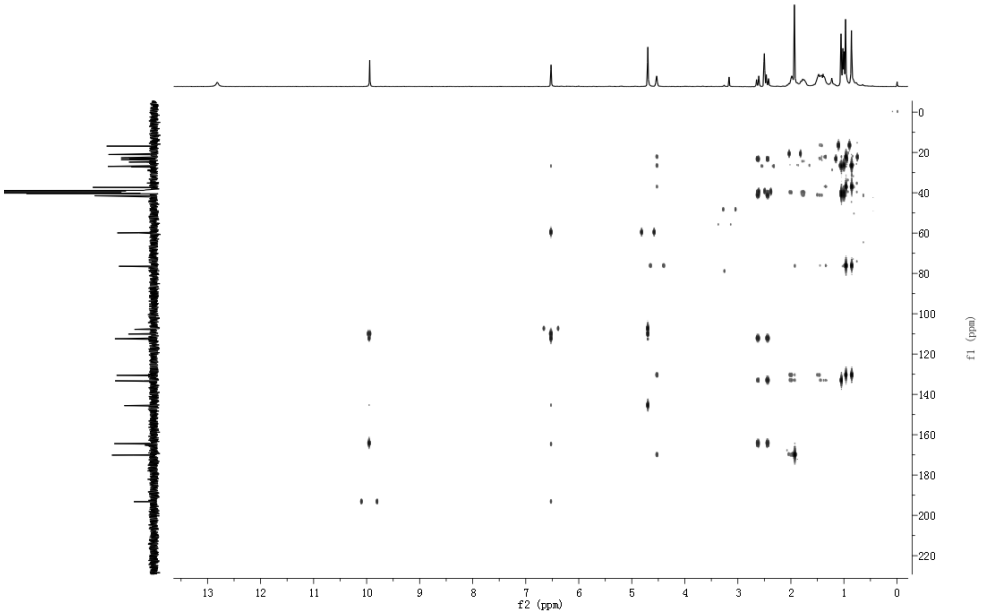

Figure S76 HMBC (600 MHz, DMSO-d_6) spectrum for myrogramin I (**11**).

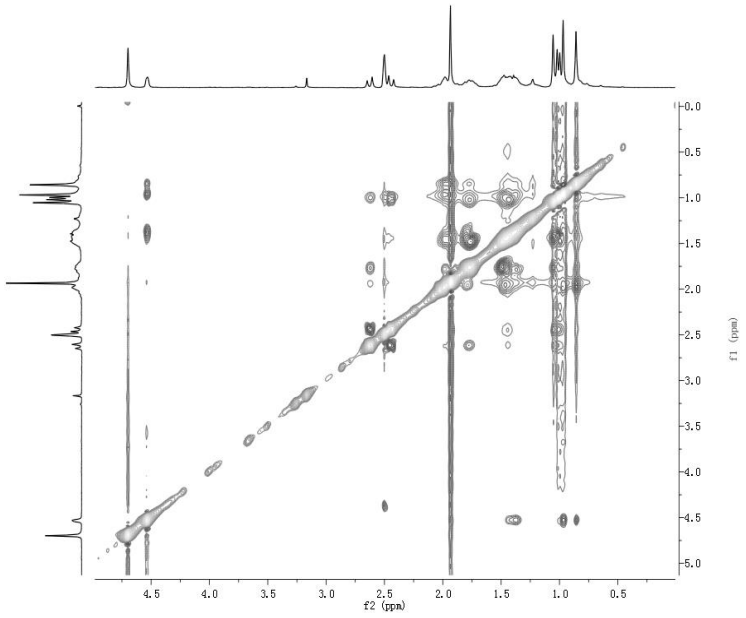

Figure S77 NOESY (600 MHz, DMSO-d_6) spectrum for myrogramin I (**11**).

7. The HR-ESI-MS spectra of compounds 1–11

Elemental Composition Report **Page 1**

Single Mass Analysis
Tolerance = 5.0 mDa / DBE: min = -1.5, max = 50.0
Element prediction: Off
Number of isotope peaks used for i-FIT = 3

Monoisotopic Mass, Even Electron Ions
142 formula(e) evaluated with 2 results within limits (up to 50 best isotopic matches for each mass)
Elements Used:
C: 0-500 H: 0-1000 O: 0-200 Na: 0-1
S537B
2014111016 215 (1.731) Cm (209:216) 1: TOF MS ES+ 1.88e+005

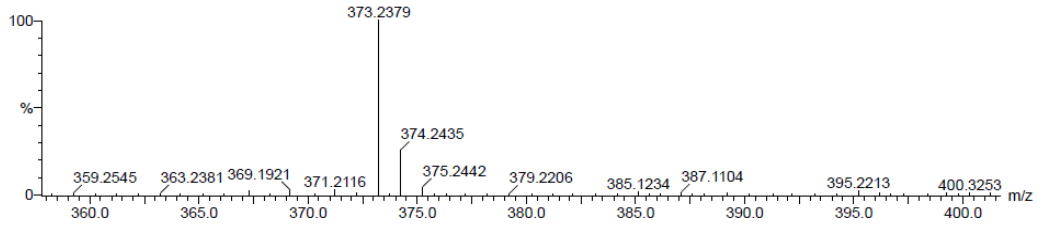

Minimum:				-1.5				
Maximum:		5.0	5.0	50.0				
Mass	Calc. Mass	mDa	PPM	DBE	i-FIT	Norm	Conf(%)	Formula
373.2379	373.2379	0.0	0.0	7.5	20.8	0.001	99.91	C23 H33 O4
	373.2355	2.4	6.4	4.5	27.8	7.000	0.09	C21 H34 O4 Na

Figure S78 HR-ESI-MS spectrum for myrogramin A (**1**).

Single Mass Analysis
Tolerance = 5.0 PPM / DBE: min = -1.5, max = 50.0
Element prediction: Off
Number of isotope peaks used for i-FIT = 3

Monoisotopic Mass, Even Electron Ions
199 formula(e) evaluated with 2 results within limits (up to 50 best isotopic matches for each mass)
Elements Used:
C: 0-500 H: 0-1000 O: 0-200 Na: 0-1
zL0801-19w4b7-1
20130527-10 243 (1.964) Cm (234:254) 1: TOF MS ES+ 1.71e+006

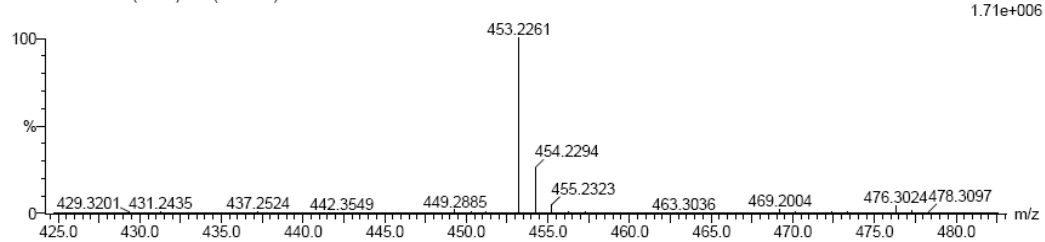

Minimum:				-1.5				
Maximum:		5.0	5.0	50.0				
Mass	Calc. Mass	mDa	PPM	DBE	i-FIT	Norm	Conf(%)	Formula
453.2261	453.2253	0.8	1.8	8.5	1287.9	0.009	99.14	C25 H34 O6 Na
	453.2277	-1.6	-3.5	11.5	1292.7	4.752	0.86	C27 H33 O6

Figure S79 HR-ESI-MS spectrum for myrothecisin C (**2**).

Single Mass Analysis
Tolerance = 5.0 PPM / DBE: min = -1.5, max = 50.0
Element prediction: Off
Number of isotope peaks used for i-FIT = 3

Monoisotopic Mass, Even Electron Ions
83 formula(e) evaluated with 1 results within limits (up to 50 best isotopic matches for each mass)
Elements Used:
C: 0-500 H: 0-1000 O: 0-200
zL0801-19w4b5c
20130527-12 198 (1.604) Cm (192:202)

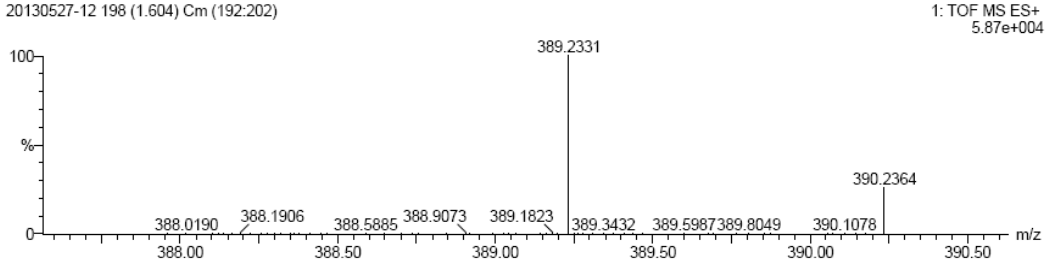

Minimum:				-1.5				
Maximum:		5.0	5.0	50.0				
Mass	Calc. Mass	mDa	PPM	DBE	i-FIT	Norm	Conf(%)	Formula
389.2331	389.2328	0.3	0.8	7.5	176.7	n/a	n/a	C23 H33 O5

Figure S80 HR-ESI-MS spectrum for myrothecisin D (**3**).

Single Mass Analysis
Tolerance = 5.0 PPM / DBE: min = -1.5, max = 50.0
Element prediction: Off
Number of isotope peaks used for i-FIT = 3

Monoisotopic Mass, Even Electron Ions
102 formula(e) evaluated with 1 results within limits (up to 50 best isotopic matches for each mass)
Elements Used:
C: 0-500 H: 0-1000 O: 0-200
ZL0801-19W4D4F-1
20130511-29 222 (1.795) Cm (214:229)

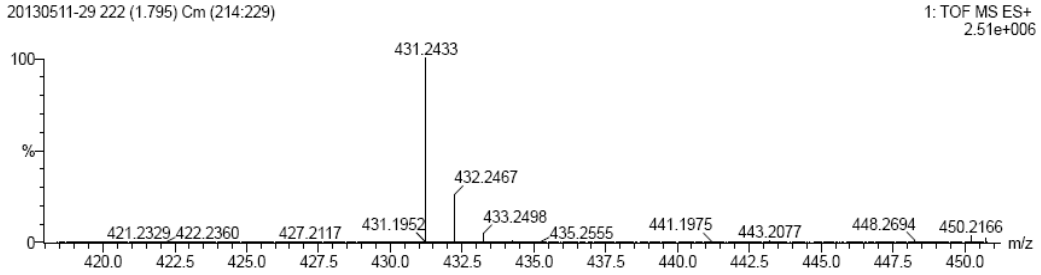

Minimum:				-1.5				
Maximum:		5.0	5.0	50.0				
Mass	Calc. Mass	mDa	PPM	DBE	i-FIT	Norm	Conf(%)	Formula
431.2433	431.2434	-0.1	-0.2	8.5	1200.5	n/a	n/a	C25 H35 O6

Figure S81 HR-ESI-MS spectrum for myrogramin B (**4**).

Single Mass Analysis
Tolerance = 5.0 mDa / DBE: min = -1.5, max = 50.0
Element prediction: Off
Number of isotope peaks used for i-FIT = 3

Monoisotopic Mass, Even Electron Ions
243 formula(e) evaluated with 4 results within limits (all results (up to 1000) for each mass)
Elements Used:
C: 0-500 H: 0-1000 O: 0-200 Na: 0-1

s574a
2015011616 253 (2.038)

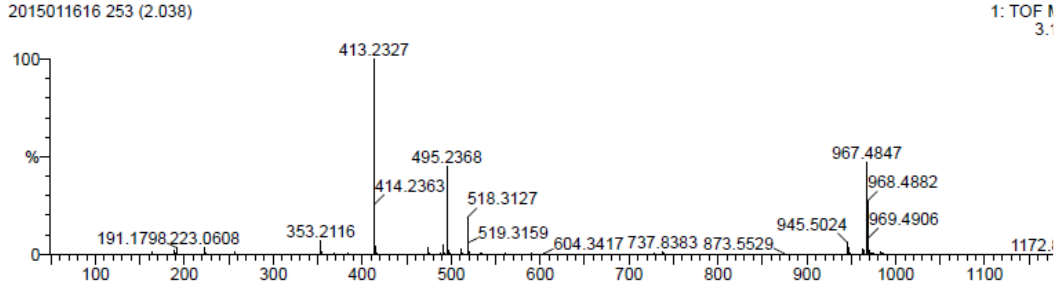

Minimum:				-1.5				
Maximum:		5.0	10.0	50.0				
Mass	Calc. Mass	mDa	PPM	DBE	i-FIT	Norm	Conf(%)	Formula
495.2368	495.2359	0.9	1.8	9.5	253.5	0.113	89.28	C27 H36 O7 Na
	495.2383	-1.5	-3.0	12.5	256.0	2.539	7.89	C29 H35 O7
	495.2417	-4.9	-9.9	0.5	257.0	3.580	2.79	C20 H40 O12 Na
	495.2324	4.4	8.9	21.5	261.2	7.773	0.04	C36 H31 O2

Figure S82 HR-ESI-MS spectrum for myrogramin C (**5**).

Elemental Composition Report **Page 1**

Single Mass Analysis
Tolerance = 5.0 PPM / DBE: min = -1.5, max = 30.0
Element prediction: Off
Number of isotope peaks used for i-FIT = 3

Monoisotopic Mass, Even Electron Ions
167 formula(e) evaluated with 2 results within limits (up to 20 best isotopic matches for each mass)
Elements Used:
C: 0-50 H: 0-100 O: 0-30 Na: 0-1

S6443C2
2015052310 216 (1.750) Cm (213:218)

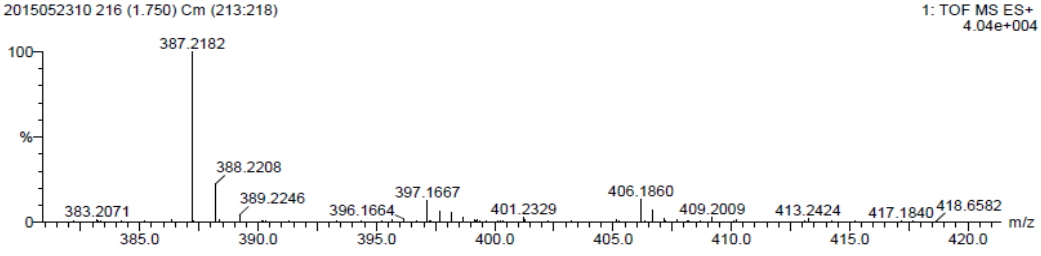

Minimum:				-1.5				
Maximum:		5.0	5.0	30.0				
Mass	Calc. Mass	mDa	PPM	DBE	i-FIT	Norm	Conf(%)	Formula
409.2009	409.2015	-0.6	-1.5	11.5	236.0	0.595	55.18	C25 H29 O5
	409.1991	1.8	4.4	8.5	236.2	0.803	44.82	C23 H30 O5 Na

Figure S83 HR-ESI-MS spectrum for myrogramin D (**6**).

Elemental Composition Report **Page 1**

Single Mass Analysis
Tolerance = 5.0 mDa / DBE: min = -1.5, max = 50.0
Element prediction: Off
Number of isotope peaks used for i-FIT = 3

Monoisotopic Mass, Even Electron Ions
211 formula(e) evaluated with 3 results within limits (all results (up to 1000) for each mass)
Elements Used:
C: 0-500 H: 0-1000 O: 0-200 Na: 0-1

S5443D2
20150032309 219 (1.773)

1: TOF MS ES+
3.08e+003

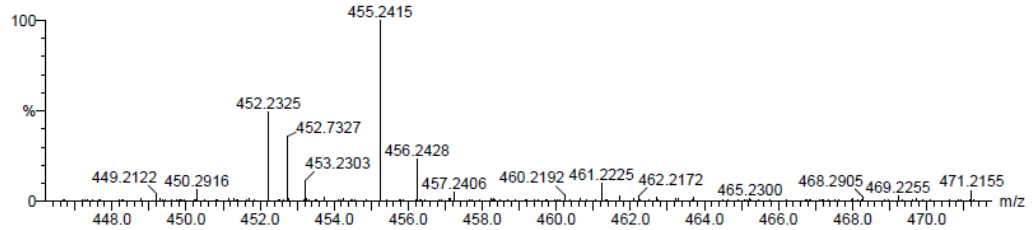

Minimum:				-1.5				
Maximum:		5.0	10.0	50.0				
Mass	Calc. Mass	mDa	PPM	DBE	i-FIT	Norm	Conf(%)	Formula
455.2415	455.2410	0.5	1.1	7.5	108.2	0.187	82.92	C25 H36 O6 Na
	455.2434	-1.9	-4.2	10.5	109.8	1.820	16.21	C27 H35 O6
	455.2375	4.0	8.8	19.5	112.7	4.739	0.87	C34 H31 O

Figure S84 HR-ESI-MS spectrum for myrogramin E (**7**).

Elemental Composition Report **Page 1**

Single Mass Analysis
Tolerance = 5.0 mDa / DBE: min = -1.5, max = 50.0
Element prediction: Off
Number of isotope peaks used for i-FIT = 3

Monoisotopic Mass, Even Electron Ions
716 formula(e) evaluated with 5 results within limits (up to 10 best isotopic matches for each mass)
Elements Used:
C: 0-500 H: 0-1000 N: 0-10 O: 0-200

S636C1
2015051607 156 (1.268)

1: TOF MS ES+
1.06e+005

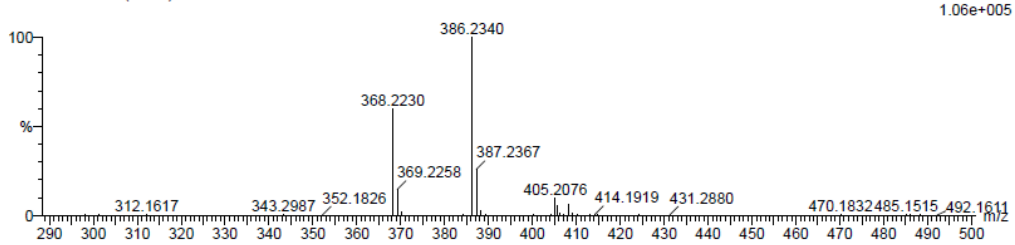

Minimum:				-1.5				
Maximum:		5.0	10.0	50.0				
Mass	Calc. Mass	mDa	PPM	DBE	i-FIT	Norm	Conf(%)	Formula
386.2340	386.2345	-0.5	-1.3	13.5	196.3	0.883	41.35	C24 H28 N5
	386.2304	3.6	9.3	9.5	196.6	1.208	29.87	C19 H28 N7 O2
	386.2331	0.9	2.3	8.5	196.7	1.278	27.87	C23 H32 N O4
	386.2291	4.9	12.7	4.5	200.2	4.753	0.86	C18 H32 N3 O6
	386.2363	-2.3	-6.0	0.5	203.2	7.804	0.04	C12 H32 N7 O7

Figure S85 HR-ESI-MS spectrum for myrogramin F (**8**).

Single Mass Analysis
Tolerance = 10.0 PPM / DBE: min = -1.5, max = 50.0
Element prediction: Off
Number of isotope peaks used for i-FIT = 3

Monoisotopic Mass, Even Electron Ions
86 formula(e) evaluated with 1 results within limits (up to 50 best isotopic matches for each mass)
Elements Used:
C: 0-500 H: 0-1000 O: 0-200
ZL0801-19W4B53-1
20130716-15 190 (1.534) Cm (183:197)

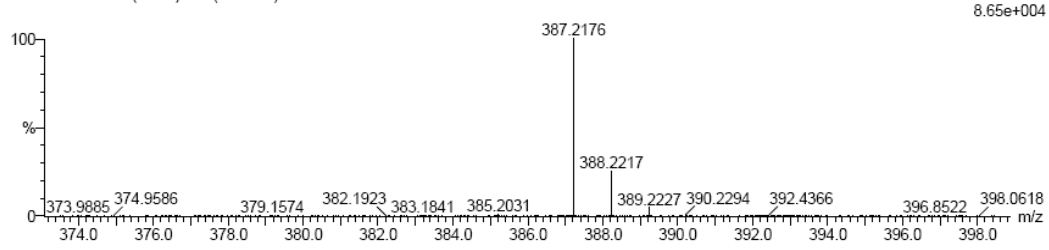

Minimum:				-1.5				
Maximum:		5.0	10.0	50.0				
Mass	Calc. Mass	mDa	PPM	DBE	i-FIT	Norm	Conf(%)	Formula
387.2176	387.2171	0.5	1.3	8.5	292.3	n/a	n/a	C23 H31 O5

Figure S86 HR-ESI-MS spectrum for myrogramin G (**9**).

Elemental Composition Report Page 1

Single Mass Analysis
Tolerance = 5.0 mDa / DBE: min = -1.5, max = 50.0
Element prediction: Off
Number of isotope peaks used for i-FIT = 3

Monoisotopic Mass, Even Electron Ions
1378 formula(e) evaluated with 10 results within limits (up to 10 best isotopic matches for each mass)
Elements Used:
C: 0-500 H: 0-1000 N: 0-10 O: 0-200 Na: 0-1

S6442b2
2015051610 174 (1.414)

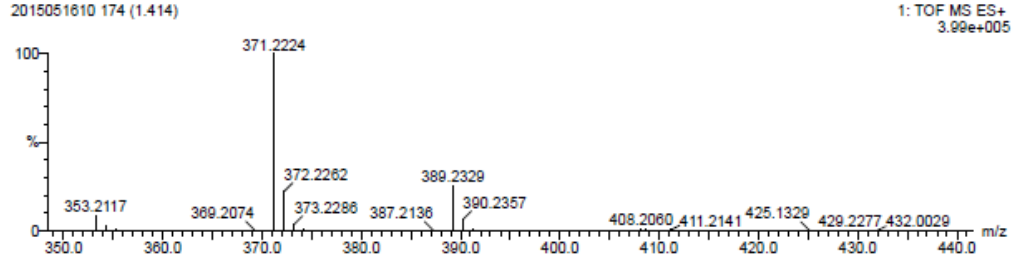

Minimum:				-1.5				
Maximum:		5.0	10.0	50.0				
Mass	Calc. Mass	mDa	PPM	DBE	i-FIT	Norm	Conf(%)	Formula
389.2329	389.2328	0.1	0.3	7.5	224.3	0.229	79.51	C23 H33 O5
	389.2304	2.5	6.4	4.5	226.3	2.235	10.70	C21 H34 O5 Na
	389.2317	1.2	3.1	9.5	226.8	2.774	6.24	C22 H30 N4 O Na
	389.2341	-1.2	-3.1	12.5	227.7	3.629	2.66	C24 H29 N4 O
	389.2301	2.8	7.2	8.5	228.9	4.890	0.75	C19 H29 N6 O3
	389.2288	4.1	10.5	3.5	230.7	6.640	0.13	C18 H33 N2 O7
	389.2376	-4.7	-12.1	0.5	233.6	9.553	0.01	C15 H34 N4 O6 Na
	389.2373	-4.4	-11.3	4.5	234.8	10.747	0.00	C13 H29 N10 O4
	389.2360	-3.1	-8.0	-0.5	234.8	10.778	0.00	C12 H33 N6 O8
	389.2349	-2.0	-5.1	1.5	235.7	11.701	0.00	C11 H30 N10 O4 Na

Figure S87 HR-ESI-MS spectrum for myrogramin H (**10**).

Elemental Composition Report **Page 1**

Single Mass Analysis
Tolerance = 5.0 mDa / DBE: min = -1.5, max = 50.0
Element prediction: Off
Number of isotope peaks used for i-FIT = 3

Monoisotopic Mass, Even Electron Ions
199 formula(e) evaluated with 3 results within limits (up to 50 best isotopic matches for each mass)
Elements Used:
C: 0-500 H: 0-1000 O: 0-200 Na: 0-1

S52524
20141201-015 213 (1.717)

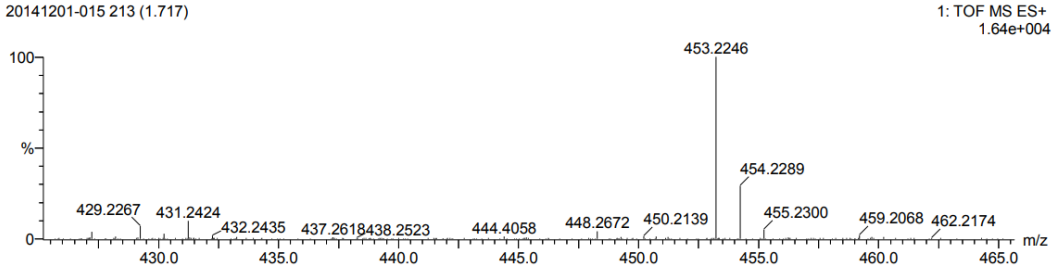

Minimum:				-1.5				
Maximum:		5.0	5.0	50.0				
Mass	Calc. Mass	mDa	PPM	DBE	i-FIT	Norm	Conf(%)	Formula
453.2246	453.2253	-0.7	-1.5	8.5	94.1	0.289	74.90	C25 H34 O6 Na
	453.2277	-3.1	-6.8	11.5	95.2	1.383	25.08	C27 H33 O6
	453.2218	2.8	6.2	20.5	102.5	8.621	0.02	C34 H29 O

Figure S88 HR-ESI-MS spectrum for myrogramin I (**11**).

8. The possible biosynthetic pathways for aureane-type sesquiterpene tetraketides

Aureane-type sesquiterpene tetraketides is a tetrakeketide meroterpenoid. The biosynthesis of tetrakeketide moiety had been reported by Li[2]. As shown in Figure S89, the biosynthetic pathways of aureane-type sesquiterpene tetraketides were hypothesized in this study. Orsinic acid is synthesized by the polyketide synthase, which accepts acetyl-CoA as the starter unit and performs malonyl-CoA extensions. Then, aromatic prenyltransferase catalyzes the transfer of the prenyl moiety to the aromatic acceptor molecule to grifolic acid, which is subsequently reduced by NRPS-like enzymes to afford a key intermediate LL-Z1272β. Subsequent, monooxygenase selectively oxidizes one double bond of prenyl to an epoxy group, which is then cyclized by terpene cyclase to generate aureane-type sesquiterpene tetraketides[3].

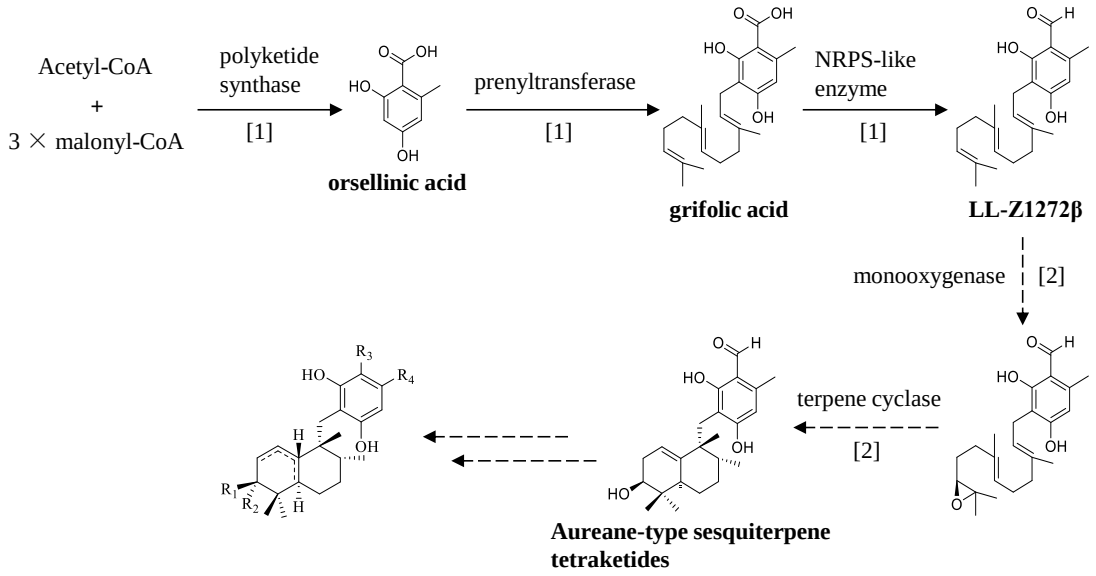

Figure S89 The possible biosynthetic pathways for aureane-type sesquiterpene tetraketide.

References

1 Dolomanov OV, Bourhis LJ, Gildea RJ, Howard JAK, Puschmann H. OLEX2: a complete structure solution, refinement and analysis program. *J Appl Crystallogr* 2009;**42**:339-41.

2 Li C, Matsuda Y, Gao H, Hu D, Yao XS, Abe I. Biosynthesis of LL-Z1272beta: Discovery of a new member of NRPS-like enzymes for aryl-aldehyde formation. *Chembiochem* 2016;**17**:904-7.

3 Itoh T, Tokunaga K, Matsuda Y, Fujii I, Abe I, Ebizuka Y, et al. Reconstitution of a fungal meroterpenoid biosynthesis reveals the involvement of a novel family of terpene cyclases. *Nat Chem* 2010;**2**:858-64.